Role of non-catalytic ligands in macromolecule function

by

Muneaki Watanabe

A dissertation submitted to graduate faculty

in partial fulfillment of the requirements for the degree of

DOCTOR OF PHILOSOPHY

Major: Biochemistry

Program of Study Committee:
Richard B. Honzatko, Major Professor
Mark S. Hargrove
Michael Shogren-Knaak
Scott W. Nelson
Guan Song

Iowa State University

Ames, Iowa

2016

To Ghada

TABLE OF CONTENTS

CHAPTER 1: GENERAL INTRODUCTION

INTRODUCTION PART I: HEXOKINASE I INTERACTIONS WITH VDAC

The mitochondrial voltage dependent anion selective channel (VDAC) was first identified in 1976. The family of VDAC proteins includes three isoforms, VDAC1, VDAC2, and VDAC3, all are located on the outer mitochondrial membrane (OMM). The most abundant isoform on the OMM is VDAC1, which is in fact, the most abundant of all embedded mitochondrial membrane proteins. It is well established that VDAC regulates the energy balance of mitochondria and the entire cell by facilitating the exchange of metabolites between mitochondria and cytoplasm (1-6). The monomer form of VDAC has a pore diameter of 36 Å, as measured from models of X-ray and NMR structures (54, 55) (Fig. 1). Most metabolites are small enough to pass through this pore; however, proteins in their folded conformation are too large to cross the membrane by way of the pore. The interior of pore has many positively charged residues that may be the basis for the anion selectivity, but VDAC also regulates levels of cytosolic and mitochondrial metabolites of respiration and ions, especially that of Ca^{2+} (7-9).

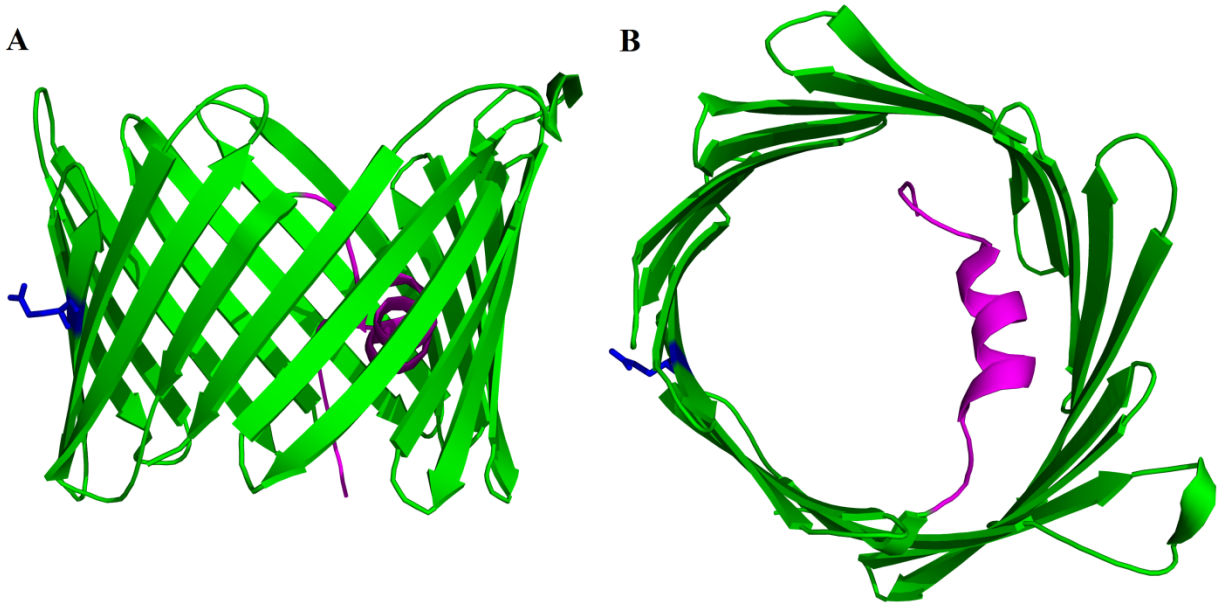

FIGURE 1. VDAC1 structure (PDB 3EMN). A and B indicate side and top views, respectively, of the19-stranded β-barrel (green). The N-terminal helix is magenta and Glu73 is blue.

VDAC is not surprisingly one of the key players in cell survival. Silencing the expression of VDAC1 inhibited cell growth through a reduction in energy production (10). Endogenous VDAC1 expression in transformed primary embryonal human kidney T-Rex-293 cells was

suppressed by 70-90% by shRNA techniques. The decrease in VDAC levels dramatically reduced cell growth, reduced ATP synthesis by five-fold and decreased cellular levels of ATP and ADP by 50% (10).

VDAC also plays a role in apoptosis. Apoptosis (Programmed Cell Death) is a natural process triggered in cells that are functionally compromised. Apoptosis is an indispensable part of the development and function of an organism. There are at least two broad pathways known as "extrinsic" and "intrinsic". The extrinsic pathway begins outside a cell in response to the extracellular environment that requires cell death. The intrinsic apoptosis pathway begins when an injury (or dysfunction) occurs within the cell. Apoptosis involving the mitochondrion is the best known intrinsic pathway (11, 12), and there is substantial evidence suggesting VDAC is a critical player in the release of apoptogenic proteins from mammalian mitochondria (2, 5, 6, 14-15). Release of cytochrome *c*, interactions between pro-apoptotic proteins and VDAC, and the triggering of cell death, are impacted by anti-VDAC antibodies, thus demonstrating the importance of VDAC in the intrinsic apoptosis pathway (16-18). Other evidence of VDAC involvement in apoptosis comes from over- and down-expression of VDAC levels *in vivo*. Over-expression of human, murine, yeast, Paralichthys olivaceus, and rive VDAC induces apoptotic cell death regardless cell type (19-23). On the other hand, siRNA-mediated down-expression of VDAC prevented cell death induced by anti-apoptotic proteins (14).

Another key player of the intrinsic apoptosis pathway relative to VDAC is hexokinase (HK). Four hexokinase isozymes are identified in mammalian tissue: I, II, III and IV (24, 25). Hexokinase I (HKI) (Fig. 2), is recognized as the “pacemaker of glycolysis” in brain tissue and the red blood cell (26). HKI is known to be highly expressed in kidneys, liver, intestines and lungs (27, 28). This enzyme binds the OMM in brain tissue (29). Mitochondrion-associated HKI may provide HKI with preferential access to newly formed mitochondrial ATP (29). HKI binding to the mitochondrion prevents the opening of the permeability transition pore (PTP) (30). The PTP presumably consists of VDAC of the outer mitochondrion membrane (31-36). HKI seems to interact with VDAC to close (or prevent) PTP opening (31, 32). Non-functional PTP causes loss of membrane potential, organelle swelling, cytosolic acidification, and the release of cytochrome *c* (30, 37). Released cytochrome *c* activates the caspase signaling pathway and initiates apoptosis (38-40).

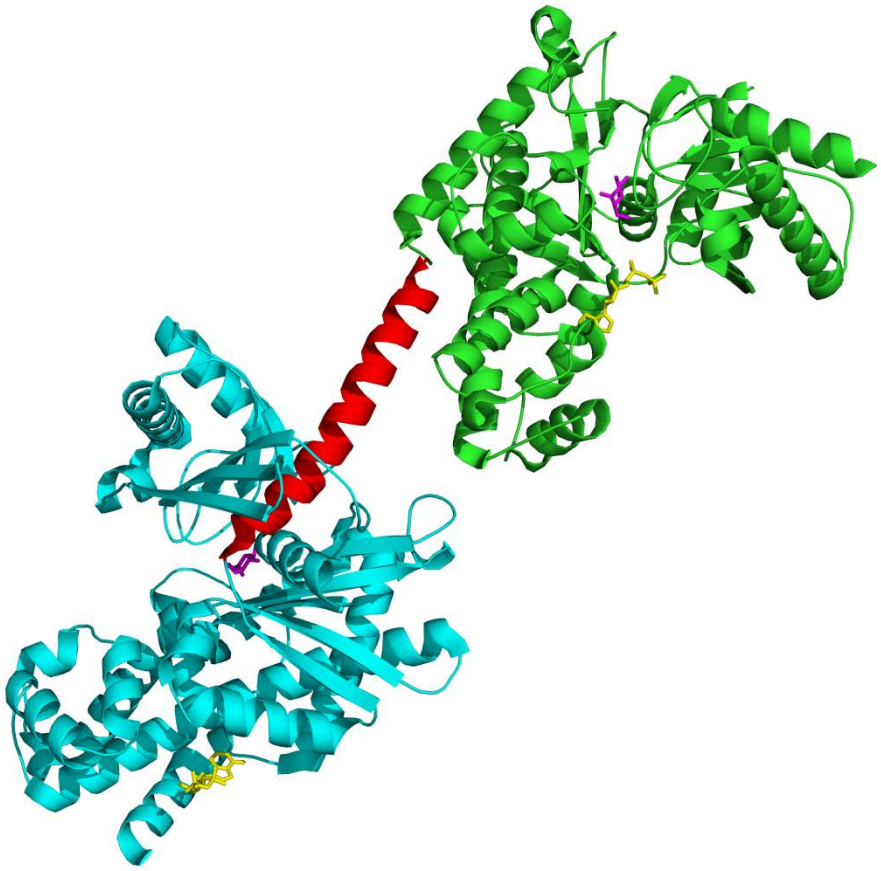

FIGURE 2. Hexokinase type I structure (PDB 1DGK) with ADP (yellow) and glucose (magenta). C-half (green), N-half (cyan), and transition helix (red).

Another line of evidence suggests that pro-apoptotic proteins (Bax, Bak, and Bim) trigger cytochrome *c* release without mitochondrial swelling (37, 41, 42). These pro-apoptotic proteins promote the assembly VDAC into the PTP (41, 42). Overexpression of VDAC causes apoptotic cell death (43, 44), however, over-expression of N-terminal truncated VDAC1 did not induce cells to release cytochrome *c* and the cells were resistant to apoptosis (13). The interaction between VDAC and HKI is governed by a specific residue in VDAC. The key residue Glu73 prevents HKI from binding to mitochondria and prevents HKI-linked protection against apoptosis in cancer cells (43, 45). Moreover, chemical modification of Glu 73 eliminated the binding of HKI to mitochondria (23). Adding HKI to VDAC1 reconstituted in lipid membrane

reduced the channel conductance (30). HKI addition to mutant (Glu 73 to glutamine) mouse VDAC reconstituted in lipid membrane did not block channel conductance, inferring the failure of HKI to bind to mutant VDAC1 (45). HKI may antagonize the formation of apoptotic channels, thus some have gone so far as to label hexokinase as "guardian of the mitochondria" (46). Other proof of HKI association with VDAC comes from its co-localization with human VDAC-1, -2 and -3 (47), and its inhibition of ATP flux through VDAC1 (45).

A number of small and physiological important ligands dissociate HKI from the mitochondrial outer membrane by binding to VDAC. Photoactive ATP analog, Bz-ATP (benzoyl-benzoyl-ATP), can bind to multiple sites on VDAC1 with low and high binding affinities (50). Mutating residues of the predicted nucleotide-binding site of VDAC1 reduced ATP cellular levels and cell growth (51). Other non-nucleotide ligands such as glucose 6-phosphate cause release of HKI from the mitochondrial outer membrane by binding to the N-terminal half of HKI (29).

This dissertation establishes the attributes of ligands that bind to VDAC and cause the release of HKI. The VDAC structure, determined by NMR and crystallographic methods, is a 19-strand β-barrel with its N-terminal helix localized within the pore (54, 55). The function of VDAC is known from ion conductance through the OMM; however, existing structures have not provided a definitive mechanism for the voltage-dependent control of ion permeability. We propose that nucleotide-induced release of HKI from mitochondria enables ion conductance, and that HKI and nucleotides compete for a common binding site on VDAC1 at the OMM. Fluorescent nucleotide analogs probe interactions of HKI with VDAC1.

INTRODUCTION PART II: STRUCTURE AND STABILITY OF β-KETOACYL-ACYL-CARRIER-PROTEIN (ACP) SYNTHASE III

Escherichia coli employs a Type II system, typical of bacteria, plants and parasites in the phylum Apicomplexa, for the synthesis of fatty acids. In contrast, lower eukayotes and mammals employ a Type I system (56, 57). The two systems differ in the organization of enzymes underlying otherwise similar chemical reactions. Type I systems employ single multi-functional enzyme complexes to conduct the sequence of reactions that leads ultimately to the final fatty acids. In the Type II system, individual enzymes are responsible for each chemical step. Focus here is on the Type II system of *E. coli*, and specifically β-ketoacyl-acyl-carrier-protein (ACP)

synthase III (abbreviated KASIII or alternatively FabH after its gene). FabH initiates the biosynthesis of fatty acids. Although KASI (FabB) and KASII (FabF) can also initiate fatty acid biosynthesis *in vitro*, the principal *in vivo* pathway relies on initiation catalyzed by FabH (Fig. 3). The principle roles of FabB and FabF instead are in the elongation of fatty acids and in the termination of fatty acid biosynthesis.

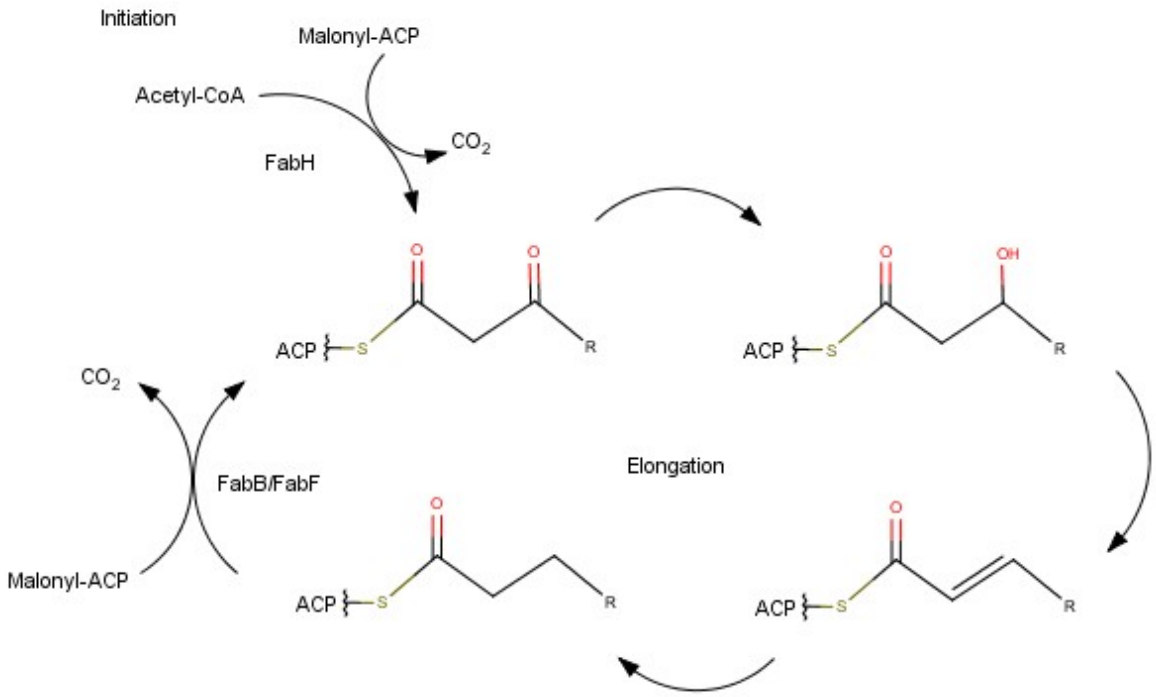

FIGURE 3. Schematic of fatty acid biosynthesis indicating roles for FabB, FabF, and FabH.

FabH catalyzes a sequence of two reactions. The first is the transfer of the acetyl group from acetyl-CoA to an active site cysteine (Cys112). The second is the decarboxylation of malonyl-ACP with the concomitant transfer of the acetyl adduct from Cys112 to form acetoacetyl-ACP. Acetoacetyl-ACP undergoes reduction, dehydration and a second reduction (three chemical steps conducted by three enzymes) resulting in butyryl-ACP. Transfer of the butyryl group from butyryl-ACP to the active site cysteine of FabB (KASI) or FabF (KASII) primes the elongation process (much like acetyl-CoA primes FabH). Another molecule of malonyl-ACP (with concomitant decarboxylation) results in formation of butyryloacetate-ACP, followed by reduction, dehydration, and further reduction to give a six-carbon thioester of ACP (58). Subsequent cycles (condensation, reduction, dehydration and reduction) produces free palmitate as the final product. The importance of enzymes (FabB and FabF) in the termination of

chain elongation and in the accumulation of specific saturated and unsaturated fatty acids in the cell has been demonstrated (59).

Most investigations of FabH focus on one of two areas: (i) enzyme inhibition as a means of limiting cell growth and (ii) enzyme engineering for the production of new fatty acids. Thiolectomycin, a known antibacterial agent, inhibits bacterial fatty acid synthases acting against FabB, FabF and FabH with IC_{50} values of 25, 6 and 110 μM, respectively (70). Cerulenin inhibits FabB, FabF and FabH with IC_{50} values of 3, 20 and >700 μM, respectively. Inhibition levels suggest similarities in the active sites of FabB and FabF that are not shared by FabH (56, 61, 62). Moreover, if the goal is the development of an effective antimicrobial agent, then FabH is the best target due its role as the principal initiator of fatty acid biosynthesis in Type II systems (60, 63, 64). FabH selects acetyl-CoA over acyl-ACP, and in fact is distinguished from FabF and FabB by its preference for acetyl-CoA as a substrate. The engineering of biosynthetic pathways in *E. coli* to produce modified fatty acids and/or fatty acids of specific chain-length is a goal of a biorenewable economy. FabH discriminates against branching at the ω-terminus of the fatty acid (the reason for this is clear from structures presented in Chapter 5 of this thesis), but fatty acid synthase initiators from other organisms do accept larger and branched alkyl groups (n-propyl, isopropyl and t-butyl). Hence, the possibility of engineering FabH to accept substrates in addition to acetyl-CoA may be possible.

Crystallographic structures of FabH with few exceptions reveal a homodimer. Previous work has revealed the presence of an acetyl adduct at Cys112 and the ordered binding of CoA at the active site that presumably closely resembles a productive complex of acetyl-CoA and the enzyme (65-68) (Fig. 4). These structural studies suggest specific functions for active-site residues in the Claisen condensation. Moreover, molecular dynamics simulations have been used to evaluate the stability of the FabH protein and models of the FabH-ACP complex. The simulations indicate that the substrate complex FabH adopts a more stable conformation than FabH itself (69).

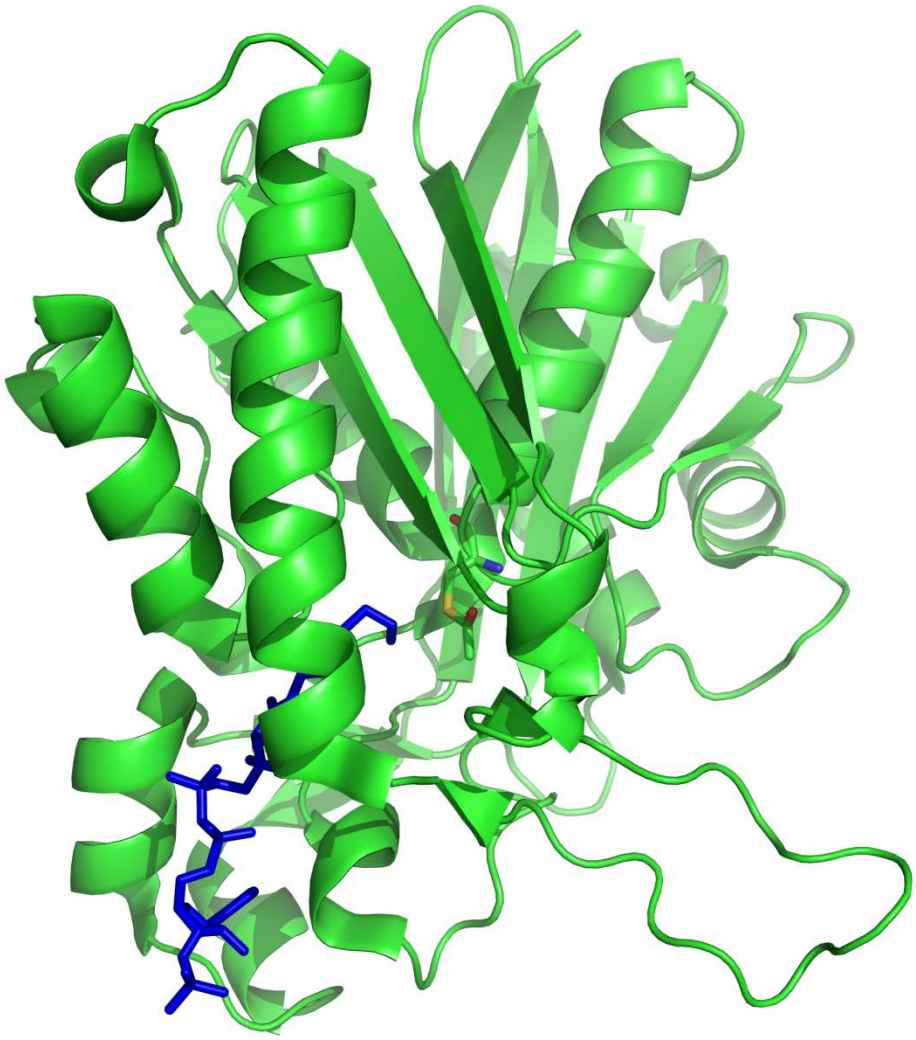

FIGURE 4. FabH structure with acetylation of active site and CoA (PDB 1HNH). FabH (green), CoA (blue), and acetylated Cysteine residue 112 (stick).

The major contribution of this thesis has been the recognition of the acetyl adduct form of FabH by halide anions. Work here verifies observations of an acetyl adduct, ordered binding of CoA to the active site and conformational disorder in the active site in the absence of ligands or adduct. The observation that FabH comes out of *E. coli* cells as the Cys112 adduct, suggest the primary *in vivo* state of the enzyme is the adduct intermediate, primed and ready to accept malonyl-ACP in the second step of the reaction mechanism.

DISSERTATION ORGANIZATION

This dissertation is organized into six chapters. Chapter 1 covers the background literature, problems and objectives related to the research projects. Chapters 2, 3, 4, and 5 are papers prepared for publication in peer reviewed journals. Chapter 2 explores the mechanism of nucleotide release of HKI from OMM. Chapter 3 explores VDAC binding to nucleotides. Chapter 4 describes the determination and localization of binding of VDAC at an artificial vesicle. Work in Chapter 5 reveals mechanisms of halide and substrate stabilization of FabH. Conclusions and recommendations for future studies are in Chapter 6.

REFERENCES

1. Colombini M (2004) Mol. Cell. Biochem. 256-257, 107-115

2. Lemasters J J; Holmuhamedov E (2006) Biochim. Biophys. Acta. 1762, 181-190

3. Shoshan-Barmatz V; Gincel D (2003) Cell Biochem. Biophys. 39, 279-292

4. Shoshan-Barmatz V; Israelson A (2005) J. Membr. Biol. 204, 57-66

5. Tsujimoto Y; Shimizu S (2002) Biochemie. 84, 187-193

6. Vyssokikh MY; Brdiczka D (2003) Acta. Biochim. Pol. 50, 389-404

7. Gincel D; Zaid H; Shoshan-Barmatz V (2001) Biochem. J. 358, 147-155

8. Deniaud A; Sharaf el dein O; Maillier E; Poncet D; Kroemer G; Lemaire C; Brenner C. (2007) Oncogene. 1-15

9. Deniaud A; Rossi C; Berquand A; Homand J; Campagna S; Knoll W; Brenner C; Chopineau J. (2007) J. Am. Chem. Soc. 23, 3898-3905

10. Abu-Hamad S; Sivan S, Shoshan-Barmatz V (2006) Proc Natl Acad Sci, 103:5787-5792

11. Wilk S. (2005) Sci. STKE. 285, tr16

12. Czerski L; Nunex G. (2004) J. Mol. Cell Cardiol. 37, 643-52

13. Abu-Hamad S; Arbel N; Calo D; Arzoine L; Israelson A; Keinan N; Ben-Romano R; Friedman O; Shoshan-Barmatz V. (2009) J. Cell. Sci. 122, 1906-1916

14. Tajeddine N; Galluzzi L; Kepp O; Hangen E; Morselli E; Senovilla L; Araujo N; Pinna G; Larochette N; Zamzami N; Modjtahedi N; Harel-Bellan A; Kroemer G. (2008) Oncogene, 27, 4221-4231

15. Yuan S; Fu Y; Wang X; Shi H; Huang Y; Song X; Li L; Song N; Luo Y. (2008) FASEB J. 22, 2809-2820

16. Madesh M; Hajnoczky G. (2001) J. Cell. Biol. 155, 1003-1010

17. Shimizu S; Matsuoka Y; Shinohara Y; Yoneda Y; Tsujimoto Y. (2001) J. Cell Biol. 152, 237-250

18. Zheng Y; Shi Y; Tian C; Jiang C; Jin H; Chen J; Almasan A; Tang H; Chen Q. (2004) Oncogene 23, 1239-1247

19. Abu-Hamad S; Zaid H; Israelson A; Nahon E; Shoshan-Barmatz V. (2008) J Biol. Chem. 283(19), 13482-13490

20. Ghosh T; Pandey N; Maitra A; Brahmachari S K; Pillai B. (2007) PLoS. ONE 2, e1170

21. Godbole A; Varghese J; Sarin A; Mathew M K. (2003) Biochim. Biophys. Acta. 1642, 87-96

22. Lu A J; Dong C W; Du C S, Zhang Q Y. (2007) Fish. Shellfish. Immunol. 23, 601-613

23. Zaid H; Abu-Hamad S; Israelson A; Nathan I; Shoshan-Barmatz V. (2005) Cell Death Differ. 12, 751-760

24. González, C; Ureta, T; Sánchez, R; Niemeyer, H. (1964) Biochem. Biophys. Res. Commun. 16, 347-52.

25. Katzen, H M; Schimke, R T. (1965) Proc. Natl. Acad. Sci. U S A. 54, 1218-25.

26. Lowry, O H; Passonneau, J V. (1964) J. Biol. Chem. 239, 31-42.

27. Katzen, H M. (1967) Adv. Enzyme. Regul. 5, 335-56.

28. Purich, D L; Fromm, H J; Rudolph, F B. (1973) Adv. Enzymol. Relat. Areas. Mol. Biol. 39, 249-326.

29. Rose, I A; Warms, J V. (1967) J. Biol. Chem. 242, 1635-45.

30. Azoulay-Zohar, H; Israelson, A; Abu-Hamad, S; Shoshan-Barmatz, V. (2004) Biochem. J. 377, 347-55.

31. Lindén, M; Gellerfors, P; Nelson, B D. (1982) FEBS Lett. 141, 189-92.

32. Fiek, C; Benz, R; Roos, N; Brdiczka, D. (1982) Biochim. Biophys. Acta. 688, 429 40.

33. Beutner, G; Ruck, A; Riede, B; Welte, W; Brdiczka, D. (1996) FEBS Lett. 396, 189-95.

34. Beutner, G; Rück, A; Riede, B; Brdiczka, D. (1997) Biochem. Soc. Trans. 25, 151-7.

35. Vyssokikh, M Y; Brdiczka, D. (2003) Acta. Biochim. Pol. 50, 389-404.

36. Vyssokikh, M Y; Goncharova, N Y; Zhuravlyova, A V; Zorova, L D; Kirichenko, W; Krasnikov, B F; Kuzminova, A E; Melikov, K C; Melik-Nubarov, N S; Samsonov, A V; Belousov, W; Prischepova, A E; Zorov, D B. (1999) Biochemistry (Mosc). 64, 390-8.

37. Machida, K; Ohta, Y; Osada, H. (2006) J. Biol. Chem. 281, 14314-20.

38. Crompton, M; Virji, S; Doyle, V; Johnson, N; Ward, J M. (1999) Biochem. Soc. Symp. 66, 167-79.

39. Zamzami, N; Kroemer, G. (2003) Curr. Biol. 13, R71-3.

40. Lemasters, J J; Qian, T; Bradham, C A; Brenner, D A; Cascio, W E; Trost, L C; Nishimura, Y; Nieminen, A L; Herman, B. (1999) J. Bioenerg. Biomembr. 31, 305-19.

41. Shimizu, S; Narita, M; Tsujimoto, Y. (2000) Nature 399, 483-87.

42. Shimizu, S; Matsuoka, Y; Shinohara, Y; Yoneda, Y; Tsujimoto, Y. (2001) J. Cell Biol. 152, 237-50.

43. Zaid, H; Abu-Hamad, S; Israelson, A; Nathan, I; Shoshan-Barmatz, V. (2005) Cell Death Differ. 12, 751-60.

44. Abu-Hamad, S; Sivan, S; Shoshan-Barmatz, V. (2006) Proc. Natl. Acad. Sci. U S A. 103, 5787-92.

45. Shoshan-Barmatz, V; Zakar, M; Rosenthal, K; Abu-Hamad, S. (2009) Biochim. Biophys. Acta. 1787, 421-30.

46.Robey R B; Hay N. (2005) Cell Cycle 4, 654-658.

47.Neumann D; Bückers J; Kastrup L; Hell S W; Jakobs S. (2010) PMC Biophys. 3, 1-15

48.Perevoshchikova I V; Zorov S D; Kotova E A; Zorov D B; Antonenko Y N. (2010) FEBS Lett. 584, 2397-2402.

49.Arzoine L; Zilberberg N; Ben-Romano R; Shoshan-Barmatz V. (2009) J. Biol.Chem. 284, 3946-3955.

50.Yehezkel G; Hadad N; Zaid H; Sivan S; Shoshan-Barmatz V. (2006) J. Biol. Chem. 281, 5938-5946.

51.Yehezkel G; Abu-Hamad S; Shoshan-Barmatz V. (2007) J. Cell. Physiol. 212, 551-561

52.Aleshin A E; Fromm H J; Honzatko R B. (1998) FEBS Lett. 434, 42-46.

53.Estabrook R W, Holowinsky A. (1961) J. Biophys. Biochem. Cytol. 9, 19-28.

54.Hiller S; Garces R G; Malia T J; Orekhov V Y; Colombini M; Wagner G. (2008) Science 321, 1206-1210

55.Bayrhuber M; Meins T; Haeck M; Becker S; Giller K; Villinger S; Vonrhein C; Griesinger C; Zweckstetter M; Zeth K. (2008) PNAS. 105(40), 15370-15375

56.Tsay, J T; Oh, W; Larson, T J; Jakowski, S; Rock, C O. (1992) J. Biol. Chem. 267, 6807-14.

57.Clough, R C; Matthis, A L; Barnum, S R; Jaworski, J G. (1992) J. Biol. Chem. 267, 20992-998.

58.Volpe, J J; Vagelos, P R. (1976) Physiol. Rev. 56, 339-417.

59.Greenspan, M D; Birge, C H; Powell, G; Hancock W S;Vagelos, P R. (1970) Science 170, 1203-1204.

60.Magnuson, K; Jackowski, S; Rock, C O; Cronan, J E Jr. (1993) Microbiol. Rev. 57, 522-5542.

61.Heath, R J; Rock, C O (1996) J. Biol. Chem. 271, 10996-11000.

62.Omura, S. (1979) Bacteriol. Rev. (1979) 40, 681-697.

63.Blatti, J L; Michaud, J; Burkart, M D. (2013) Curr. Opin. Chem. Biol. 17, 496-505.

64.Howard, T P; Middelhaufe, S; Moore, K; Edner, C; Kolak, D M; Taylor, G N; Parker D A; Lee, R; Smirnoff, N; Aves, S J; Love, J. (2013) Proc. Natl. Acad. Sci. U.S.A. 110, 7636-41.

65.Davies, C; Heath R J; White, S W; Rock, C O. (2000) Structure 8, 185-195.

66.Qiu, W; Janson, C A; Konstantinidis, A K; Nwagwu, S; Silverman, C; Smith, W W; Khandekar, S; Lonsdale, J; Abdel-Meguid, S S. (1999) J. Biol. Chem. 274(51), 36465-71.

67.Qiu, X; Janson, C A; Smith, W W; Head M; Lonsdale J; Konstantinidis A K. (2001) J. Mol. Biol. 307, 341-56.

68.Gajiwala, K S; Margosiak, S; Lu, J; Cortez, J; Su, Y; Nie, Z; Appelt, K. (2009) Febs Lett. 583, 2939-46.

69.Misra, N; Patra, M C; Panda, P K; Sukla, L B; Mishra B K. (2013) J. Biomol. Struct. Dyn. 31(3), 241-57.

70. Khandekar, S S; Gentry, R D; Van Aller, S G; Warren, P; Xiang, H; Silverman, C; Doyle, L M; Konstantinidis, K A; Brandt, M; Daines, A R; Lonsdale, T J. (2001) J. Biol. Chem. 276(32), 30024-30.

CHAPTER 2. MECHANISM OF ATP-DEPENDENT RELEASE OF WILD-TYPE AND MUTANT HUMAN BRAIN HEXOKINASES FROM MITOCHONDRIA[1]

A paper to be submitted to the Journal of Biological Chemistry

Nimer Mehyar[2], Muneaki Watanabe[2], Lu Shen[2], Andrew D. Skaff[2], and Richard B. Honzatko[2,3]

From the Roy J. Carver Department of Biochemistry, Biophysics and Molecular Biology

Iowa State University, Ames, IA 50011

Running title: Human brain HK release from mitochondria

Keywords: human brain hexokinase, VDAC1, mitochondria, apoptosis, nucleotides

Background: Hexokinase I binding to mitochondrion prevent apoptosis in the cells. Adenosine 5'-triphosphate (ATP) releases HKI from mitochondria.
Results: ATP and fluorescent nucleotide analogue 2',3'-O-(2,4,6-trinitro-phenyl) adenosine 5'-diphosphate (TNP-ADP) release wild-type Hexokinase I, mHKI and N-domain from mitochondrion. TNP-ADP does not bind to N-domain HKI. TNP-ADP binds to VDAC1.
Conclusion: ATP releases HKI from mitochondria by binding to VDAC1 on OMM.
Significance: Propose a mechanism for nucleotide induced release of brain of HKI from mitochondria.

ABSTRACT

Adenosine 5'-triphosphate (ATP) can release hexokinase I (HKI) from its binding site on the outer mitochondrial membrane, but the mechanism of ATP release of HKI from mitochondria is unclear. ATP binds to the C-terminal half of HKI as a substrate and to the N-terminal half near the membrane binding element. ATP may also bind to the voltage dependent anion channel (VDAC), the integral membrane component that putatively targets HKI to the mitochondrion. The fluorescent nucleotide analogue 2',3'-O-(2,4,6-trinitrophenyl) adenosine 5'-diphosphate (TNP-ADP) binds with high affinity to the C-terminal half of HKI (Kd = 2.8 ± 0.4 μM) and to VDAC (Kd = 1.3 ± 0.1 μM), but not to the N-terminal half of HKI (Kd not available).

---

[1] This research was supported in part by National Institute of Health Research Grant NS 10546.
[2] Graduate student and professor, respectively, Department of Biochemistry, Biophysics and Molecular Biology, Iowa State University. Research conducted and manuscript written by Mehyar with assistance from Muneaki, Shen, Skaff and Honzatko.
[3] To whom correspondence should be addressed.

ATP competes with TNP-ADP for binding sites on HKI (KA = 46 ± 6 μM) and VDAC (KA = 550 ± 40 μM), but CTP does not displace TNP-ADP from either HKI or VDAC. Other trinitophenyl nucleotides (TNPATP, TNP-AMP, and TNP-CTP) bind with high affinity to HKI and VDAC. ATP and trinitrophenyl nucleotides individually release wild-type HKI from mitochondria; however, CTP is ineffective as an agent of release. ATP and ADP-TNP release the truncated N-domain of HKI from mitochondria, excluding nucleotide binding to either the N- or C-half of HKI in the release mechanism. Results here are consistent with a release mechanism caused by the binding of ATP or TNP-ADP to VDAC.

INTRODUCTION

Mammalian tissue contains four hexokinase isozymes: I, II, III and IV (1). Hexokinase I (HKI) or brain hexokinase has long been recognized as the “pacemaker of glycolysis” in brain tissue and the red blood cell (2). Human brain comprises less than 2% of body weight and yet it utilizes at least one-quarter of the circulating blood glucose and approximately one-fifth of the oxygen consumed by the body (3). Nevertheless, HKI is at least 95% inhibited under normal physiological conditions in brain tissue (2). A number of ligands inhibit HKI; however, glucose 6-phosphate (Glc-6-P) is probably the primary physiological inhibitor of the Type-I enzyme (4). On the other hand, inorganic orthophosphate (Pi) is capable of ameliorating Glc-6-P inhibition under normal physiological conditions (5), although at elevated levels it inhibits HKI by binding to the active site (6). Hexokinase II (HKII) is functionally similar to HKI; however, Pi does not relieve Glc-6-P inhibition of the Type-II isozyme (7).

HKI and HKII have evolved by the duplication and fusion of a primordial hexokinase gene similar to that of yeast hexokinase (8). Each half of HKI and HKII exhibits significant sequence similarities (9). For HKII both halves support catalysis and are each sensitive to inhibition by Glc-6-P (10), whereas only the C-terminal half of HKI supports activity (11). Nonetheless, both halves of HKI can bind Glc-6-P with high affinity, and moreover the binding of Glc-6-P to either half inhibits activity (12, 13). Pi binds with high affinity to the N-terminal half of HKI (14-15), and relieves Glc-6-P inhibition by an allosteric mechanism that couples both halves of the enzyme (15).

HKI and HKII associate with the outer mitochondrial membrane in brain tissue (16). This interaction requires fifteen, largely hydrophobic amino acid residues at its N-terminus (17). HKI

association with outer mitochondrial membrane allows preferential access to newly formed mitochondrial ATP (16). HKI likely interacts with the voltage-dependent anion channel (VDAC) of the outer mitochondrial membrane (18-19). HKI binding to the mitochondrion prevents the opening of the permeability transition pore (PTP) (20). The PTP is a multicomponent system that includes the adenylate translocator (ANT) of the inner mitochondrion membrane, and the voltage dependent anion channel (VDAC) of the outer mitochondrion membrane (18-24), and is regulated by cyclophilin D of the inner mitochondrion matrix and the binding of hexokinase I and II (25-27). Opening of the PTP results in loss of membrane potential, organelle swelling, cytosolic acidification, and the release of cytochrome c (20, 25). Cytochrome c that escapes the mitochondrion after the PTP opening activates the caspase family of proteases, which ultimately results in apoptosis (27-29).

Others maintain that the opening of the PTP initiates necrosis, but not apoptosis, and that a proapoptotic protein such as Bax, triggers the release of cytochrome c without mitochondrial swelling (25,30-31). Nevertheless, mitochondrion associated hexokinase II clearly antagonizes the action of pro-apoptotic factors such as Bax (32-34). Pro-apoptotic proteins (Bax, Bak, and Bim) interact with VDAC in the assembly of large pores that presumably serve as conduits for the release of cytochrome c (30-31,35). Indeed, overexpression of VDAC-1 causes apoptotic cell death (36-37). Hexokinase I and II, through their own associations with VDAC, may antagonize the formation of apoptotic channels. Some have gone so far as to label hexokinase as “guardian of the mitochondria” (38). Hexokinase co-localizes differentially with human VDAC1, 2 and 3 (39). Hexokinase binding to mitochondria inhibits ATP flux through VDAC-1 (40). Over expression of N-terminally truncated VDAC-1 did not induce cells to release cytochrome c and the cells were resistant to apoptosis (41). The N-terminal peptide of VDAC-1 and other VDAC-1 based peptides bind to immobilized HKI. These peptides prevented protection of cells by HKI (42). Chemical modification of Glu 72 eliminated the binding of HKI to mitochondria (36). Mutating Glu 72 and other residues abolished overexpressed HKI protection against apoptosis in different cancer cells (43). Adding HKI to VDAC-1 reconstituted in lipid membrane reduced the channel conductance (20). HKI addition to mutant (Glu 72 to glutamine) mouse VDAC reconstituted in lipid membrane did not lessen channel conductance, indicating failure of HKI to bind to mutant VDAC-1 (43).

A number of small and physiological important ligands are capable of dissociating HKI from the mitochondrial outer membrane. These compounds include Glc-6-P and ATP (16). Skaff et al. (44) demonstrated a wild-type recombinant HKI with properties comparable to native brain hexokinase, including those of mitochondrial binding and release. Their recombinant construct has an intact membrane targeting element and a formyl group attached to the amino terminus of the polypeptide chain. The release properties of mutant constructs demonstrated the significance of Glc-6-P binding to the N-terminal half of HKI in promoting the release of the mitochondrion associated enzyme. The Glc-6-P release phenomenon adheres to a simple equilibrium model. To date, little is known regarding the mechanism of ATP-induced release of HKI from mitochondria (16, 45-47). Three binding sites exist on HKI for adenine nucleotides: the active site at the C-terminal half (11), the Pi binding site at the N-terminal half at which the nucleotide may bind through its terminal phosphoryl group (48), and the nucleotide pocket of unknown function near the N-terminal membrane targeting element (48-49). Photoactive ATP analog, Bz-ATP (benzoylbenzoyl-ATP), can bind to more than one sites on VDAC-1 with low and high affinities (50). Mutating residues in predicted nucleotide-binding site in VDAC-1 reduced ATP cellular levels and caused retarded cell growth (51).

The purpose of the present study was to investigate the mechanism of HKI release from mitochondria by adenosine nucleotides, and which, if any, of the adenine nucleotide binding sites of HKI or VDAC are responsible for that release. The fluorescent ADP analog, 2',3'-O-(2,4,6-trinitrophenyl) adenosine 5'-diphosphate (TNP-ADP), binds with high affinity to single sites at the C-terminal domain of HKI and to VDAC. Nevertheless, TNP-ADP releases the N-terminal domain of HKI (a domain to which it does not bind) from mitochondria. The data here are consistent with a site on VDAC that binds HKI and ADP-TNP in a mutually exclusive manner.

EXPERIMENTAL PROCEDURES

Materials— ATP, ADP, chloramphenicol, deoxyribonuclease (DNase I), bovine serum albumin (BSA), leupeptin, protease cocktail inhibitor and phenylmethylsulfonyl fluoride came from Sigma. Kanamycin sulfate and 2',3'-O-(2,4,6-trinitrophenyl)-derivatives of ATP, ADP, AMP, and CTP came from Invitrogen. DEAE HPLC was from Tosoh. Nickel-nitrilotriacetic acid-agarose (NiNTA) and Rosetta (DE3) competent cells were from Novagen. Glucose-6-phosphate dehydrogenase was obtained from Roche Molecular Biochemicals. Isopropyl-1-thio-

β-D-galactopyranoside (IPTG) came from Anatrace. His-tag anitbodies, N-terminal HKI antibodies and C-terminal HKI antibodies were from Abcam. Substrates for the 3,3',5,5'-tetramethylbenzidine enzyme-linked imunoabsorbant assay (TMB-ELISA) and western blotting chemiluminescence came from Pierce. Oligonucleotides came from the Iowa IDT. Lauryldimethylamine-N-oxide (LADO) was purchased from Affymetrix.

Construction of Wild-type Hexokinase and N domain Plasmids— Human brain hexokinase (HKI) was cloned into pET-24b vector with a 10-residue histidine tag at its C-terminus (pET-24b-HKI-10xHis) as reported previously (44). Hexokinase mutants were created through PCR modification. An NdeI cut site was created at Ala454 in pET-24b-HKI-10xHis using the forward primer, 5'-GCAGCGGCAAGGGGGCTCATATGGTGACGGCGGTGGC-3', and its reverse complement. Mutant plasmid was digested with NdeI and then ligated to produce pET24b-N-C half-HKI-10xHis. This plasmid encodes residues 454-917 of HKI with a C-terminal polyhistidyl tag (hereafter mHKI). An EcoRI cut site was created at Ala454 in pET-24b-HKI-10xHis using the forward primer, 5'GCAGCGGCAAGGGGGCTCGAATTCGTGACGGCGGTGGC-3', and its reverse complement. Mutant plasmid was digested with NdeI and then ligated to produce pET24b-NHKI-10xHis. This plasmid encodes residues 1-454of HKI with a C-terminal polyhistidyl tag (hereafter N domain HKI).

Mitochondrion Purification— Pig livers were obtained from the Iowa State University Meats Laboratory shortly after slaughter. Mitochondrial purification is described (52) with modification as discussed elsewhere (44). Both outer mitochondrial membrane (OMM) and inner mitochondrial membrane (IMM) integrities were measured as described previously (53-54). Mitochondria were stored at –80º C in the presence of 5% dimethyl sulfoxide.

Expression and Purification of Wild-Type HKI and N-domain HKI— *E.coli* strain Rosetta (DE3) cells were transformed with wild-type or N-domain HKI plasmids. Expression and purification HKI enzymes are discussed in detail by Skaff et al (44). The determination of protein concentration employed the Bradford method with bovine serum albumin as a standard (55).

HKI Activity Assay— Hexokinase activity was measured using the glucose 6-phosphate dehydrogenase (G6PDH)-coupled spectrophotometric assay. All assay solutions had 3mM $MgCl_2$, 3 mM DTT, 0.3 mM NADP, 10 μg/mL G6PDH and 50 mM Tris-HCl, pH 8.0.

Concentrations of substrate (either glucose or ATP:Mg^{2+} at1:1 ratio) varied from 1/5 to 5 times Km. NADPH production was monitored at 340 nm. G6PDH was in sufficient excess so that a doubling of HKI concentration resulted in a doubling of initial velocity. Assays were initiated by addition of 0.5 μg HKI. Initial rates were determined from slopes of linear progress curves (monitored for 3 minutes). Initial-rate data were analyzed using the GraFit computer program (56). The mechanism of TNP-ADP inhibition was determined by assays in the presence of saturating glucose (1.6 mM) and systematic variations in the concentration of ATP:Mg^{2+} at1:1 (0.3-4.5 mM) and TNP-ADP (0-40 μM). Mitochondrion-bound hexokinase was added to the assay cocktail with saturating glucose (1.6 mM) and saturating ATP:Mg^{2+}, 1:1 (6 mM). Initial velocity data were fit to models described in the Results section by nonlinear least squares using GraFit (56).

Mitochondrial Binding and Release— Purified HKI was dialyzed twice against mitochondrial binding buffer (250 mM sucrose, 5 mM Glc, 50mM NaCl, 5 mM $MgCl_2$ and 50 mM HEPES, pH7.4), and then diluted to 2 mg/mL using the same buffer. Thirty mg wet weight of mitochondrion (0.24 mg mitochondrial protein), thawed on ice, was suspended in 1 mL of mitochondrial-binding buffer, and then collected by centrifugation at 11,000 × g for 5 minutes. Suspension and centrifugation steps were repeated twice. The pellet was suspended in 1 mL of mitochondrial binding buffer with added HKI (2 mg/mL), protease cocktail inhibitor (0.25 mg/mL) and PMSF (1 mM). After 60 minutes on ice, the mixture of HKI and mitochondria was centrifuged at 11,000 × g for 5 minutes. Unbound HKI in the supernatant fluid was decanted. Pelleted mitochondria were suspended in mitochondrial binding buffer, less the $MgCl_2$, NaCl, and Glc, and centrifuged again. This wash step was twice repeated. HKI-bound mitochondria, prepared as above, is suspended in release buffer (250 mM sucrose and 50 mM HEPES, pH 7.4). One hundred μL aliquots of this suspension were distributed to plastic micro-centrifuge tubes, to which were added a release agent (ATP or TNP-nucleotide) at various concentrations. After 30 minutes at room temperature, the mitochondria were pelleted by centrifugation. HKI solubilized by nucleotide was removed by decanting the supernatant liquid. The mitochondrial pellet was suspended in wash buffer (250 mM sucrose and 5 mM HEPES, pH 7.4), and centrifuged. After discarding the supernatant fluid, pelleted mitochondria were suspended in 100 μL wash buffer and then assayed for hexokinase activity or suspended in 100 μL of coating buffer (100 mM sodium carbonate/bicarbonate, pH 9.6) for ELISA assays.

HKI ELISA Assay— Fifty μL of HKI-bound mitochondrial suspension in coating buffer (100mM Na_2CO_3/$NaHCO_3$ pH 9.6) was loaded in each well of the ELISA plate and incubated overnight at 4 C. Plates were washed four times with PBST (137mM NaCl, 2.7mM KCl, 8.1mM Na_2HPO_4, 1.76mM KH_2PO_4, pH 7.4, 0.05% Tween-20). Wells were blocked with 200 μL of 1% BSA in PBST at room temperature for 2 hours and then washed four times with 200 μL PBST. Wells were incubated with 100 μL of anti-His-tag primary antibodies (1:1000 dilution) for 2 hours at room temperature, and then washed four times with PBST. One hundred μL of anti-rabbit IgG secondary antibodies solution (1:10000 dilution) was added to each well, incubated for 2 hours at room temperature, and then washed four times with PBST. A volume of 100 μL of 1-Step Ultra TMB-ELISA solution was added to each well. A Biotek (Ceres 900) plate reader was used to measure change in absorbance at wavelength 620 nm. A reading was taken every 10 seconds, a total of 75 for each well. HKI was used as a positive control and mitochondria as a negative control. Slopes of linear progress curves were determined by regression analysis, and used in nonlinear least square fits (using GraFit) to models described in the Results section.

Mitochondria western blotting— Mitochondria with and without bound HKI were re-suspended in 15 μL water plus 3μL of loading buffer (1M Tris-HCl, pH 6.8, 10% SDS, 3% glycerol, 0.12 mg/mL bromophenol blue) and boiled for 5 minutes prior to polyacrylamide gel electrophoresis (SDSPAGE). After removal of SDS, proteins were transferred by blotting from gel to nitrocellulose membranes (57). Membranes were blocked with 3% bovine serum albumin in 50 mM Tris, 150 mM NaCl, 0.05% Tween 20, pH 7.6, (TBST buffer) for one hour at room temperature and then washed three times with TBST buffer. Membranes were exposed to primary antibody (His-Tag antibodies, C-terminal HKI antibodies, or N-terminal HKI antibodies) in TBST buffer for one hour at room temperature, and then washed three times with TBST buffer. Membranes were subsequently treated with rabbit IgG secondary antibodies for one hour at room temperature and washed three times with TBST buffer. Finally, x-ray film was exposed for 1 minute to membranes treated with Pierce chemiluminescence substrate and then developed.

Cloning of Wild-type human VDAC-1— A plasmid with the coding sequence of human VDAC-1 (hVDAC-1) was purchased from Open Biosystems. NdeI and SacI cut sites were created in the plasmid using the polymerase chain reaction (PCR) and NdeI primer 5'CGCGGCAGCCATATGATGGCTGTGCCACCCACG3' and SacI primer

5'GGACTGGAATTTCAAGCA TCGAGCTCCGTCGACAAGC3'. The PCR product and vector pET-24a were digested by NdeI and SacI restriction enzymes. After separation on agarose gel, the DNA fragment for hVDAC-1 was ligated to pET-24a. The construct was confirmed by DNA sequencing facility at Iowa State University.

Expression and purification of hVDAC-1— Wild-type human VDAC-1 containing plasmid was transformed into *E. coli* strain BL21 (DE3). Cells were grown in LB media at 37 °C, kanamycin was added to a final concentration of (30 μg/mL). Growth was monitored by absorbance at wavelength 600 nm. At A600 of 0.9, the temperature was reduced to 16 °C and IPTG was added to a final concentration of 0.3 mM. Cells were collected after 16-20 hours of induction and suspended in lysis buffer (30mM Tris-HCl, pH8.0, 150mM NaCl, 1mM EDTA, and 1mM DTT). DNase (50 μg/mL), leupeptin (5 μg/mL), and PMSF (1 mM) were all added to the solution. Cells were lysed by sonication. Inclusion bodies were pelleted at 32460g for 1 hour. Pelleted inclusion bodies were subjected to the following procedures three times: separation from the supernatant fraction, suspension in wash buffer (30 mM Tris-HCl, pH 8.0, 150 mM NaCl, 1 mM EDTA, 1 mM DTT) and centrifugation at 15,000rpm 32460g for 30 minutes. Inclusion bodies were suspended in 30 mL of wash buffer plus 1% Triton X-100, incubated for 30 minutes at 37 °C, and then suspended and washed twice with wash buffer.

Refolding of Wild-Type Human VDAC1— Human VDAC1 purification and folding follows protocols in the literature (51, 58) with modifications. Washed inclusion bodies were solubilized in 150 mL dissolving buffer (6M guanidine hydrochloride, 10 mM DTT, 0.1 mM EDTA, 100 mM Tris-HCl, pH8.0) to a final protein concentration of 15 mg/mL. Inclusion bodies dissolved completely in 12 hr. at 4 °C. Twenty five milliliters of unfolded human VDAC-1were diluted by slow addition into 300 mL of refolding buffer (0.1 mM EDTA, 1 mM DTT, 100 mM Tris-HCl, pH8.0, 2% LDAO) at 4 °C. Refolded protein was concentrated and dialyzed against 50 mM Tris-HCl. pH 7.5, 0.1% LDAO buffer for 24 hr at 4 °C. Solution was loaded onto a nickel-nitrilo triacetic acid (Ni-NTA) column. The column was washed with buffers containing 50 mM Tris-HCl, pH7.5, 300 mM NaCl, 0.1% LDAO and 5 mM imidazole and then 50 mM imidazole. Finally, human VDAC-1 was eluted with the same buffer containing 300 mM imidazole.

HKI and VDAC-1 Fluorescence Experiments— Purified HKI and human VDAC-1 were dialyzed against 2 mM glucose and 50 mM Tris-HCl, pH 7.5. Fluorescence measurements were made at room temperature using a 1-cm^2 quartz cuvette on a SLM Amico 8000 fluorimeter with

entrance/exit slits of 4 mm in the presence of 10% polyethyleneglycol, MW ~10,000 (PEG) in the case of HKI. For TNP-nucleotides the excitation wavelength was 409 nm, and emission scans were from 450 to 600 nm. Fluorescence scans (a total of three for each datum) were performed after additions of small volumes of TNP-nucleotide to 2mL of 2.5μM HKI or human VDAC-1. TNP-nucleotide displacement was accomplished by the addition of the alternative nucleotide to 1 mL solution of 2 .5 μM HKI or human VDAC-1 and 1 μM TNP-nucleotide. For each kind of experiment, the total concentration of added titrant did not exceed 5% of the initial volume of solution, and the total concentration of titrant was corrected for volume changes. The analysis of fluorescence data followed the approach of Fallar (59), modified as described in the Results section, using GraFit to perform nonlinear least squares fitting.

RESULTS

Mitochondria integrity and absence of native hexokinase— Cytochrome c oxidase activity indicated 90% integrity of OMM (data not shown). Uptake of carbocyanine dye JC-1 indicated intact IMM (data not shown). Western blotting of pig liver mitochondria and staining with polyclonal antibodies raised against HKI indicated the absence of native hexokinase (data not shown).

TNP-ADP inhibits HKI— Wild-type HKI (kcat = 73 ± 4 s^{-1}, Km Glc = 77 ± 6 μM, Km ATP = 1.1 ± 0.1μM) exhibited no measurable activity with TNPADP as a replacement substrate for ATP, placing an upper limit on kcat of 0.001 s^{-1}. TNP-ADP has no effect on the activity glucose 6-phosphate dehydrogenase (coupling enzyme) up to a concentration of 100 μM. On the other hand, TNP-ADP is a competitive inhibitor with respect to ATP (Ki = 4.9 ± 0.5 μM) (Fig.1).

TNP-nucleotide binding to Wild-type hexokinase I and displacement by ATP— The observed fluorescence from a mixture of TNP-ADP and HKI comes from free TNP-ADP, TNP-ADP bound to HKI, and HKI itself:

$$F_{obs} = F_{free} + F_{bound} + F_{protein} \quad (1)$$

$F_{protein}$ is small relative to other contributions as HKI has no native fluorophore sensitive to an excitation wavelength of 409 nm. $F_{free}=a + b[L] +c[L]^2$, where a, b, and c are determined by a fit of fluorescence versus [L] in the absence of protein under buffer conditions identical to those used in the titration of HKI. $F_{bound} = \gamma b(L_0 – [L])$, where γ is a fluorescence enhancement factor

of the bound relative to the free state of the fluorescent ligand and Lo and [L] are the total and free concentrations of fluorescent ligand.

A single binding-site model adequately accounts for the observed fluorescence of the bound state

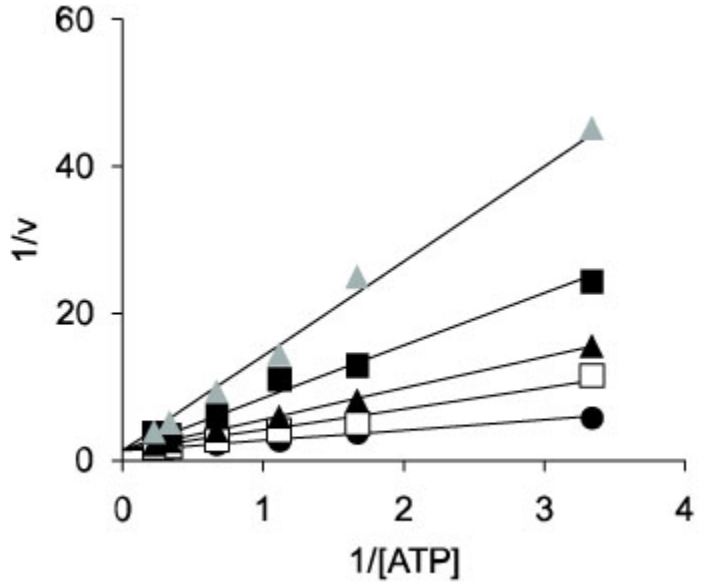

FIGURE 1. TNP-ADP and ATP binding to WTHKI. TNP-ADP inhibition of HKI competitive with ATP HKI activity was measured using the Glc-6-P dehydrogenase assay in 100 mM Tris, pH 8.0, glucose 1.6 mM, ATP 0.3-4.5 mM and TNP-ADP 0 μM (●), TNP-ADP 2.5 μM (□), TNP-ADP 10 μM (▲), TNP-ADP20 μM (■), and TNP-ADP 40 μM (▲).

and for the displacement of the TNP-nucleotide by a non-fluorescent nucleotide:

$$P + L = PL, \quad K_L = \frac{[P][L]}{[PL]}$$

$$P + A = PA, \quad K_A = \frac{[P][A]}{[PA]}$$

Scheme I

In Scheme I, L represents the TNP-nucleotide and A the displacing ligand. The equilibrium relationships of Scheme I with mass conservation relationships for L_0 (total fluorophore concentration), A_0 (total concentration of displacing ligand) and P_0 (total concentration of protein) leads to a third-order equation in the concentration of free protein [P]. For circumstances here, $K_A >> [P]$, allowing an approximation that reduces the third order equation to one of second order:

$$\left(1 + \frac{A_0}{K_A}\right) \times [P]^2 + \left(\frac{K_A - P_0 + A_0 K_L}{K_L + L_0}\right) \times [P]^2 - P_0 K_L = 0 \qquad (2)$$

The physical root of this quadratic relationship is the concentration of free protein, and determines the concentration of free fluorophore [L] = L_0K_L / (K_L + [P]) at a given total concentration of fluorophore, L_0. GraFit software optimizes the fit of the observed fluorescence to the right-hand side of Eq. 1 at fixed P_0 and varying Lo and Ao by adjusting parameters K_A, K_L, γ and Fprotein. TNP-ADP binds with high affinity to wild-type HKI (K_L = 2.8 ± 0.4 μM, γ = 6.0 ± 0.2, and $F_{protein}$ = 0.13 ± 0.03) and to mHKI (K_L = 5.2 ± 1.5 μM, γ = 3.2 ± 0.3, and $F_{protein}$ = 0.03 ± 0.01), however; it binds weakly to the N-domain of HKI (K_L , not available) (Fig. 2). ATP displaces TNP-ADP from wild-type hexokinase (K_A = 46 ± 6 μM) (Fig. 3) and mHK (KA = 97 ± 19 μM) (data not shown).

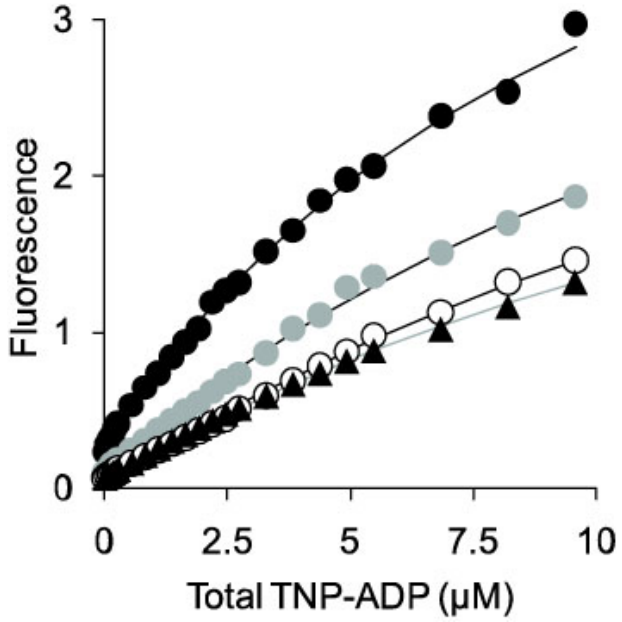

FIGURE 2. Titration of HKI constructs with TNP-ADP. Plots represent the fluorescence at varying total concentrations of TNP-ADP in 2 mM glucose, 10% PEG (MW ~10,000) and 50 mM Tris-HCl, pH 7.5, with no protein (▲), wild-type HKI 2.5 μM (○), mHKI 2.5 μM (●) and N-domain HKI 2.5 μM (●). Black lines for wild-type HKI, mHKI and N-domain HKI represent Eq. 1 with Ao of 0 μM, Po of 2.5 μM and parameters *K*L, *K*A, γ and Fprotein given in the Results section. The gray line is the fit of observed fluorescence in the absence of protein to the second-order polynomial, a + b(Lo) + c(Lo)2.

TNP-nucleotide binding to wild-type human VDAC-1 and displacement by nucleotides— Single binding site model of Scheme I also account for TNP-ADP binding to VDAC-1 and its displacement by ATP. Analog TNP-ADP binds to VDAC-1 with high affinity (K_L = 1.3 ± 0.1 μM, γ = 16.7 ± 0.3, $F_{protein}$ = 0.06 ± 0.02) (Fig. 4) and is displaced by ATP (K_A = 550 ± 40 μM)

(Fig. 5). CDP does not displace TNP-ADP from VDAC-1 (Fig. 6). Analogs TNP-ATP, TNP-AMP and TNP-CTP bind to VDAC-1 similarly to TNP-ADP (Table 1).

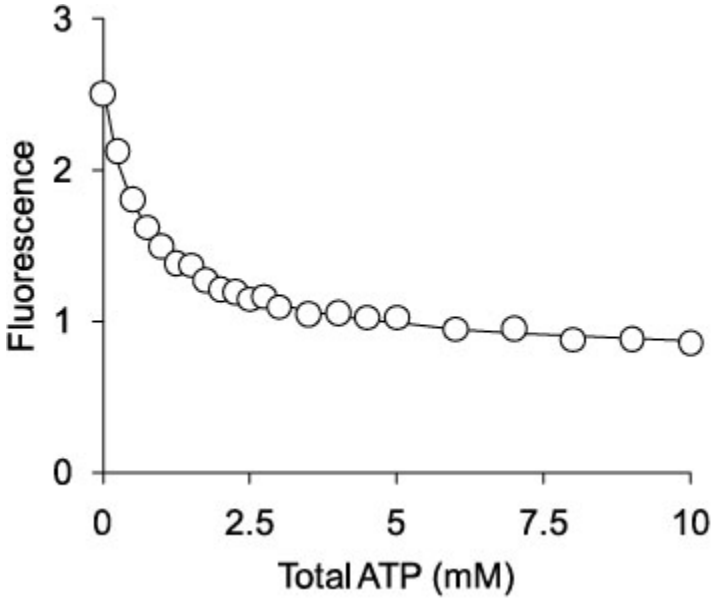

FIGURE 3. Titration of wild-type HKI bound TNP-ADP with ATP. Plot represents the fluorescence at varying total concentrations of ATP (○) added to 2.5 μM wild-type HKI and 5 μM TNP-ATP in 2mM glucose, 10% PEG (MW ~10,000) and 50 mM Tris pH 7.5. The solid line represents is a fitted curve using Eq. 1 with Lo of 5 μM, Po of 2.5 μM.

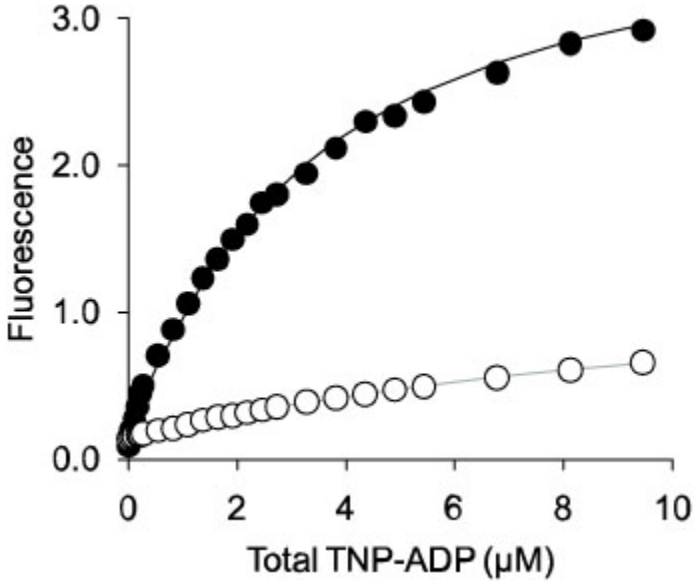

FIGURE 4. Titration of wild-type human VDAC-1 with TNP-ADP. Plots represent the fluorescence at varying total concentrations of TNP-ADP in 2 mM glucose and 50 mM Tris-HCl, pH 7.5, with no protein (○) or with wild-type human VDAC-1 2.0 μM (●). The black line represents Eq.1 with Po of 2 μM, Ao of 0 μM and parameters *K*L, *K*A, γ and Fprotein given in the Results section. The gray line is the fit of observed fluorescence in the absence of protein to the second-order polynomial, $a + b(\mathrm{Lo}) + c(\mathrm{Lo})2$.

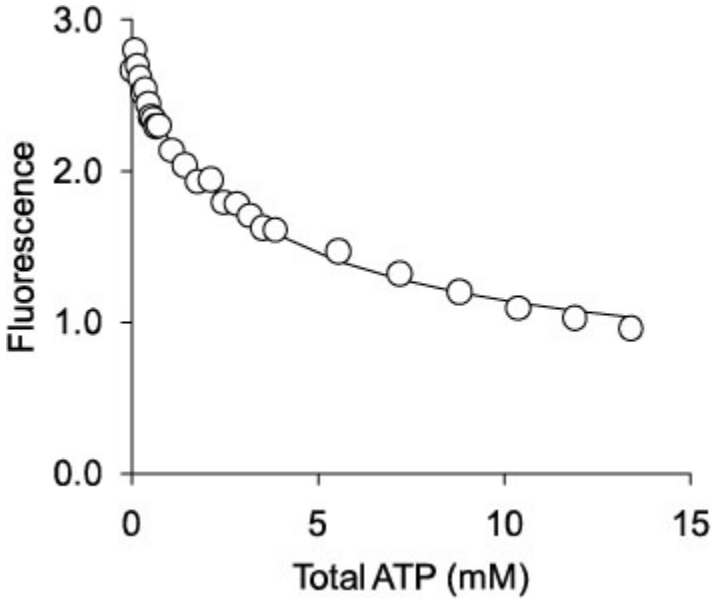

FIGURE 5. Titration of wild-type human VDAC-1 bound TNP-ADP with ATP. Plot represents the fluorescence at varying total concentrations of ATP (○) added to 2.0 μM wild-type human VDAC-1 and 5 μM TNP-ATP in 2mM glucose and 50 mM Tris, pH 7.5. The black line represents Eq. 1 with Po of 2 μM, Lo of 5 μM.

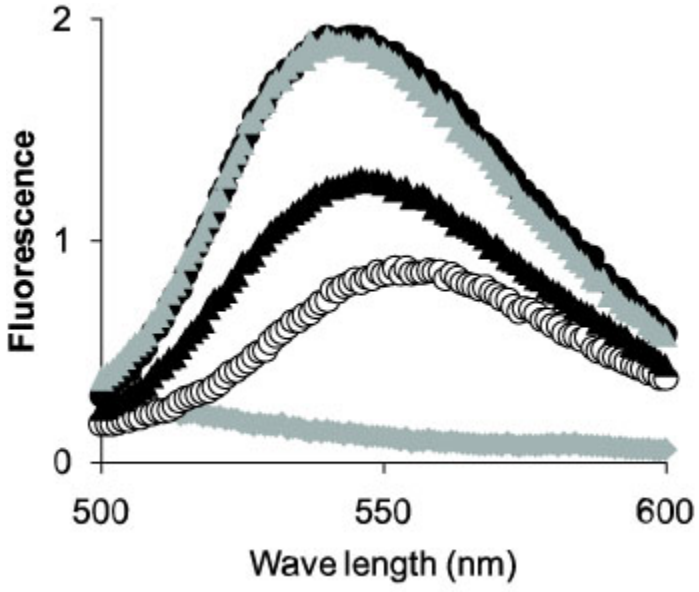

FIGURE 6. Human VDAC-1 bound TNP-ADP displacement by nucleotides. Fluorescence scans of 2.0 μM human VDAC-1 in 2mM glucose and 50 mM Tris, pH 7.5. human VDAC-1 only (○) , 5μM ANP-ADP only (○), human VDAC-1 plus 5 μM TNP-ADP (●), human VDAC-1 plus 5 μM TNP-ADP and 10mM ATP (▲), and human VDAC-1 plus 5 μM TNP-ADP and 10 mM CDP (▲).

TABLE 1. TNP-nucleotides binding to wild-type human VDAC-1.

TNP-nucleotide	K_L (μM)	γ	$F_{protein}$
TNP-ATP	0.5 (2)	16.4 (9)	0.40 (9)
TNP-ADP	1.3 (1)	16.7 (3)	0.06 (2)
TNP-AMP	2.0 (1)	20.4 (3)	0.13 (2)
TNP-CTP	0.7 (1)	11.2 (3)	0.22 (2)

Parameters are from a single binding site model. KL, γ and Fprotein are constants for the dissociation of TNP-nucleotides from human VDAC-1. Fluorescence was measured at varying total concentrations of TNP-nucleotides in 2 mM glucose and 50 mM Tris-HCl, pH 7.5. Standard deviations in the last significant digits are given in parentheses.

Nucleotide release of wild-type HKI— Incubation times of twenty and sixty minutes produced identical release curves, indicating an equilibrium phenomenon. Scheme II represents the simplest equilibrium model that accounts for ATP release of wild-type and mutant enzymes from mitochondria.

$$E + Q = EQ, \quad K_1 = \frac{[EQ]}{[E][Q]}$$
$$E + P = EP, \quad K_2 = \frac{[EP]}{[E][P]}$$
$$Q + A = QA, \quad K_3 = \frac{[QA]}{[Q][A]}$$

Scheme II

In Scheme II, K1 and K2 represent association constants for the binding of HKI (represented by E) to specific mitochondrial binding sites Q, and nonspecifically to the membrane at sites P. The association constant K3 represents the binding of A competitively with E for the specific binding sites Q. The fraction of E bound to mitochondria depends explicitly on the concentrations of Q and P, and implicitly on the concentration of A as follows:

$$R([A]) = \frac{K_1[Q]+K_2[P]}{1+K_1[Q]+K_2[P]} = \frac{(K_1[Q]+K'_2)}{1+K_1[Q]+K'_2} \qquad (3)$$

The concentration of free nonspecific binding sites for hexokinase is overwhelmingly large allowing a pseudo constant K'_2 to approximate the product $K_2[P]$. The concentration of free specific mitochondrial sites Q is itself a function of the concentrations of enzyme and competitive binding ligand. Algebraic manipulation of the equilibrium expression in Scheme II

and relationships for mass conservation of total enzyme E_0 and total specific sites Qo results in a quadratic relationship in Q:

$$a[Q]^2 + b[Q] + c = 0$$

where $a = K_1(1 + K_3[A])$, $b = K_1(E_0 - Q_0) + (1 + K'_2)(1 + K_3[A])$, and $c = -Q_0(1 + K'_2)$. The general solution to the quadratic equation gives [Q]:

$$[Q] = \frac{-K_1(E_0-Q_0)-(1+K'_2)(1+K_3[A])+\sqrt{K_1^2(E_0-Q_0)+2K_1(E_0-Q_0)(1+K'_2)(1+K_3[A])+(1+K'_2)^2(1+K_3[A])^2+4K_1(1+K_3[A])Q_0(1+K'_2)}}{2K_1(1+K_3[A])}$$

(4)

Substitution of Eq. 4 into Eq. 3 provides a relationship for the fraction of enzyme bound to the mitochondria R([A]), explicitly as a function of [A].

The fitting relationship is:

$$V = sR[A] \quad (5)$$

where s is a proportionality constant that relates the fraction of bound enzyme R([A]) to velocity V in μmoles/min. Eq. 5 includes undefined quantities s, E_0, Q_0, K_1, K'_2 and K_3; all six cannot be determined by a nonlinear least squares fit of data from a single experiment. Hence, values for some of these quantities must come from other determinations. Firstly, one assumes the HKI-VDAC complex has an equal number of HKI and VDAC subunits. The value for Q_o (7.1×10^{-8} M) then is an estimate based on 42,000 VDAC molecules per mitochondrion (60), 7.2×10^9 mitochondria per 1 mg of total mitochondrial protein (61), and 0.014 mg of mitochondria in each 100 μL assay. In binding HKI to mitochondria, the concentration of enzyme (10^{-6} M) is 10-fold greater than the estimated concentration of specific binding sites. After washing away excess enzyme, we assume all specific sites have bound enzyme, and that the condition $E_0=Q_0$ applies to the system. The release of HKI is complete at the highest levels of nucleotide, $R([A]\rightarrow\infty) = 0$, which requires $K'_2 = 0$. Moreover, s = Qo × (specific activity) × (assay volume), where the specific activity for HKI is 6×10^9 μmole/min^{-1} mole-1 and the assay volume is liters. Hence, if the assumption of a 1:1 ratio of the HKI-VDAC complex is correct, then data can be fit to Eq. 5 using K_1 and K_3 alone as adjustable parameters. Moreover, as K_1 represents the binding affinity of HKI for the mitochondrion, all experiments using wild-type HKI should provide comparable values for K_1 regardless of the release agent. Listed in Table 2 are values for K_1 and K_3 for 8 release experiments involving ATP and ADP. Although correlations in K_1 and K_3 are evident,

one finds values of K_1 within a single order with an average value of $4.1 \pm 1.0 \times 10^8\ M^{-1}$. In release experiments involving the HKI activity assay, K_1 is set to its average value, and only K_3 is optimized in fitting the data. The true uncertainty in K_3 then is on par with that for the average value of K_1; however, on a comparative basis the K_3 values in Table 3 accurately reflect the relative binding efficacies of nucleotides to VDAC. Characteristic release curves are in Fig. 7. All TNP-nucleotides tested were effective in the release of wild-type HKI from mitochondria.

TABLE 2. ATP and ADP release of wild-type HKI from pig liver mitochondria in the determination of *K*1.

	K_1 (M^{-1})	K_3^{ATP} (M^{-1})	K_3^{ADP} (M^{-1})
Experiment 1	6.0×10^8 (1.2×10^8)	5.2×10^4 (1.7×10^4)	-
Experiment 2	5.1×10^8 (7.8×10^7)	4.9×10^4 (8.9×10^3)	-
Experiment 3	6.6×10^8 (2.4×10^8)	1.5×10^4 (6.1×10^4)	-
Experiment 4	8.1×10^8 (3.3×10^8)	1.7×10^5 (7.7×10^4)	
Experiment 5	1.3×10^8 (1.5×10^7)	3.6×10^4 (6.7×10^3)	
Experiment 6	1.2×10^8 (1.3×10^7)	3.7×10^4 (6.6×10^3)	
Experiment 7	2.7×10^8 (6.9×10^7)	-	9.6×10^3 (3.7×10^3)
Experiment 8	2.1×10^8 (4.4×10^7)	-	8.5×10^3 (2.6×10^3)

Parameters are from an equilibrium model in which the binding of nucleotide and WHKI and nucleotide to the mitochondrion is mutually exclusive. K1, K_3^{ATP} and K_3^{ADP} are constants for the association in M^{-1} of HKI, ATP and ADP from the mitochondrion. Mitochondria with HKI bound in 250mM sucrose and 50 mM HEPES, pH7.5, were exposed to different nucleotides for 30 minutes. Remaining mitochondria bound HKI was measured by activity. Standard deviations in the last significant digits are given in parentheses.

TABLE 3. Release of wild-type HKI from pig liver mitochondria by TNP-nucleotides.

TNP-nucleotide	K_3 (M^{-1})
ATP	9.9×10^4 (3.0×10^3)
ADP	1.8×10^4 (3.5×10^3)
TNP-ATP	2.7×10^5 (2.7×10^4)
TNP-ADP	3.7×10^5 (5.2×10^4)
TNP-AMP	3.1×10^5 (5.2×10^4)
TNP-CTP	1.9×10^5 (4.8×10^4)

Parameters are defined in the Results section and by Scheme II. *K*1 is set to its average value of $4.1x10^8\ M^{-1}$ and K_3 determined by fitting Eq. 5 to data as described in the Results section. Standard deviations in the last significant digit are given in parentheses

Nucleotide induced release of N-domain HKI from mitochondria— Validation of the ELISA assay is provided by Fig. 8. Release of wild-type HKI, determined as a percent of total release, is measured comparably by the ELISA and the HKI activity assays. Measures of nucleotide affinity constants come from the fitting data to Eq. 5. The parameter s, however, is difficult to determine, requiring the optical path length of a plate reader, and the assumption of one to one

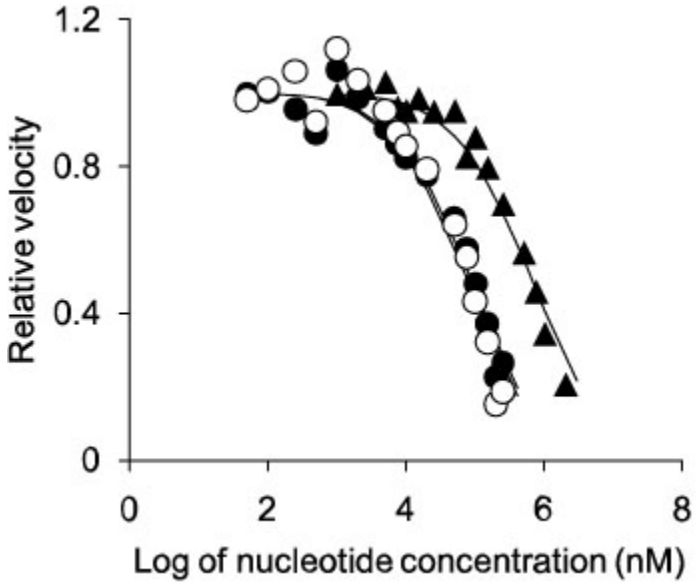

FIGURE 7. Nucleotide-induced release of wild-type HKI from pig liver mitochondria. Mitochondria with HKI bound in 250 mM sucrose and 50 mM HEPES, pH 7.5, were exposed to different nucleotides for 30 minutes. Plots represent relative velocities from mitochondria-bound HKI that remains after exposure to varying concentrations of ATP (▲), TNP-ATP (○), or TNP-ADP (●). The solid lines represent fitted curves using Eq. 5 with parameters given in Table 3.

correspondences between the hexokinase construct, primary antibody, and secondary antibody/peroxidase components. Moreover, nonzero background levels in the presence of high concentrations of nucleotide require a nonzero K'_2. Hence, fitting of data from ELISA assays employs s, K'_2 and K_3 as parameters. TNP-ADP and ATP release wild-type HKI and N-domain HKI from mitochondria to a comparable extent (Fig. 8), and provide values for K3 that compare favorably to those of the determined from the HKI assays (Table 4).

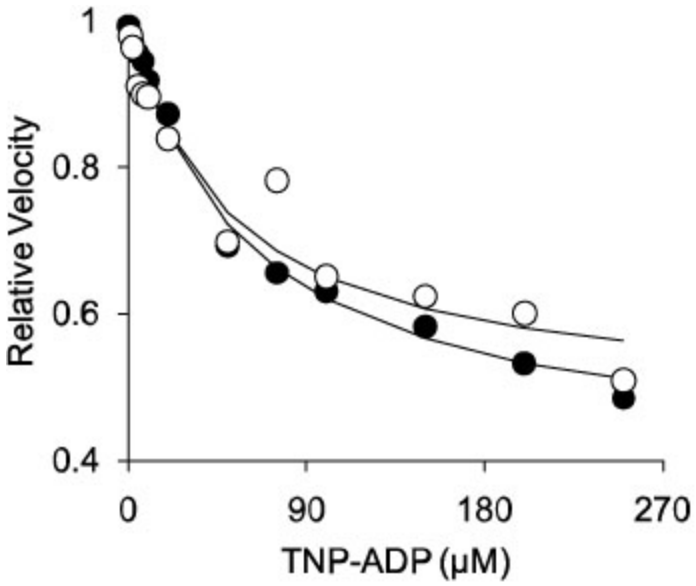

FIGURE 8. Nucleotides induced release of wild-type HKI and N-domain HKI from pig liver mitochondria measured by kinetic ELISA. Mitochondria with HKI bound in 250 mM sucrose and 50 mM HEPES, pH 7.5, were exposed to different nucleotides for 30 minutes. Plots represent wild-type HKI (●) or N-domain HKI (○) that remains bound to mitochondria as measured by His-Tag antibodies and ELISA. The solid lines represent fitted curves using Eq. 5 with parameters given in Table 4.

TABLE 4. Nucleotide-dependent release of HKI constructs from pig-liver mitochondria.

HKI Construct	Nucleotide	s (μmol/min)	K_2' (M^{-1})	K_3 (M^{-1})
Wild-type[a]	ATP	0.0213*	0**	3.1×10^4 (2.9×10^3)
	TNP-ADP	0.0213*	0**	2.3×10^5 (6.8×10^4)
Wild-type[b]	ATP	0.098 (3)	0.14 (3)	1.3×10^4 (8.2×10^3)
	TNP-ADP	0.110 (1)	0.24 (1)	1.8×10^5 (3.8×10^4)
N-domain[b]	ATP	0.190 (2)	0.44 (2)	2.8×10^4 (5.9×10^3)
	TNP-ADP	0.069 (1)	0.73 (2)	1.3×10^5 (4.1×10^4)

Parameters are defined in the Results section and by Scheme II. K_1 is set to its average value $4.1x10^8$ M^{-1} and *s*, *K2'* and *K3* determined by fitting to Eq.5 to data as described in the Results section. Mitochondria with HKI bound in 250 mM sucrose and 50 mM HEPES, pH 7.5, were exposed to different nucleotides for 30 minutes. Remaining mitochondria bound HKI was measured by activity and/or ELISA. Standard deviations in the last significant digit are in parentheses.

[a]Measured by HKI activity

[b]Measured by His-tag antibodies and kinetic-ELISA

* Calculated as described in the Results section

** Fixed at zero as described in the Results section

DISCUSSION

Previous reports demonstrated the release of HKI from mitochondria by ATP and other nucleotides at millimolar concentrations (16, 45-47). The importance of the hexokinase mitochondrion interaction to apoptosis motivated our efforts to quantify and determine the mechanism of nucleotide release of HKI from mitochondria. Four general mechanisms can account for ATP-release of HKI from mitochondria (Fig. 9): ATP binds to the C-terminal domain of HKI causing release. ATP and HKI bind with mutual exclusion to human VDAC-1. ATP binds to the N-terminal domain of HKI causing release. HKI converts ATP and glucose to Glc-6-P, which in turn binds to the N-terminal half of HKI triggering release.

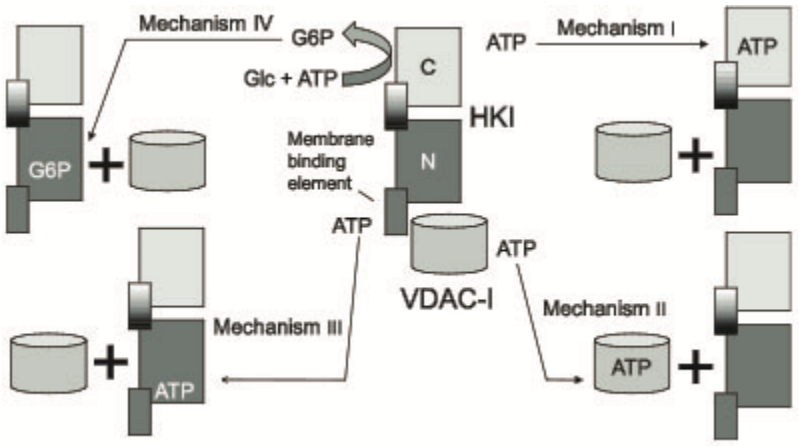

FIGURE 9. Four mechanisms by which ATP could release HKI from mitochondria. VDAC-1 (cylinder) HKI (rectangles) interact directly. ATP binds to HKI, C-terminal half, (Mechanism I), to VDAC (Mechanism II), or to HKI, N-terminal half (Mechanism III) to disrupt the HKI-VDAC-1 complex. HKI produces glucose 6-phosphate from ATP, which in turn binds to N-terminal half of HKI (Mechanism VI) to disrupt the HKI-VDAC-1 complex.

The experimental protocols adopted here avoid the combination of glucose and ATP, which in the presence of Mg^{2+} and HKI would result in the generation of Glc-6-P. TNP-nucleotides are not substrates for HKI (current study) or for yeast hexokinase (62). TNP-ADP binds to HKI and yeast hexokinase at micromolar concentrations and is displaced by ATP. In the absence of Mg^{2+} both TNP-ADP and ATP release HKI from mitochondria. Under such conditions, the evolution of Glc-6-P from ATP and glucose is an unlikely cause for ATP release, and cannot be the mechanism by which TNP-ADP releases HKI from the mitochondrion (Mechanism IV).

A test of Mechanisms II and III requires an assay for N-domain HKI, which has no hexokinase activity. Data of Fig. 10 validate the kinetic ELISA assay to measure levels of N-domain HKI bound to mitochondria. The kinetic ELISA measures the HKI construct in any state (active or inactive), whereas the HKI activity assay measures only HKI in an active state. The presence of substantial peroxidase activity in the presence of high levels of nucleotide indicates residual HKI bound to the mitochondrion. This bound fraction of HKI must not be active, as it would be detected by the HKI activity assay. Blank samples (mitochondria not exposed to an HKI construct) in the ELISA assay have low peroxidase activity, consistent with Western blots which indicate no bound HKI on the surface of the pig-liver mitochondria. Released HKI, as a fraction of total released HKI, is nonetheless in excellent agreement for the two assay methods (Fig. 10).

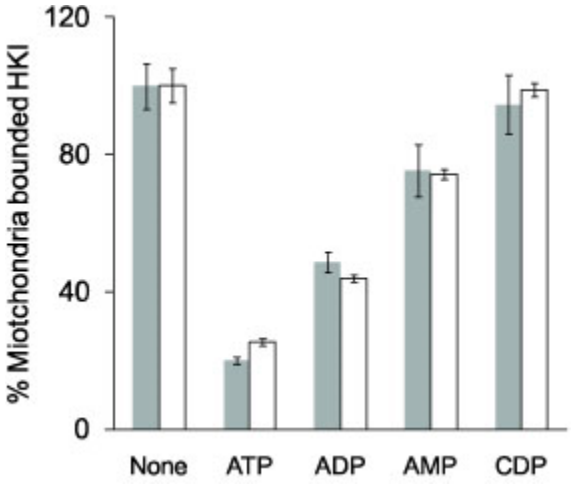

FIGURE 10. Nucleotide release of wild-type HKI and N-domain HKI from pig liver mitochondria. Plots represent wild-type HKI (■) remained bound to mitochondria and measured by activity and N-domain HKI (□) remained bound to mitochondria and measured by His-tag antibodies and ELISA.

Release of HKI and N-domain HKI are indistinguishable by the kinetic ELISA assay (Fig. 8). Evidently, the C-terminal half of HKI plays no significant role in the binding of HKI to the mitochondrion. Indeed, other evidence is consistent with this view. Polyclonal antibodies directed to the C-terminal half of HKI do not release HKI from mitochondria, whereas antibodies directed toward the N-terminal half of HKI cause release (63). Mutations to the Glc-6-P binding site at the N-terminal half greatly diminish release of HKI by Glc-6-P, but mutation to the Glc-6-P site at the C-terminal half has little effect on release (44). The indistinguishable release of HKI

and N-domain-HKI but ATP and TNP-ADP is inconsistent with Mechanism I, which attributes release to nucleotide association with the C-terminal half of HKI.

A single-site binding model accounts for TNPADP association with HKI. That binding site is not part of the N-terminal half, as TNP-ADP binds weakly to N-domain HKI. Potent competitive inhibitor of TNP-ADP with respect to ATP is consistent with a high-affinity site at or near the active site of the C-terminal half. TNP-ADP does not bind to N-domain HKI and yet releases N-domain HKI from mitochondria, observations clearly inconsistent with Mechanism III.

Although it is relatively straightforward to exclude mechanisms of release, to actually prove the remaining mechanism (Mechanism IV) requires the accumulation of overwhelming experimental evidence. The approach here is to demonstrate correlations between nucleotide release of HKI from mitochondria and high affinity binding to human VDAC-1. In fact if Mechanism IV is correct, newly-discovered agents that bind to human VDAC-1 competitively with respect to TNP-ADP should also release HKI from mitochondria. The TNP-nucleotides (TNP-ATP, TNP-ADP, TNP-AMP, and TNP-CTP) bind to human VDAC-1 with high affinity (Table 1), and each is effective in the release of HKI from the mitochondrion (Table 3). The affinity of TNP-nucleotides to the mitochondrion, as measure by the release experiments (K3) and by fluorescence titrations (KL) are in reasonable agreement. Moreover, CDP does not displace TNP-ADP from human VDAC-1, and is not effective as a release agent (Figs. 6 and 10). These findings are consistent with Mechanism IV. If the target protein is not VDAC, then it must be another protein of equal abundance, able to bind TNP-nucleotides with similar high affinities, but not CDP. As VDAC is reportedly the most abundant protein in the outer leaflet, another protein with these attributes seems a remote possibility.

One should note, however, an apparent discrepancy within the body of data presented here. Firstly, 1/K3 for ATP release of HKI is ~5x10-5 M, whereas KA for ATP measured by fluorescence is ~5x10-4 M. The basis for this difference is unclear. Mg^{2+} is necessary for the association of HKI with mitochondria, and quite possibly ATP releases HKI not only through its interaction with VDAC, but also by chelation of Mg^{2+}. ATP and ADP, however, are nearly equal in efficacy of HKI release. Moreover, release of HKI by TNP-nucleotides show no dependence on the number of phosphoryl groups, release efficacies and binding affinities being linked to the trinitrophenol functionality. Although TNP-ADP does not bind to the N-terminal half of HKI,

one cannot rule-out a release effect due to the binding of ATP (or ADP) to the N-terminal half. Mutations of residues at the ATP binding site of the N-terminal half, however, seem not to influence ATP release (Skaff, Honzatko, and Fromm, unpublished). ATP could bind to an additional site on VDAC which does not exclude the binding of TNP-ADP. An azido photo-affinity label modifies VDAC at three positions that could map to distinct sites (50).

Although the focus here is on a mechanism of release, one can glean some basic understanding of the subunit stoichiometries in the HKI-VDAC-1 complex. Firstly, the ratio of HKI to VDAC must be at least one to one. If HKI is present at ratios less than unity with VDAC, then the observed reaction velocities in the absence of release agent are unachievable. A ratio of 1:2 HKI to VDAC requires a doubling of the estimated number of VDAC molecules in the mitochondrion. HKI forms dimers (15, 48), and at least one report in the literature indicates a subunit tetramer of mitochondrion-bound hexokinase (64). An assumption of 4:1 HKI to VDAC for release data presented here decrease K1 by 20-fold (~107 M^{-1}) and K3 by 4-fold, but the relative values of K3 remain unchanged. Hence, the affinity constants presented here are fairly insensitive to radical departures from the assumed 1:1 subunit ratio of the HKI-VDAC complex. Disruption of the hexokinase-mitochondrion association is the intention of potential anti-cancer drugs (66). Hexokinases I&II are often overexpressed in cancer cell lines, presumably to block pro-apoptotic signals which act through the release of cytochrome c from the mitochondrion. Remove hexokinase from the mitochondrion, and cancer cell succumb to apoptosis or have heightened sensitivity to existing treatments for cancer. Small molecules such as clotrimazole, bifonazole (67), 3-bromopyruvate (68) and methyl jasmonate (69) dissociate hexokinase from the mitochondrion. In most cases, the mechanism of release has not been determined, as has been here for the TNP-nucleotides and for Glc-6-P (44). VDAC evidently is a target for small molecules that release mitochondrion-bound hexokinase. As the trinitrophenol group seems critical to binding affinity and not the phosphoryl groups or nucleotide base, one has a reasonable expectation of finding a molecule of high specificity and within the parameters that define substances of potential pharmacological value.

Multimers of mitochondrion-bond HKI, to the extent that they form, must not involve interactions of C-terminal halves to be consistent with observations here. In fact, the simplest structural model consistent with release data is complex involving the N-terminal half of HKI with VDAC. Using the X-ray structure of mouse VDAC-1 (65), the N-terminal hydrophobic tail

of HKI most likely interacts with lipid and the external surface of the VDAC β-barrel. TNP-ADP, however, is highly anionic, having at pH 7.5 formal charges on the phosphoryl and nitro groups. The most probably binding site for this anion is somewhere at the inner surface of the VDAC barrel, which is lined with positively charged side chains. The model here is one of completion between TNP-ADP and HKI for VDAC, and leaves two possibilities: Either the binding of TNP-ADP cause such significant conformational change in VDAC as to disrupt interactions involving the N-terminal resides of HKI or another set of surfaces residues of the N-terminal half of HKI are essential to the stability of the HKI-VDAC complex.

REFFERENCES

1. Katzen, H M; Schimke, R T. (1965) Proc. Natl. Acad. Sci. U S A 54, 1218-25.
2. Lowry, O H; Passonneau, J V. (1964) J. Biol. Chem. 239, 31-42.
3. Wilson, J E. (1980) Curr. Top. Cell. Regul. 16, 1-54.
4. Crane, R K; Sols, A. (1954) J. Biol. Chem. 210, 597-606.
5. Rose, I A; Warms, J V; O'Connell. (1964) Biochem. Biophys. Res. Commun. 15, 33-7.
6. Ellison, W R; Lueck, J D; Fromm, H J. (1975) J. Biol. Chem. 250, 1864-71.
7. Wilson, J E. (1995) Rev. Physiol. Biochem. Pharmacol. 26, 65-198.
8. Wilson, J E. (2003) J. Exp. Biol. 206, 2049-57.
9. Schwab, D A; Wilson, J E. (1989) Proc Natl Acad Sci U S A 86, 2563-2567.
10. Ardehali, H; Yano, Y; Printz, R L; Koch, S; Whitesell, R R; May, J M; Granner, D K. (1996) J. Biol. Chem. 271, 1849-52.
11. White, T K; Wilson, J E. (1989) Arch. Biochem. Biophys. 274, 375-93.
12. Fang, T Y; Alechina, O; Aleshin, A E; Fromm, H J; Honzatko, R B. (1998) J. Biol. Chem. 273, 19548-53.
13. Liu, X; Kim, C S; Kurbanov, F T; Honzatko, R B; Fromm, H J. (1999) J. Biol. Chem. 274, 31155-9.
14. Tsai, H J; Wilson, J E. (1995) Arch. Biochem. Biophys. 316, 206-14.
15. Aleshin, A E; Zeng, C; Bartunik, H D; Fromm, H J; Honzatko, R B. (1998) J. Mol. Biol. 282, 345-57.
16. Rose, I A; Warms, J V. (1967) J. Biol. Chem. 242, 1635-45.
17. Xie, G C; Wilson, J E. (1988) Arch. Biochem. Biophys. 267, 803-10.

18. Lindén, M; Gellerfors, P; Nelson, B D. (1982) FEBS Lett. 141, 189-92.

19. Fiek, C; Benz, R; Roos, N; Brdiczka, D. (1982) Biochim. Biophys. Acta. 688, 429-40.

20. Azoulay-Zohar, H; Israelson, A; Abu-Hamad, S; Shoshan-Barmatz, V. (2004) Biochem. J. 377, 347-55.

21. Beutner, G; Ruck, A; Riede, B; Welte, W; Brdiczka, D. (1996) FEBS Lett. 396, 189-95.

22. Beutner, G; Rück, A; Riede, B; Brdiczka, D. (1997) Biochem. Soc. Trans. 25, 151-7.

23. Vyssokikh, M Y; Brdiczka, D. (2003) Acta. Biochim. Pol. 50, 389-404.

24. Vyssokikh, M Y; Goncharova, N Y; Zhuravlyova, A V; Zorova, L D; Kirichenko, W; Krasnikov, B F; Kuzminova, A E; Melikov, K C; Melik-Nubarov, N S; Samsonov, A V; Belousov, W; Prischepova, A E; Zorov, D B. (1999) Biochemistry (Mosc). 64, 390-8.

25. Machida, K; Ohta, Y; Osada, H. (2006) J. Biol. Chem. 281, 14314-20.

26. Zoratti, M; Szabò, I. (1995) Biochim. Biophys. Acta. 1241, 139-76.

27. Crompton, M; Virji, S; Doyle, V; Johnson, N; Ward, J M. (1999) Biochem. Soc. Symp. 66, 167-79.

28. Zamzami, N; Kroemer, G. (2003) Curr. Biol. 13, R71-3.

29. Lemasters, J J; Qian, T; Bradham, C A; Brenner, D A; Cascio, W E; Trost, L C; Nishimura, Y; Nieminen, A L; Herman, B. (1999) J. Bioenerg. Biomembr. 31, 305-19.

30. Shimizu, S; Narita, M; Tsujimoto, Y. (2000) Nature 399, 483-87.

31. Shimizu, S; Matsuoka, Y; Shinohara, Y; Yoneda, Y; Tsujimoto, Y. (2001) J. Cell Biol. 152, 237-50.

32. Pastorino, J G; Shulga, N; Hoek, J B. (2002) J. Biol. Chem. 277, 7610-8.

33. Majewski, N; Nogueira, V; Bhaskar, P; Coy, P E; Skeen, J E; Gottlob, K; Chandel, N S; Thompson, C B; Robey, R B; Hay, N. (2004) Mol. Cell 16, 819-30.

34. Majewski, N; Nogueira, V; Robey, R B; Hay, N. (2004) Mol. Cell. Biol. 24, 730-40.

35. Shimizu, S; Ide, T; Yanagida, T; Tsujimoto, Y. (2000) J. Biol. Chem. 275, 12321-5.

36. Zaid, H; Abu-Hamad, S; Israelson, A; Nathan, I; Shoshan-Barmatz, V. (2005) Cell Death Differ. 12, 751-60.

37. Abu-Hamad, S; Sivan, S; Shoshan-Barmatz, V. (2006) Proc. Natl. Acad. Sci. U S A 103, 5787-92.

38. Robey, R B; Hay, N. (2005) Cell Cycle 4, 654-8.

39. Neumann, D; Bückers, J; Kastrup, L; Hell, S W; Jakobs, S. (2010) PMC Biophys. 3, 1-15.

40. Perevoshchikova, I V; Zorov, S D; Kotova, E A; Zorov, D B; Antonenko, Y N. (2010) FEBS Lett. 584, 2397-402.

41. Abu-Hamad, S; Arbel, N; Calo, D; Arzoine, L; Israelson, A; Keinan, N; Ben-Romano, R; Friedman, O;Shoshan-Barmatz, V. (2009) J. Cell Sci. 122, 1906-16.

42. Arzoine, L; Zilberberg, N; Ben-Romano, R; Shoshan-Barmatz, V. (2009) J. Biol. Chem. 284, 3946-55.

43. Shoshan-Barmatz, V; Zakar, M; Rosenthal, K; Abu-Hamad, S. (2009) Biochim. Biophys. Acta. 1787, 421-30.

44. Skaff, D A; Kim, C S; Tsai, H J; Honzatko, R B; Fromm, H J. (2005) J. Biol. Chem. 280, 38403-9.

45. Wilson, J E. (1968) J. Biol. Chem. 243, 3640-7.

46. Hochman, M S; Shimada, Y; Sacktor, B. (1974) J. Neurochem. 23, 861-3.

47. Bustamante, E; Pedersen, P L. (1980) Biochemistry, 19, 4972-7.

48. Aleshin, A E; Kirby, C; Liu, X; Bourenkov, G P; Bartunik, H D; Fromm, H J; Honzatko, R B. (2000) J. Mol. Biol. 296, 1001-15.

49. Rosano, C; Sabini, E; M, Rizzi; Deriu, D; Murshudov, G; Bianchi, M; Serafini, G; M, Magnani; Bolognesi, M. (1999) Structure 7, 1427-37.

50. Yehezkel, G; Hadad, N; Zaid, H; Sivan, S; Shoshan-Barmatz, V. (2006) J. Biol. Chem. 281, 5938-46.

51. Yehezkel, G; Abu-Hamad, S; Shoshan-Barmatz, V. 2007, J. Cell. Physiol. 212, 551-61.

52. Graham, J M. (1993) Methods Mol. Biol. 19, 29-40.

53. Wojtczak, L; Zaluska, H; Wroniszewska, A; Wojtczak, A B. (1972) Acta. Biochim. Pol. 19, 227-34.

54. Rice, J E; Lindsay, J G. (1997) in Subcellular Fractionation, A Practical Approach (Graham J M; Rickwood, D, ed) pp 107-142, Oxford University Press, New York, NY.

55. Bradford, M M. (1976) Anal. Biochem. 72, 248-54.

56. Leatherbarrow, R J. (2001) GraFit, Version 5, Erithacus Software Ltd., Horley, UK

57. Towbin, H; Staehelin, T; Gordon, J. (1979) Proc. Natl. Acad. Sci. U S A. 76, 4350–4.

58. Engelhardt, H; Meins, T; Poynor, M; Adams, V; Nussberger, S; Welte, W; Zeth, K. (2007) J. Membrane Biol. 216, 93-105.

59. Fallar, L D. (1990) Biochemistry 29, 3179-86.

60. Aleshin, A E; Fromm, H J; Honzatko, R B. (1998) FEBS Lett. 434, 42-6.

61. Estabrook, R W; Holowinsky A. (1961) J. Biophys. Biochem. Cytol. 9, 19-28.

62. Arora, K K; Shenbagamurthi, P; Fanciulli, M; Pedersen, P L. (1990) J. Biol. Chem. 265, 5324-8.

63. Smith, A D; Wilson, J E. (1991) Arch. Biochem. Biophys. 287, 359-66

64. Xie, G and Wilson, J E. (1990) Arch. Biochem. Biophys. 276, 285-93

65. Ujwal, R; Cascio, D; Colletier, J P; Faham, S; Zhang, J; Toro, L; Ping, P; Abramson, J. (2008) Proc. Natl. Acad. Sci. USA 105, 17742-7

66. Mathupala, S P, Ko; Y H; Pedersen, P L. (2006) Oncogene 25, 4777-86.

67. Penso, J; Beitner, R. (1998) Eur. J. Pharmacol. 342, 113-7.

68. Kim, W; Yoon, J H; Jeong, M; Cheon, G J; Lee, T S; Yang, J I; Park, S C; Lee, H S. (2007) Mol. Cancer Ther. 6, 2554-62.

69. Cohen, S; Flescher, E. (2009) Phytochemistry 70, 1600-9.

CHAPTER3: RESIDUES OF THE VOLTAGE DEPENDENT ANION CHANNEL (VDAC) CRITICAL FOR THE BINDING OF ATP

A paper to be submitted to the Journal of Biological Chemistry

Muneaki Watanabe[4] and Richard B. Honzatko[1,5]

From the Roy J. Carver Department of Biochemistry, Biophysics and Molecular Biology

Iowa State University, Ames, IA 50011

Running title: ATP binding to hVDAC-1

Keywords: VDAC; mitochondria; ATP; TNP-ATP; fluorescence

Background: Human VDAC-1 (hVDAC-1), the most abundant protein of the outer mitochondrial membrane, allows passage of ATP and ADP in/out of the mitochondrion.
Results: The mutation of 15 lysine residues in the pore of hVDAC-1, generally reduced the binding affinity of ATP and TNP-AMP to hVDAC-1 by comparable levels ranging from 5- to 20-fold; however, K256M impacts the binding affinity of ATP and TNP-AMP by more than 100-fold, whereas mutations of Lys61 and Lys113 have little, if any, effect.
Conclusion: The side chains of most lysines in the pore contribute to the binding of ATP and TNP-AMP. The role of Lys256 seems by comparison critical to high-affinity binding, whereas lysines 61 and 113 seem unimportant.
Significance: Lys256 is the first determinant of hVDAC-1linked to the high-affinity binding of ATP.

ABSTRACT

Hexokinase I (HKI) blocks the conducting state of the Voltage Dependent Anion Channel (VDAC) and blocks the formation of a permeability transition pore (PTP) associated with the release of cytochrome *c* from mitochondria during apoptosis. Metabolites of respiration (for instance, ATP and glucose 6-phosphate), as well as a fluorescent analog of ATP analog, TNP-ATP, release HKI from the mitochondrion. Putatively, the site of ATP-binding in the release of HKI from mitochondria lies somewhere on VDAC, however, no firm evidence maps a high-affinity binding of ATP to a specific site. Presented here is evidence for the binding of TNP-AMP (K_d~1 μM) to a single site on isoform Type-1 of human VDAC (hereafter hVDAC-1). ATP displaces TNP-AMP from hVDAC-1 binding with high-affinity (K_d~10 μM). The individual

[4] Graduate student and professor, respectively, Department of Biochemistry, Biophysics and Molecular Biology, Iowa State University.
[5] To whom correspondence should be addressed.

mutations of 15 lysine residues located in the pore of hVDAC-1 reduces ATP and TNP-AMP binding affinities comparably by 5- to 20-fold; however, K256M reduces ATP and TNP-AMP affinities by 100-fold whereas K51M and K113M have little or no effect. The results clearly establish a high-affinity binding site for ATP on hVDAC-1, and establish the side-chain of Lys256 as a critical determinant in ATP binding.

INTRODUCTION

VDAC regulates the energy balance of mitochondria and the entire cell by modulating the passage of metabolites between the organelle and cytoplasm (1-9). Silencing VDAC1 expression inhibits cell growth through a reduction in energy production (10). Endogenous VDAC1 expression in transformed cells, suppressed by 70-90% using shRNA methodology, greatly impacts cell growth, reduced ATP synthesis by five-fold and decreased cellular levels of ATP and ADP by 50% (10).

The pore diameter of a VDAC monomer is about 36 Å (measured from diametrically opposed Cα atoms), sufficiently large to pass most metabolites (such as ATP and ADP) but not large enough to pass proteins such as cytochrome *c*. The VDAC pore has many positively charged residues that should favor the entry of anions, and an N-terminal helix that partially blocks the pore (19, 20). Hence, the structural attributes of a mechanism to control the permeability of the outer mitochondrial membrane (OMM) is an integral part of VDAC.

Regulation of OMM permeability, however, involves more than VDAC. Hexokinase Type I (HKI) and Hexokinase Type II (HKII) bind at high levels to the outer mitochondrial membrane, but not to vesicle or plasmid membranes. The abundance of bound HKI and/or HKII and the specificity of binding to the mitochondrion are consistent with an interaction between VDAC (the most abundant protein in the OMM) and HKI and/or HKII (11-16). In patch clamp studies, the addition of HKI abolishes ion conductance through VDAC (21). Moreover, HKII is overexpressed in cancer cells (by as much as 10-fold), presumably as an anti-apoptotic strategy (13). An overabundance of HKII covers the mitochondrion and blocks the formation of the permeability transition pore that leads to mitochondrial death. But if HKI and/or HKII remain bound to the OMM at all times, blocking anion conductance through VDAC, then how do adenine nucleotides exchange between the cytosol and mitochondrion? A mechanism must exist to modulate the interactions of HKI (and HKII) with the mitochondrial OMM, allowing at least

transitory passage of ATP and ADP. One possible player in the transitory release of HKI (and perhaps HKII) from the mitochondrial membrane is glucose 6-phosphate (G6P), which binds with high affinity to the N-terminal half of HKI and releases mitochondrion-bound enzyme (22-25). ATP (and ADP) may be also play a role, as both are effective in the release of HKI from the mitochondrion (Chapter 2, this thesis).

Although several studies have shown ATP binding to VDAC (17, 18), crystallographic and NMR studies of VDAC did not reveal an ATP binding site (19, 20). Given that VDAC allows the passage of ATP/ADP to supply the energy needs of the cell and to regenerate ATP from ADP, the presence of a binding site for adenine nucleotides on VDAC is not an unreasonable expectation.

Our approach here assumes the existence of an adenine nucleotide binding site somewhere on the interior surface of the VDAC pore, and that a subset of lysine side chains facilitate ATP/ADP binding and transport. The fluorescent analogs TNP-ATP, -ADP, -AMP and -CTP all bind to human VDAC-1 (hereafter hVDAC-1) with high affinity; however, ATP displaces TNP-AMP revealing a site with high affinity for ATP. Mutation of 15 lysine residues in the pore to methionine, reveals Lys256 as a significant determinant in the high-affinity binding of ATP. The affinity of ATP for this site (dissociation constant of ~10 μM) approximately matches the concentration of ATP necessary to release 50% of HKI from the mitochondrial membrane (Chapter 2, this thesis).

EXPERIMENTAL PROCEDURES

Materials— ATP, ADP, AMP, deoxyribonuclease (DNase I), protease cocktail inhibitor and phenylmethylsultonyl fluoride came from Sigma. Kanamycin sulfate and 2’3’-O-(2,4,6-trinitrophenyl)-derivatives of ATP were came from Invitrogen. 2’3’-O-(2,4,6-trinitrophenyl)-derivatives of ADP, AMP, CTP came from Jena Bioscience. Nickel-nitrilotriacetic acid-agarose (NiNTA) was from Novagen. Isopropyl-1-thio-β-D-galactopyranoside (IPTG) and Lauryldimethylamine-N-oxide (LADO) were from Anatrace. Oligonucleotides came from the Iowa IDT. Other materials came from Fisher Scientific.

Cloning of Wild-type human VDAC-1 and mutant VDAC-1— A plasmid with the coding sequence of human VDAC-1 (hVDAC-1) was purchased from Open Biosystems. NdeI and SacI cut sites were created in the plasmid using the polymerase chain reaction (PCR) and NdeI primer

5'CGCGGCAGCCATATGATGGCTGTGCCACCCACG3' and SacI primer 5'GGACTGGAATTTCAAGCA TCGAGCTCCGTCGACAAGC3'. The PCR product and vector pET-24a were digested by NdeI and SacI restriction enzymes. After separation on agarose gel, the DNA fragment for hVDAC-1 was ligated to pET-24a. Mutagenesis of conserved amino acids at the putative interior pore of hVDAC1 was acquired by PCR site-directed mutagenesis method. The interior lysine resides are located at residue numbers 28, 32, 61, 74, 96, 113, 115, 119, 174, 197, 224, 236, 256, and 274. These resides were changed to methionine. The construction of each mutant employed designed primers as follows: for K28M, 5'-GCTATGGATTTGGCTTAATAATGCTTGATTTG-3' (forward) and 5'-CAAATCAAGCATTATTAAGCCAAATCCATAGC-3' (reverse); for K32M, 5'-TAATAAAGCTTGATTTGATGACAAAATCTGAG- 3' (forward) and 5'-CTCAGATTTTGTCATCAAATCAAGCTTTATTA-3' (reverse); for K61M, 5'-GGGCAGTCTGGAAACCATGTACAGATGGACTG-3' (forward) and 5'-CAGTCCATCTGTACATGGTTTCCAGACTGCCC-3' (reverse); for K74M, 5'-CGGCCTGACGTTTACAGAGATGTGGAATACCG-3' (forward) and 5'-CGGTATTCCACATCTCTGTAAACGTCAGGCCG-3' (reverse); for K96M, 5'-CAGCTTGCACGTGGACTGATGCTGACCTTCGA-3' (forward) and 5'-TCGAAGGTCAGCATCAGTCCACGTGCAAGCTG-3' (reverse); for K113M, 5'-CTGGGAAAAAAAATGCTATGATCAAGACAGGG-3' (forward) and 5'-CCCTGTCTTGATCATAGCATTTTTTTTCCCAG-3' (reverse); for K115M, 5'-GCTAAAATCATGACAGGGTACAAGCGGGAGCA-3' (forward) and 5'-TGCTCCCGCTTGTACCCTGTCATGATTTTAGC-3' (reverse); for K119M, 5'-CAAGACAGGGTACATGCGGGAGCACATTAACC-3' (forward) and 5'-GGTTAATGTGCTCCCGCATGTACCCTGTCTTG-3' (reverse); for K174M, 5'-GCAGTTGGCTACATGACTGATGAATTCCAGCT -3' (forward) and 5'-AGCTGGAATTCATCAGTCATGTAGCCAACTGC -3' (reverse); for K197M, 5'-GGCGGCTCCATTTACCAGATGGTGAACAAGAA-3' (forward) and 5'-TTCTTGTTCACCATCTGGTAAATGGAGCCGCC-3' (reverse); for K224M, 5'-GCGCTTCGGAATAGCAGCCATGTATCAGATTG-3' (forward) and 5'-CAATCTGATACATGGCTGCTATTCCGAAGCGC-3' (reverse); for K236M, 5'-CTGCTTCTCGGCTATGGTGAACAACTCCAGCC-3' (forward) and 5'-

GGCTGGAGTTGTTCACCATAGCCGAGAAGCAG-3’ (reverse); for K256M, 5’-CTAAAGCCAGGTATTATGCTGACACTGTCAGC-3’ (forward) and 5’-GCTGACAGTGTCAGCATAATACCTGGCTTTAG-3’ (reverse); for K274M, 5’-CAATGCTGGTGGCCACATGCTTGGTCTAGGAC-3’ (forward) and 5’-GTCCTAGACCAAGCATGTGGCCACCAGCATTG-3’ (reverse). The N-terminal helix of hVDAC-1 was truncated by restriction enzyme digestion and ligation method introducing an additional NdeI cut site between residues 20 and 21. This site was introduced by PCR using 5’-TTCACCAAGCATATGGGCTATGGATTTGGCTTA-3’ (forward) and 5’-TAAGCCAAATCCATAGCCCATATGCTTGGTGAA-3’ (reverse). All the constructs were confirmed by the DNA sequencing facility at Iowa State University.

Expression and purification of hVDAC-1— hVDAC-1 purification and folding follows protocols in the literature (18, 26) with modifications. hVDAC-1 containing plasmid was transformed into *E. coli* strain BL21 (DE3). Cells were grown in LB media at 37 °C, kanamycin was added to a final concentration of (30 μg/mL). Growth was monitored by absorbance at wavelength 600 nm. At A600 of 0.9, the temperature was reduced to16 °C and IPTG was added to a final concentration of 0.3 mM. Cells were collected after 16-20 hours of induction and suspended in lysis buffer (30 mM Tris-HCl, pH8.0, 150 mM NaCl, 1mM EDTA, and 1mM DTT). DNase (50 μg/mL), leupeptin (5 μg /mL), and PMSF (1 mM) were all added to the solution. Cells were lysed by sonication. Inclusion bodies were pelleted at 16,0000 rpm for 1 hr. Pelleted inclusion bodies were subjected to the following procedures three times: separation from the supernatant fraction, suspension in wash buffer (30 mM Tris-HCl, pH 8.0, 150 mM NaCl, 1 mM EDTA, 1 mM DTT) and centrifugation at 15,000 rpm for 30 minutes. Inclusion bodies were suspended in 30 mL of wash buffer plus 1% Triton X-100, incubated for 45 minutes at 37 °C, and then suspended and washed twice with wash buffer. Washed inclusion bodies were solubilized in 10 mL dissolving buffer (6 M guanidine hydrochloride, 10 mM DTT, 0.1 mM EDTA, 100 mM Tris-HCl, pH8.0). Inclusion bodies dissolved completely in 12 hr. at 4 °C. About 20 mL of unfolded solubilized hVDAC-1 were added dropwise into 300 mL of refolding buffer (0.1 mM EDTA, 1 mM DTT, 100 mM Tris-HCl, pH8.0, 2% LDAO) at 4 °C to reduce concentration of guanidine hydrochloride around 0.4~0.8 M. Refolded protein was concentrated and dialyzed against 50 mM Tris-HCl. pH 7.5, 0.1% LDAO buffer for 24 hrs. at 4 °C. Solution was loaded onto a nickel-nitrilo triacetic acid (Ni^{2+}-NTA) column. The column was washed with

buffers containing 50 mM Tris-HCl, pH7.5, 300 mM NaCl, 0.1% LDAO and 5 mM imidazole and then 50 mM imidazole. Finally, hVDAC-1 was eluted with the same buffer containing 300 mM imidazole.

Conformational analysis of VDAC-1 mutants—Far-UV circular dichroism spectroscopy was used to verify similar folds for wild-type and mutant hVDAC-1. Spectra were recoded from 260-190 nm with 1 nm increments. Secondary structure was estimated from the wild-type spectrum by DichroWeb, provided by Prof. B. A. Wallace at the University of London. Spectra were collected for mutants to confirm unperturbed secondary structure relative to the wild-type protein.

hVDAC-1 fluorescence experiments— Purified hVDAC-1 were dialyzed against 2 mM glucose and 50 mM Tris-HCl, pH 7.5. Fluorescence measurements were made at room temperature using a 1-cm^2 quartz cuvette on a SLM Amico 8000 fluorimeter. For TNP-nucleotides the excitation wavelength was 409 nm, and emission scans were from 450 to 600 nm. An excitation wavelength of 295 nm was chosen to avoid exciting tyrosyl side chains for tryptophan fluorescence experiments. Emission spectra were recoded from 310 to 400 nm. Fluorescence scans (a total of three for each datum) were performed after additions of small volumes of TNP-nucleotide to 2 mL of 2.5 μM hVDAC-1. TNP-nucleotide displacement was accomplished by the addition of the alternative nucleotide to 1 mL solution of 2.5 μM hVDAC-1 and 1-μM TNP-nucleotide. For each kind of experiment, the total concentration of added titrant did not exceed 5% of the initial volume of solution, and the total concentration of titrant was corrected for volume changes. The analysis of fluorescence data followed the approach of Fallar (59), modified as described in the Results section, using GraFit to perform nonlinear least squares fitting.

RESULTS

Validation of mutant hVDAC-1 — Circular dichroism spectra where taken of wild-type (Fig.1) and 14 methionine mutants. The wild type spectrum indicated 16% of all residues as α-helix and 81% β-strand (Table 1). These numbers compare favorably to those determined from the crystal structure of VDAC. The spectra of all methionine mutants matched that of wild-type hVDAC-1.

TABLE 1. Wild-type hVDAC-1 analysis by Dichroweb (Lee Whitmore and B. A. Wallace).

	Helix1	Helix2	Strand1	Strand2	Turns	Unordered	Total
wt-hVDAC-1	0.000	0.157	0.117	0.694	0.008	0.024	1.000

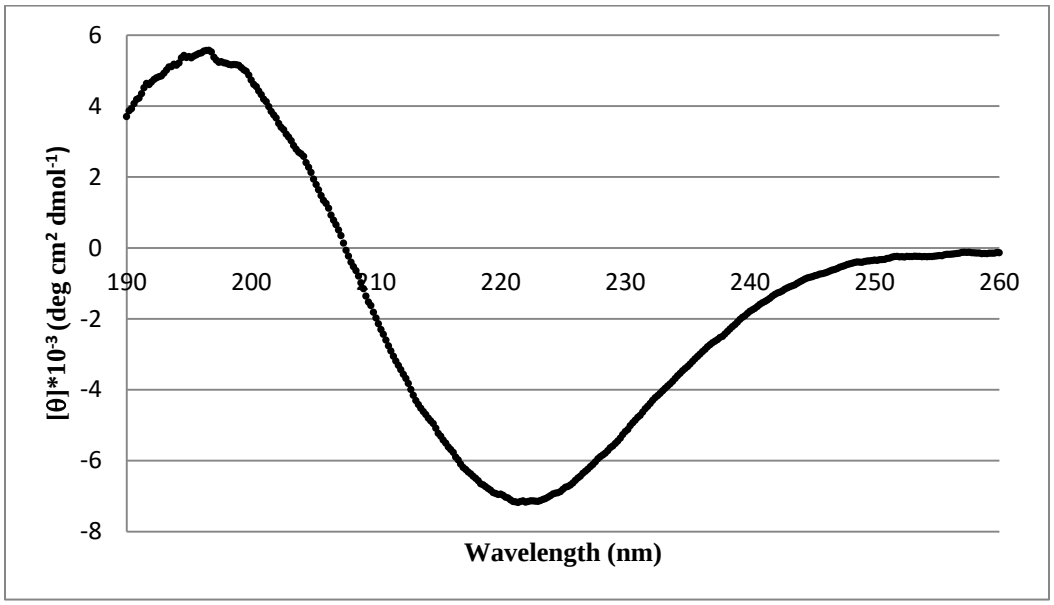

FIGURE 1. CD spectrum of wild type hVDAC-1.

TNP-nucleotides binding to wild-type hVDAC-1— The experiment employed the same method as previously described (Chapter 2, this thesis). The observed fluorescence comes from free TNP-nucleotides, TNP-nucleotides bound to hVDAC-1, and hVDAC-1 itself: $F_{\text{obs}} = F_{\text{free}} + F_{\text{bound}} + F_{\text{scatter}}$. The term F_{scatter} accounts for all intensity not directly from the fluorophore TNP-ATP. The principle contribution to F_{scatter} is the protein, and as the concentration of protein is fixed and has no fluorophore subject to excitation at 409 nm, F_{scatter} has a small constant value. $F_{free} = a + b[L] - c[L]^2$, where *a*, *b*, and *c* are determined by a fit of fluorescence versus free concentrations of fluorescent ligand *[L]* in the absence of protein under buffer conditions identical to those used in the titration of hVDAC-1. $F_{bound} = \gamma b(L_o - [L])$, where γ is a fluorescence enhancement factor of the bound relative to the free state of the fluorescent ligand and L_o is the total concentrations of fluorescent ligand. The value for *[L]* above goes into the relationship for F_{obs}: $F_{obs} = a + b[L] - c[L]^2 + \gamma b(L_o - [L]) + F_{scatter}$ (Eqn. 1). The derivation of this equation assumes one site per protein molecule, but it also has a simple solution if there are *N* identical, independent sites per protein molecule (Chapter 2, this thesis). Mass conservation

relations for total protein $P_o = [P] + [PL]$ and total ligand $L_o = [L] + [PL]$, when combined results in a quadratic equation in free ligand concentration $[L]$, the positive root of which represents $[L]$ in terms of L_o, P_o and an equilibrium dissociation constant $K_L = [P]*[L] / [PL]$. Substitution of the positive root into Eqn. 1 gives F_{obs} as a function of $F_{scatter}$, P_o, L_o and adjustable parameters K_L and γ. GraFit software optimizes the fit of the observed fluorescence at fixed *P*o and varying *L*o by adjusting parameters K_L and γ. Analog TNP-ATP binds to hVDAC-1 with high affinity ($K_L = 0.5 \pm 0.2$ μM, $\gamma = 16.4 \pm 0.9$, $F_{scatter} = 0.5 \pm 0.08$) (Fig. 2). Analogs TNP-ADP, TNP-AMP and TNP-CTP bind to hVDAC-1 similarly to TNP-ATP (Table 2). Picric acid, the TNP fluorophore exhibits no binding.

Although the single-site model generally accounts for observed fluorescence, the observed fluorescence for the TNP-ATP titration departs systematically from the fitted curve for a single-site model. One possible explanation for the departure is the presence of an additional binding site for TNP-ATP. Other analytical models were attempted (two independent binding sites, two populations of VDAC); however, the improvement of the goodness of fit did not justify the increase in the number of adjustable parameters of more complex models. Results in the next section, however, are consistent with multiple binding sites for TNP-ATP. On the other hand, a single-site model accounts for the observed fluorescence from the titration of hVDAC-1 by TNP-AMP.

TABLE2. TNP-nucleotides and picric acid binding to wild-type hVDAC-1. Parameters are from a single binding site model. K_L, γ and $F_{scatter}$ are constants for the dissociation of substrates from hVDAC-1. Fluorescence was measured at varying total concentrations of ligands in 2 mM glucose and 50 mM Tris-HCl, pH 7.5. Standard deviations in the last significant digits are given in parentheses.

Ligand	K_L(μM)	γ	$F_{scatter}$
TNP-ATP	0.5 (2)	16.4 (9)	0.45 (8)
TNP-ADP	1.2 (2)	21.4 (8)	0.06 (2)
TNP-AMP	2.0 (1)	20.4 (3)	0.13 (2)
TNP-CTP	0.7 (1)	11.2 (3)	0.22 (2)

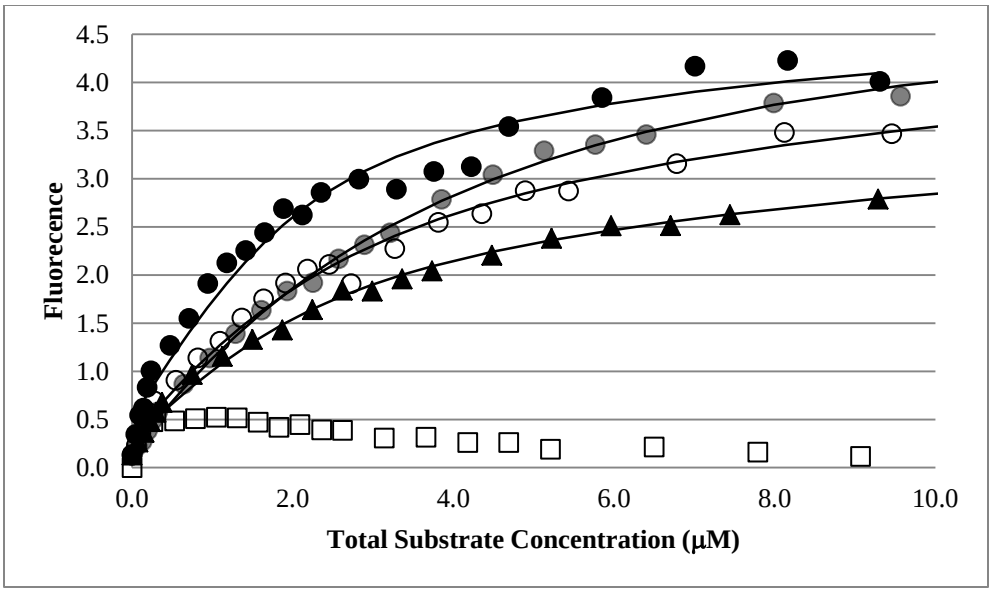

FIGURE 2. Titration of wild-type hVDAC-1 with fluorescent ligands. Plots represent fluorescence at varying total concentrations of ligand in 2 mM glucose and 50 mM Tris-HCl, pH 7.5, with 2.0 μM wild-type hVDAC-1 and 1-μM TNP-nucleotide. TNP-ATP (●), TNP-ADP (○), TNP-AMP (●), TNP-CTP (▲) and picric acid (□).

Displacement of TNP-nucleotides by ATP— As before, the observed fluorescence is given by Eqn. 1; however, F_{obs} must be cast as a function of total ligand concentration A_o used in displacement titration of the bound fluorophore. Mass conservation and equilibrium relationships are as follows: $L_o = [L] + [PL]$, $A_o = [A] + [PA]$, $P_o = [P] + [PA] + [PL]$, $K_L = [P]*[L] / [PL]$, and $K_A = [P]*[A] / [PA]$. The equilibrium relationships and mass conservation relations for L_o and A_o can be used to rewrite mass conservation relationship for protein as $P_o = [P] + [P]*A_o / (K_A + [P]) + [P]*L_o / (K_L + [P])$. Assuming $[P] << K_A$ one obtains a quadratic in $[P]$, the positive root of which can be substituted into Eqn.1 to give F_{obs} as a function of $F_{scatter}$, P_o, A_o, L_o, K_A, K_L and γ. Using values from Table 1 for K_L, and experimentally determined values for P_o, A_o and L_o, curve fitting employed $F_{scatter}$, K_A and γ.

ATP released each of the TNP-nucleotides (Fig. 3) with the following values for K_A: for TNP-ATP, K_A = 1100 ± 300 μM; for TNP-ADP, K_A = 550 ± 40 μM; for TNP-AMP, K_A = 14 ± 1 μM and for TNP-CTP, K_A = 210 ± 20 μM. If each TNP-nucleotide binds to the same site on hVDAC-1, then K_A (representing the dissociation constant of ATP from its binding site on hVDAC-1) should be the same. Clearly, this is not the case. ATP interacts relatively weakly ($<K_A>$~600 μM) at sites occupied by TNP-ATP, TNP-ADP and TNP-CTP. In contrast, ATP binds strongly (K_A~10 μM) to the site occupied by TNP-AMP. Given the good agreement

between the single-site model and titration binding curve for TNP-AMP (Fig. 1), and given the likelihood of a high-affinity binding site for ATP by its displacement of TNP-AMP, further analysis of mutant forms of hVDAC-1 employs TNP-AMP as a fluorescence probe.

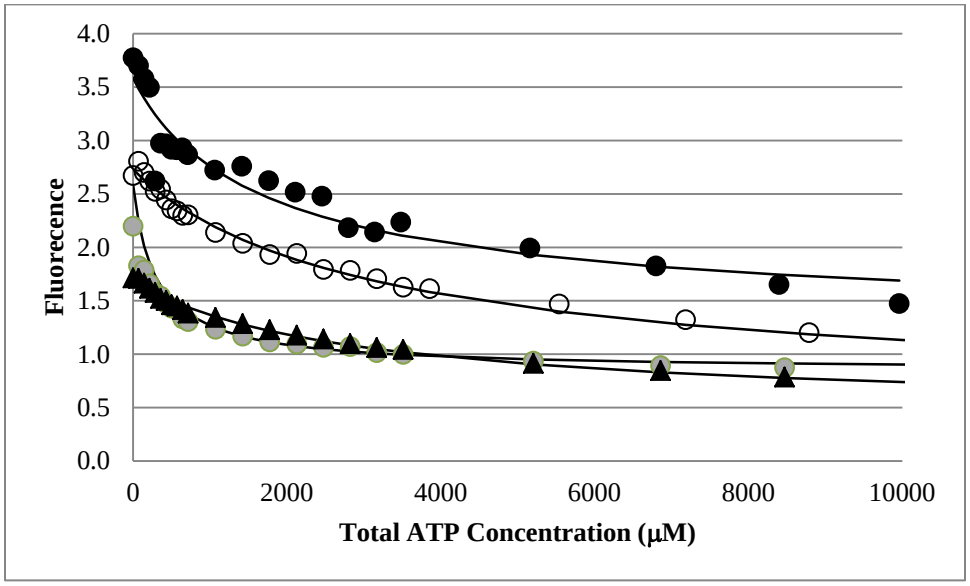

FIGURE 3. ATP titrations of wild-type hVDAC-1 ligated with TNP-nucleotides. Plot represents the fluorescence at varying total concentrations of ATP in 2 mM glucose and 50 mM Tris-HCl, pH 7.5, with 2.0 μM wild-type hVDAC-1 and 1-μM TNP-nucleotide. TNP-ATP (●), TNP-ADP (○), TNP-AMP (●), TNP-CTP (▲)

TNP-AMP binding to mutants of hVDAC-1— ATP displacement of bound TNP-AMP probed the effects of mutations on ATP binding to hVDAC-1. This approach requires a determination of binding affinity of TNP-AMP to each mutant form of hVDAC-1 first in order to determine the binding affinity of ATP. Fluorescence titrations and subsequent fitting followed the procedure above for wild-type hVDAC-1. The results are in Table 3, and the K_L for TNP-AMP relative to that of wild-type hVDAC-1 appears in Fig. 4. N-terminal helix-truncated hVDAC-1 was also tested for TNP-AMP binding affinity exhibiting a 10-fold reduction relative to wild-type hVDAC-1 (K_L = 6 ± 1 μM, γ = 4.4 ± 0.4, $F_{scatter}$ = 0.06 ± 0.01).

TNP-AMP displacements by ATP— Displacement of TNP-AMP by ATP measures the binding affinity of the high-affinity site for ATP. The displacement titration and analysis of observed fluorescence follows the protocol above in previous displacement titrations using ATP. Results are in Table 4. ATP-displacement of TNP-AMP from N-terminal helix-truncated hVDAC-1 produced a K_A = 430 ± 3 μM with γ = 4.0 ± 0.1 and $F_{scatter}$ = 0.10 ± 0.01).

TABLE 3. TNP-AMP binding to different constructs of hVDAC-1. Parameters K_L, γ and $F_{scatter}$ are from a single-site binding model, where K_L is the dissociation constant for TNP-AMP from its protein-ligand complex, γ is the fluorescence enhancement factor and $F_{scatter}$ represents background radiation. Fluorescence was measured at varying total concentrations of TNP-AMP in 2 mM glucose and 50 mM Tris-HCl, pH 7.5. Standard deviation in the last significant digit is given in parentheses.

	K_L (μM)	γ	$F_{scatter}$
WT	0.5 (1)	5.1 (1)	0.09 (1)
K28M	3.6 (6)	5.9 (3)	0.07 (1)
K32M	2.5 (4)	3.0 (1)	0.05 (5)
K61M	0.8 (2)	3.3 (1)	0.06 (9)
K74M	3.0 (1)	3.9 (3)	0.07 (1)
K96M	8.0 (1)	8.2 (5)	0.09 (8)
K113M	0.3 (1)	4.0 (1)	0.08 (1)
K115M	3.8 (6)	5.2 (3)	0.06 (9)
K119M	1.9 (4)	4.3 (2)	0.08 (1)
K174M	2.9 (5)	4.4 (2)	0.08 (9)
K197M	3.0 (1)	6.2 (7)	0.04 (3)
K224M	4.1 (9)	4.8 (3)	0.07 (1)
K236M	2.9 (5)	4.4 (2)	0.08 (9)
K256M	40 (30)	10 (6)	0.06 (5)
K274M	7.0 (2)	4.4 (7)	0.05 (1)

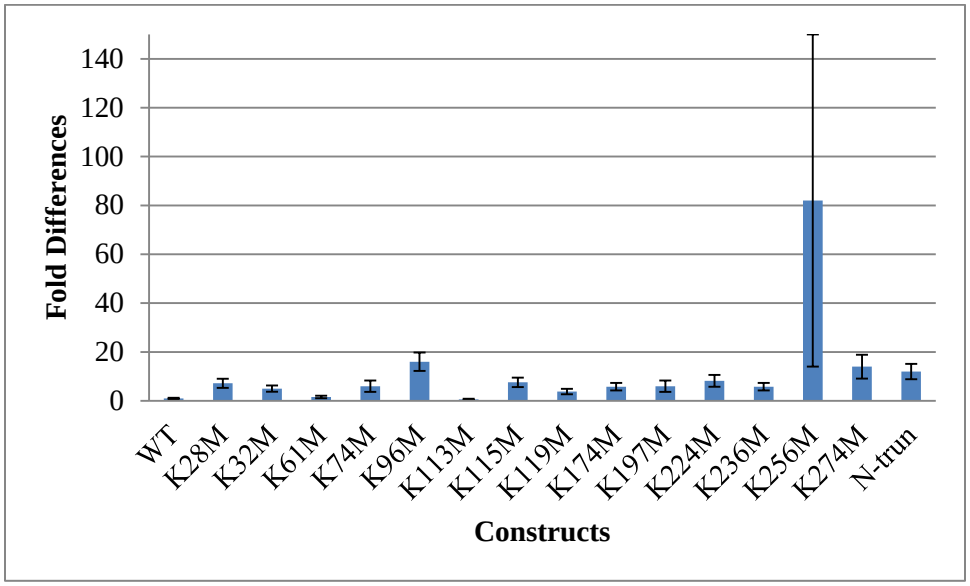

FIGURE 4. Change in binding affinity of TNP-AMP for mutant relative to wild-type hVDAC-1. The height of each bar indicates the ratio of K_L-mutant/K_L-wildtype. K61M and K113M had essentially no effect on TNP-AMP binding, whereas K256M weakened binding by 80-fold. Error bars are one sigma-(A/B) = SQRT[$(1/B)^2$*(sigma-A)^2 + $(A/B^2)^2$*(sigma-B)^2], where A and B are values for K_L-mutant and K_L-wildtype, respectively. Uncertainty in the parameters for K256M is high simply because the K_L is far above the limiting concentration of 14 μM for TNP-AMP titrations.

TABLE 4. TNP-AMP displacement by ATP for constructs of hVDAC-1. Parameters are from a single binding-site model. K_A, γ and $F_{scatter}$ are constants for the displacement of TNP-AMP by ATP from hVDAC-1. Fluorescence was measured at varying total concentrations of ATP in 2 mM glucose and 50 mM Tris-HCl, pH 7.5, with 2.0 μM wild-type hVDAC-1 and 1-μM TNP-AMP. Standard deviation in the last significant digits is given in parentheses.

Construct	K_A [μM]	γ	$F_{scatter}$
WT	14 (1)	9.0 (2)	0.23 (2)
K28M	210 (20)	6.7 (2)	0.19 (2)
K32M	180 (20)	3.8 (1)	0.10 (1)
K61M	35 (4)	5.5 (2)	0.19 (1)
K74M	480 (50)	7.5 (2)	0.18 (2)
K96M	340 (60)	4.9 (2)	0.10 (3)
K113M	36 (7)	5.3 (2)	0.14 (3)
K115M	500 (60)	5.4 (1)	0.16 (2)
K119M	160 (30)	4.7 (2)	0.15 (2)
K174M	300 (40)	8.1 (2)	0.25 (3)
K197M	290 (30)	5.6 (1)	0.22 (1)
K224M	160 (20)	4.9 (1)	0.25 (1)
K236M	140 (20)	6.6 (2)	0.33 (2)
K256M	900 (100)	7.4 (3)	0.21 (1)
K274M	660 (70)	6.4 (2)	0.27 (1)

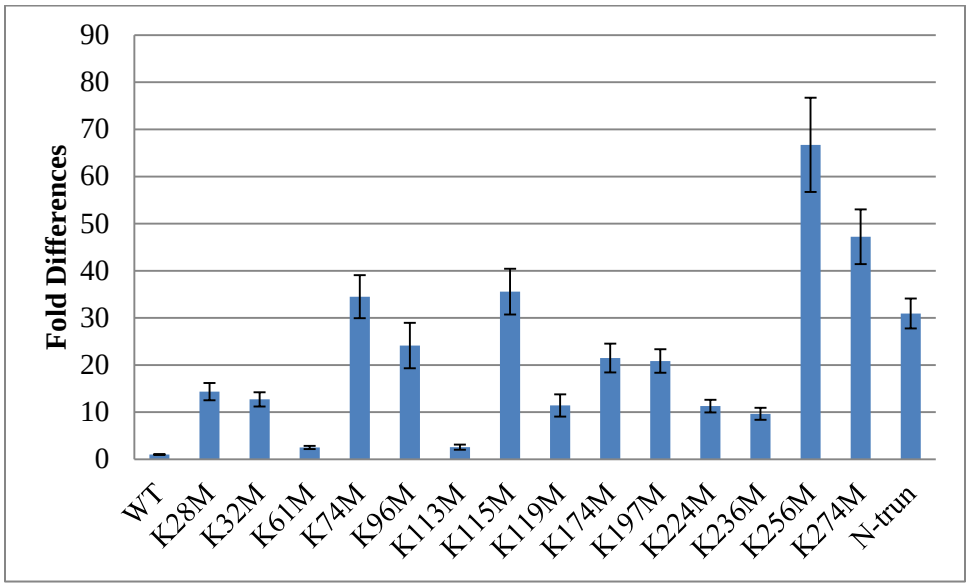

FIGURE 5. Change in binding affinity of ATP for mutant relative to wild-type hVDAC-1. The height of each bar indicates the ratio of K_A-mutant/K_A-wildtype. K61M and K113M had essentially no effect on ATP binding (consistent with the absence of an effect on TNP-AMP binding affinity), whereas K256M weakened binding by at more than 10-fold. Error bars are one sigma-(A/B) = SQRT[$(1/B)^2$*$(\text{sigma-A})^2$ + $(A/B^2)^2$*$(\text{sigma-B})^2$], where A and B are values for K_A-mutant and K_A-wildtype, respectively.

Effect of TNP-ATP on tryptophan fluorescence of wild-type of hVDAC-1 and tryptophan mutants of hVDAC-1— The following line of investigation probed whether TNP-nucleotides displace the N-terminal helix of hVDAC-1 from the barrel, and provided independent confirmation of the measured value of K_L for the binding of TNP-ATP. Tryptophan mutations of Tyr7 and Phe18, both part of the N-terminal helix of hVDAC-1, introduced fluorophores at two positions. Using an excitation wavelength of 295 nm, tryptophan fluorescence could be monitored in response to the titration of TNP-ATP. Titration curves were analyzed by following equation: $\frac{\Delta F}{F_0} = \frac{(\Delta F_{max/F_0})L^n}{K_L + L^n}$ (Eqn. 2) (Biochem 39, 36, 11100-11106). ΔF is the change in fluorescence due to the presence of ligand L, F_o is the fluorescence in the absence of ligand, F_{max} is the fluorescence at the highest concentration of ligand, K_L the dissociation constant and n the Hill coefficient. Changes in tryptophan fluorescence in response to the binding of TNP-ATP (Fig. 6) established a 2-fold difference in the determination of K_L by the two methods (Table 5). Moreover, the increase in fluorescence as TNP-ATP increases indicates a tighter binding of the N-terminal helix a TNP-ATP increases. TNP-ATP did not exhibit fluorescence at an excitation wavelength of 295 nm.

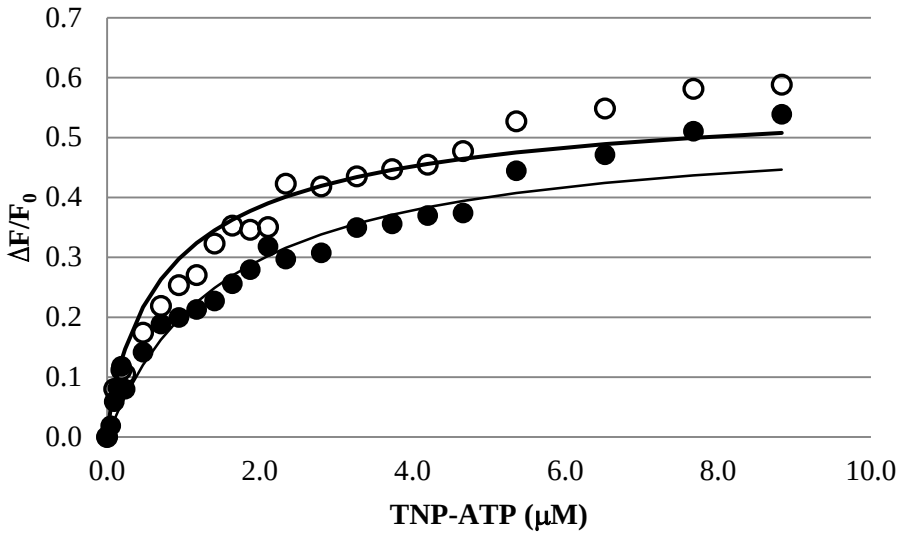

FIGURE 6. TNP-ATP titration of the tryptophan mutants. Plot represents the fluorescence at varying total concentrations of TNP-ATP in 2 mM glucose and 50 mM Tris-HCl, pH 7.5, with mutant hVDAC-1 2.0 μM. Y7W (○), F18W (●)

TABLE 5. Comparison of dissociation constant determined by TNP-ATP excitation (409 nm) and tryptophan excitation (295 nm). Parameters are from each fluorescence analysis model as describe in the text. Fluorescence was measured at varying total concentrations of TNP-ATP in 2 mM glucose and 50 mM Tris-HCl, pH 7.5. Standard deviations in the last significant digit are in parentheses.

Excitation wavelength (nm)		K_L (μM)	γ	$F_{scatter}$	*n*
409	WT	0.5 (2)	16.4 (9)	0.5 (1)	NA
	Y7W	0.6 (6)	6.8 (2)	0.16 (2)	NA
	F18W	0.7 (6)	6.7 (1)	0.10 (2)	NA
295	Y7W	0.9 (1)	NA	NA	0.8 (1)
	F18W	1.5 (1)	NA	NA	1.0 (1)

DISCUSSION

TNP-nucleotides bind with high affinity to hVDAC-1. The TNP-ATP dissociation constant is twofold lower than that of TNP-ADP, and four-fold lower than that of TNP-AMP, but roughly the same as that for TNP-CTP. The data indicate a weak dependence on the number of phosphoryl groups and no dependence on the type of nucleotide base. The TNP moiety is essentially picric acid, but picric acid alone does not bind with high affinity to hVDAC-1. Binding seems determined by the phosphoryl groups, but may be limited primarily to the α-phosphoryl group, or may preclude interactions involving multiple phosphoryl groups. These observations suggest that anions present in buffers could have a significant impact on apparent binding affinities of nucleotides. Work here employed Tris-HCl, making Cl^- the dominant anion in the system at a concentration of approximately 25 mM.

TNP-ATP exhibited a titration curve not consistent with a single fluorophore binding to hVDAC-1. Fluorescence increased smoothly and began to plateau after the total concentration of TNP-ATP reached 2 μM. Higher concentrations of TNP-ATP resulted in a reproducible rise in fluorescence, not linked to any discernable aspect in the delivery of titrant (such as changing the volume settings on the pipette). The behavior is indicative of the binding of a second molecule of TNP-ATP; however, fitting such data proved problematic because of the introduction of a second K_L and γ to account for another binding interaction. Multiple binding of ATP analogs to VDAC have been observed previously (17). Two molecules of benzoyl-benzoyl-ATP bind to VDAC indicating high- and low-affinity sites, and resulting in multiple sites of labeling after photoexcitation.

The titration curve using TNP-AMP exhibited no evidence of anything more complicated than the binding of a single fluorophore. Hence, with reasonable confidence ATP displacement of TNP-AMP reflects a simple exchange of molecule of ATP for one molecule of TNP-AMP, consistent with the model (mutually exclusive binding of TNP-AMP and ATP) used for the analysis of data. The K_A value (1100 μM) for ATP in its displacement of TNP-ATP indicates a low affinity interaction, whereas the K_A value (14 μM) for ATP in its displacement of TNP-AMP indicates a high affinity site of interaction.

The binding of TNP-AMP and displacement by ATP through interactions that involve primarily a phosphoryl group implicates one or more positively charged lysine residues in the pore of hVDAC-1. There are 15 candidates, and most seem involved, perhaps through indirect electrostatic interactions, but certainly lysines 61 and 113 (co-localized on one side of the barrel) are not involved, whereas Lys256 and Lys274 (co-localized on the opposite side of the barrel) are involved significantly (Fig. 7). ATP and TNP-AMP have common patterns of interaction.

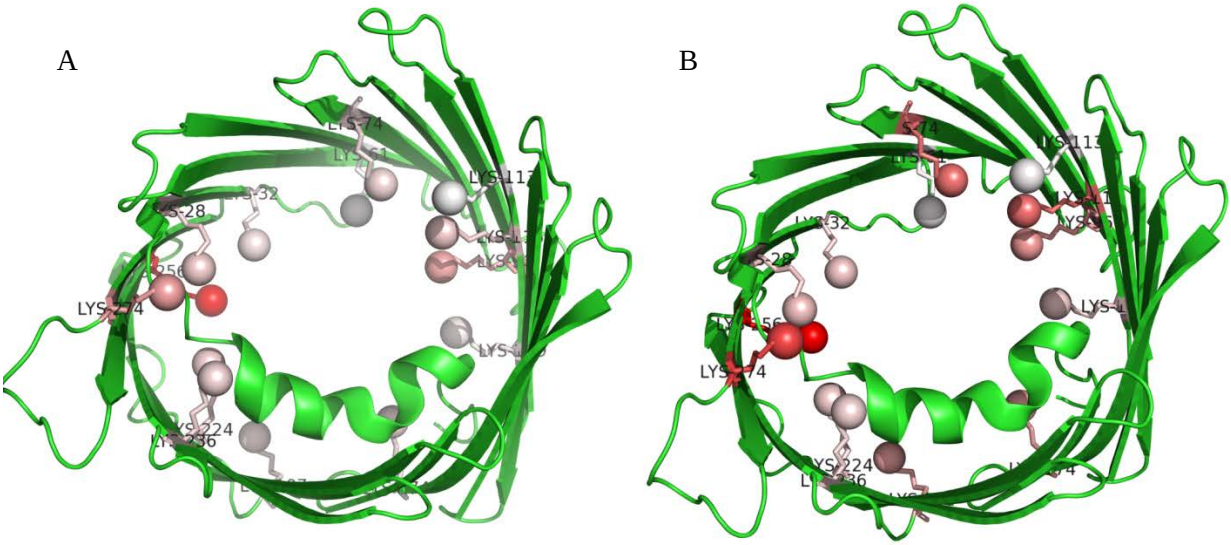

FIGURE 7. Mapping pore lysine residues to VDAC structure (PDB 3EMN). The color of lysine residues represents the effect of the mutation relative to K256M, calculated by $(K^{mutant}–K^{wildtype})/(K^{K256M}–K^{wildtype})$, where K represents K_L for TNP-AMP or K_A for ATP. The effects of mutations range from 0 to 1 relative to K256M, with 1=100% red and 0=0% red (i.e., white). Panels A and B are effects of mutation on the binding affinities of TNP-AMP and ATP, respectively.

In other words, mutations have similar impacts on ATP (three phosphoryl groups and no TNP moiety) and TNP-AMP (one phosphoryl group and one TNP group). Structurally, these molecules differ significantly, and the active site of an enzyme should have little difficulty in distinguishing ATP from TNP-AMP. The VDAC pore, however, is not an active site, but a channel for the passage of anions. TNP-AMP and ATP have nearly the same formal charge (–4) at pH 7.5, and it may be that Lys256 and Lys274 form hydrogen bonds with the α-phosphoryl group of each ligand with other lysine residues interacting electrostatically over distances beyond 3.5 Å.

The passage of an anion through hVDAC-1 must overcome the N-terminal helix which resides in the pore. The truncation of the N-terminal helix substantially decreases the binding affinities of TNP-AMP and ATP (Tables 4 & 5). The involvement of the N-terminal helix in interacting with ATP and TNP-AMP is evident from the substitution of Phe18 or Tyr7 with tryptophan. Tryptophan fluorescence increases in response to the titration of TNP-ATP, indicating diminished access of the tryptophan sidechains at positions 7 and 18 to solvent, which would be consistent with nucleotide binding within the pore without the displacement of the helix. Hence, the ATP and TNP-AMP complexes here represent anion binding to a close state of hVDAC-1 (Fig. 8).

How does hVDAC-1 pass ATP if the high-affinity state for ATP is associated with a closed pore? Conceivably, under a membrane potential difference of a respiring mitochondrion, this closed state may open. Another mechanism may exist that involves a second, low-affinity binding site for ATP (Fig. 8). The ATP molecule stationed at the high-affinity site may indeed stabilize a close hVDAC-1. The binding of a second molecule of ATP, which would occur only in the presence of a high mitochondrial concentration of ATP, would then weaken the high-affinity interaction (the second molecule of ATP antagonizes the binding of first molecule) which in turn destabilizes the closed pore (gate opens in response to the second binding event). A mechanism of this kind opens the pore only when a molecule of ATP is in position to leave.

Work of Maskey (MS thesis) favors the binding of the N-terminal helix of HKI to the outside of the hVDAC-1 barrel, placing the N-terminal half over the pore of hVDAC-1. The displacement of the N-terminal helix of hVDAC-1 could force reorientation of HKI so that its high-affinity binding site for ADP at the N-terminal half faces the pore opening. As ATP exits the open pore, a molecule of ADP bound to HKI is positioned to enter the pore. Are any of these

ideas subject to experimental verification? Perhaps through the introduction of CRISPR/CAS9 methods mutant forms of hVDAC-1 (for instance, K256M) and/or HKI (elimination of the N-terminal ADP site) could determine whether specific binding sites have significant impact on cell growth and ATP levels.

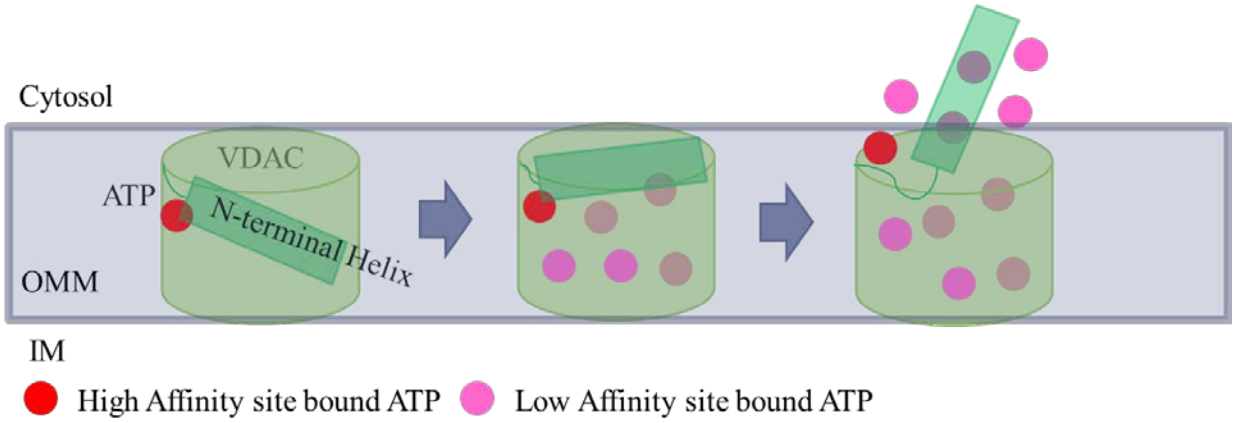

FIGURE 8. Possible mechanism of ATP movement through hVDAC-1. The N-terminal helix (parallelogram) resides in the interior of closed hVDAC-1 (left). ATP molecules (circles) bind to the hVDAC-1 interior causing a significant change in net electrostatic charge, which then triggers helix movement (middle). N-terminal helix opens to the cytosolic side of the outer mitochondrial membrane when ATP molecules fill the low affinity biding site (or sites) (right). OMM represents outer mitochondrial membrane. IM means the inner membrane space of the mitochondrion.

REFFERENCES

1.Colombini, M. (2004) Mol. Cell. Biochem. 256-257, 107-15.

2.Lemasters, J J; Holmuhamedov, E. (2006) Biochim. Biophys. Acta. 1762, 181-90.

3.Shoshan-Barmatz, V; Gincel, D. (2003) Cell Biochem. Biophys. 39, 279-92.

4.Shoshan-Barmatz, V; Israelson, A. (2005) J. Membr. Biol. 204, 57-66.

5.Tsujimoto, Y; Shimizu, S. (2002) Biochemie. 84, 187-93.

6.Vyssokikh, M Y; Brdiczka, D. (2003) Acta. Biochim. Pol. 50, 389-404.

7.Gincel, D; Zaid, H; Shoshan-Barmatz, V. (2001) Biochem. J. 358, 147-55.

8.Deniaud, A; Sharafeldein, O; Maillier, E; Poncet, D; Kroemer, G; Lemaire, C; Brenner, C. (2007) Oncogene. 1-15.

9.Deniaud, A; Rossi, C; Berquand, A; Homand, J; Campagna, S; Knoll, W; Brenner, C; Chopineau, J. (2007) J. Am. Chem. Soc. 23, 3898-905.

10.Abu-Hamad, S; Sivan, S; Shoshan-Barmatz, V. (2006) Proc. Natl. Acad. Sci. 103, 5787-92.

11.Zaid, H; Abu-Hamad, S; Israelson, A; Nathan, I; Shoshan-Barmatz, V. (2005) Cell Death Differ. 12, 751-60.

12.Perevoshchikova, I V; Zorov, S D; Kotova, E A; Zorov, D B; Antonenko, Y N. (2010) FEBS Lett. 584,2397-402.

13.Shoshan-Barmatz, V; Zakar, M; Rosenthal, K; Abu-Hamad, S. (2009) Biochim. Biophys. Acta. 1787, 421-30.

14.Azoulay-Zohar, H; Israelson, A; Abu-Hamad, S; Shoshan-Barmatz, V. (2004) Biochem. J. 377, 347-55.

15.Xie, G C; Wilson, J E. (1988) Arch. Biochem. Biophys. 267, 803-10.

16.Mulichak, A M; Wilson, J E; Padmanabhan, K; Garavito, R M. (1998) Nat. Struct Biol. 5, 555-60.

17.Yehezkel, G; Hadad, N; Zaid, H; Sivan, S; Shoshan-Barmatz, V. (2006) J. Biol. Chem. 281, 5938-46.

18.Yehezkel, G; Abu-Hamad, S; Shoshan-Barmatz, V. (2007) J. Cell. Physiol. 212, 551-61.

19.Hiller, S; Garces, R G; Malia, T J; Orekhov, V Y; Colombini, M; Wagner, G. (2008) Science 321, 1206-10.

20.Bayrhuber, M; Meins, T; Haeck, M; Becker, S; Giller, K; Villinger, S; Vonrhein, C; Griesinger, C; Zweckstetter, M; Zeth, K. (2008) PNAS. 105(40), 15370-75.

21.Abu-Hamad S; Arbel N; Calo D; Arzoine L; Israelson A; Keinan N; Ben-Romano R; Friedman O; Shoshan-Barmatz V. (2009) J. Cell. Sci. 122, 1906-1916.

22. Fang, T Y; Alechina, O; Aleshin, A E; Fromm, H J; Honzatko, R B. (1998) J. Biol. Chem. 273, 19548-53.

23.Liu, X; Kim, C S; Kurbanov, F T; Honzatko, R B; Fromm, H J. (1999) J. Biol. Chem. 274, 31155-9.

24.Tsai, H J; Wilson, J E. (1995) Arch. Biochem. Biophys. 316, 206-14.

25.Aleshin, A E; Zeng, C; Bartunik, H D; Fromm, H J; Honzatko, R B. (1998) J. Mol. Biol. 282, 345-57.

26.Engelhardt, H; Meins, T; Poynor, M; Adams, V; Nussberger, S; Welte, W; Zeth, K. (2007) J. Membrane Biol. 216, 93-105.

CHAPTER 4: CONFOCAL MICROSCOPIC VISUALIZATION OF THE INTERACTION BETWEEN FLUORESCENCE-LABELED CONSTRUCTS OF HEXOKINASE TYPE I (HKI) WITH VOLTAGE DEPENDENT ANION CHANNELS (VDAC) LOCALLIZED TO THE MEMBRANE OF GIANT UNILAMELLAR VESICLES (GUV)

A paper to be submitted to the Journal of Biological Chemistry

Muneaki Watanabe[6], Richard B. Honzatko[1,7]

From the Roy J. Carver Department of Biochemistry, Biophysics and Molecular Biology

Iowa State University, Ames, IA 50011

Running title: Interaction of HKI Constructs with VDAC

Keywords: VDAC; HKI; mitochondria; ATP; Glucose-6-P; fluorescence; confocal microscopy
Background: Evidence suggests the direct interaction of HKI with VDAC of the outer mitochondrial membrane.
Results: VDAC embedded in the outer membrane of artificial vesicles binds and releases fluorescence-tagged constructs of HKI comparably to intact mitochondria.
Conclusion: The presence of VDAC alone is sufficient to bind constructs of HKI to membrane. The presence of the first 26-resdues of the N-terminal tail of HKI is sufficient to localize constructs of HKI to membranes containing VDAC.
Significance: Data here represent the first evidence for a direct interaction between VDAC and HKI.

ABSTRACT

Human hexokinases Type I and Type II (HKI & HKII) bind the outer mitochondrial membrane, being among the first enzymes of the cytosol to have access to ATP, while desensitizing mitochondria toward pro-apoptotic signals. Several lines of evidence show correlations between the status of the voltage dependent anion channel (VDAC) and the binding of HKI or HKII to the outer mitochondrial membrane, but no investigation has provided evidence for a direct interaction between VDAC and either HKI or HKII. Giant unilamellar vesicles (GUVs) of lipid composition comparable to that of the outer mitochondrial membrane do not bind fluorescent constructs of HKI as visualized by confocal microscopy; however, such vesicles bind HKI constructs when recombinant VDAC is embedded in the membrane. N-terminal half HKI tagged with either green fluorescent protein (GFP) or FlAsH-modified tetracysteine is released from vesicles by glucose 6-phosphate (G6P) or ATP, comparable to the

release of HKI from pig liver mitochondria. A construct composed of the first 26-residues of HKI tagged with GFP or FlAsH-modified tetracysteine binds to VDAC-embedded GUVs as well. ATP releases such constructs but G6P does not, consistent with different mechanisms of action for each ligand. The observations reported here can be reconciled only by a direct interaction of HKI with VDAC.

INTRODUCTION

Apoptosis is a naturally occurring process by which a cell is programed to self-destruct. Apoptosis is based on genetic information that is an indispensable part of the development and function of an organism. There are at least two broad pathways of apoptosis known as an "extrinsic" and "intrinsic". The extrinsic pathway begins when conditions in the extracellular environment determine that a cell must die. Intrinsic apoptosis begins when an injury (or malfunction) occurs within the cell. Mitochondrially-linked apoptosis is the best known intrinsic apoptosis pathway (1, 2). Substantial evidence suggests VDAC as a critical player in the release of apoptogenic proteins from mammalian mitochondria (3-8). Cytochrome *c* release, interactions between the pro-apoptotic proteins and VDAC, and the initiation of cell death are impeded by anti-VDAC antibodies, indicating the central importance of VDAC in the intrinsic apoptosis pathway (9-11).

The other evidence for VDAC involvement is demonstrated by over-expression and down-expression of VDAC *in vivo*. Over-expression of human, murine, yeast, Paralichthys olivaceus, and rive VDAC was found to induce apoptotic cell death regardless of cell type (12-16). On the other hand, siRNA-mediated down-expression of VDAC prevented cell death induced by pro-apoptotic proteins (7). Hexokinase Type-I (HKI) and Type-II (HKII) antagonize the formation of apoptotic channels. Some have gone so far as to label hexokinase as “guardian of the mitochondria” because of its anti-apoptotic properties (17). Hexokinase co-localizes differentially with human VDAC-1, -2 and -3 (18). HKI binding to mitochondria inhibits ATP flux through VDAC-1 (19). Over expression of N-terminally truncated VDAC-1 did not induce cells to release cytochrome *c* and the cells were resistant to apoptosis (6). The N-terminal peptide of VDAC-1 and other VDAC-1 based peptides bind to immobilized HKI. These peptides prevented protection of cells by HKI (20).

Specific residues in VDAC are likely to be important for the interaction between VDAC and HKI. Chemical modification of Glu73 eliminated the binding of HKI to mitochondria (16). Mutating Glu73 of VDAC abolished anti-apoptotic effects due to the overexpression of HKI in different cancer cells (21). Adding HKI to VDAC1 reconstituted in lipid membrane reduced channel conductance (22). The addition of HKI to Glu73Gln VDAC did not terminate ion conductance, indicating the failure to form a HKI-mutant VDAC complex (21). A number of small and physiological important ligands dissociate HKI from the mitochondrial outer membrane. For instance, a photoactive ATP analog, Bz-ATP (benzoyl-benzoyl-ATP), can bind to sites on VDAC-1 with low and high binding affinities (23). Mutating residues in predicted nucleotide-binding site in VDAC-1 reduced ATP cellular levels and caused sluggish cell growth (24).

Giant unilamellar vesicles (GUVs) could function as an artificial substitute for the outer membrane of the mitochondrion, offering the prospect of a “simplified” outer mitochondrial membrane with known constituents. Stability, flexibility, and viscosity of the GUV membrane can be adjusted as necessary in order to capture integral membrane proteins. The challenge in developing a “functional” GUV comes in the capture of VDAC molecules with orientation and conformation that approximates VDAC molecules in the outer membrane of the mitochondrion. Based on the previous study (Chapters 2&3, this thesis) TNP-ATP binds with high affinity to VDAC. In this study, we exhibit the capture of VDAC in the membrane of GUVs. The VDAC-embedded GUVs bind fluorescent constructs of HKI, consistent with HKI binding to the mitochondrion. Moreover, glucose 6-phosphate (G6P) and ATP release constructs of HKI comparably to the release of HKI from mitochondria. Work here represents the first evidence for a direct interaction between HKI and VDAC, showing VDAC allow is sufficient and necessary to localized HKI to a membrane.

EXPERIMENTAL PROCEDURES

Materials— ATP, deoxyribonuclease (DNase I), protease cocktail inhibitor and phenylmethylsultonyl fluoride came from Sigma. Kanamycin sulfate was from Invitrogen. Nickel-nitrilotriacetic acid-agarose (NiNTA) was from Novagen. Isopropyl-1-thio-β-D-galactopyranoside (IPTG) and Lauryldimethylamine-N-oxide (LADO) came from Anatrace.

Oligonucleotides came from the Iowa IDT. Phosphatidylcholine (PC) and Cholesterol were from Avanti.

N-domain constructs of HKI— Human brain hexokinase (HKI) was cloned into pET-24b vector with a polyhistidyl tag at its C-terminus (pET-24b-HKI-10*x*His) as reported previously (26). Hexokinase mutants were created through PCR modification. An NdeI cut site was created at Ala454 in pET-24b-HKI-10*x*His using the forward primer, 5'-GCAGCGGCAAGGGGGCTCATATGGTGACGGCGGTGGC-3', and its reverse complement. N-terminal half HKI plasmid was digested with NdeI and then ligated to produce pET24b-HKI$^{1–454}$-10*x*His. This plasmid encodes residues 1–454 of HKI with a C-terminal polyhistidyl tag.

Green Fluorescence Protein (GFP) was incorporated between the C-terminal end of HKI$^{1–454}$ and the polyhistidyl tag by the double digestion using MscI and HindIII cut sites to produce pET24b-HKI$^{1–454}$-GFP-10*x*His. A StuI cut site was introduced after the N-terminal first 26 residues of pET24b-HKI$^{1–454}$-GFP-10*x*His using the forward primer, 5'-ATTACTTCACGGAGCTGAAGGAAGGCCTTCCATGAATGGATGACCAGGTCAA-3', and its reverse complement. Digestion with StuI and HindIII and ligation to pET24b resulted in pET24b-HKI$^{27–454}$-GFP-10*x*His. The N-terminal 26 residues of HKI were removed by double digestion using NdeI and StuI and then ligated into pET24b-GFP to produce pET24b-HKI$^{1–26}$-GFP-10*x*His.

Several constructs employed the tetracysteine motif (to be subsequently reacted with FlAsH). A tetracysteine motif was inserted between C-terminal end of N-terminal half HKI and the polyhistidyl tag using the forward primer, 5'-GTCGACAAGCTTGCGGCCTGTTGTCCAGGATGTTGTGCACTCGAGCACCACCAC-3', and its reverse complement. The resulting construct (pET24b-HKI$^{1–454}$-tetracysteine-10*x*His) has 1-454 residues of HKI followed by the tetracysteine motif and the polyhistidyl tag at C-terminal end. A ClaI cleavage site was created after the N-terminal first 26 residues using the forward primer, 5'-ATTGACAAGTATCTGTGTTGTCCAGGATGTTGTCATGCCATGGCATGTATGCCATGCGGCTCTC-3', and its reverse complement. A plasmid containing the residues 1–26 of HKI with the tetracysteine motif was digested with ClaI and ligated with the pET24b vector to produce pET24b-HKI$^{1–26}$-tetracysteine-10*x*His. The construct encodes residues 1–26 of HKI, the tetracysteine motif, and a C-terminal polyhistidyl tag.

All plasmid constructs were confirmed by DNA sequencing at the DNA Sequencing Facility at Iowa State University.

Expression and purification of N-domain HKI constructs— E.coli strain BL21 (DE3) cells were transformed with plasmids of HKI constructs. Expression and purification HKI constructs employed Ni-NTA agarose chromatography as previously described (26). Protein purity was monitored by SDS-polyacrylamide gel electrophoresis. The determination of protein concentration employed the method of Bradford with bovine serum albumin as a standard (27).

Cloning of Wild-type human VDAC-1— A plasmid with the coding sequence of human VDAC-1 (hVDAC-1) was purchased from Open Biosystems. NdeI and SacI cut sites were created in the plasmid using the polymerase chain reaction (PCR) and NdeI primer 5'CGCGGCAGCCATATGATGGCTGTGCCACCCACG3' and SacI primer 5'GGACTGGAATTTCAAGCA TCGAGCTCCGTCGACAAGC3'. The PCR product and vector pET-24a were digested by NdeI and SacI restriction enzymes. After separation on agarose gel, the DNA fragment for hVDAC-1 was ligated to pET-24a. The construct was confirmed by DNA sequencing at Iowa State University.

Expression and purification of hVDAC-1— E.coli strain BL21 (DE3) cells were transformed with hVDAC-1 or mutant hVDAC-1 plasmids. The expression and purification hVDAC-1 are discussed elsewhere (28, 29). The determination of protein concentration and secondary structure employed UV absorbance at 280 nm and CD spectra, respectively.

Reconstitution of gigantic unilamellar vesicle (GUV) embedding hVDAC-1— Reconstitution of GUVs used the dehydration method (30) with modification as described here briefly. Composition of GUV employed the major components of the outer mitochondrial membrane, phosphatidylcholine (PC) and phosphatidylethanolamine (PE). The lipids were dissolved in chloroform, each to a concentration of 0.1 M. 20 μl of this solution was added to a 50 mL round-bottom flask containing 980 μL of chloroform and 200 μL of methanol. The aqueous phase (7 mL of 5 mM Hepes, pH7.4) was carefully added along the flask wall. Liposomes formed in the aqueous phase. VDAC to be embedded in vesicles were added up to a concentration of 2 μM to the aqueous phase prior to evaporation of the organic solvent. The organic solvent was removed in a rotary evaporator under reduced pressure at 40 °C and 40 rpm. As a consequence of the different boiling temperatures of chloroform and methanol, two major boiling events were observed. After evaporation for 2 min, an opalescent fluid was obtained in a volume of about 6.5

ml. The resulting aqueous solution contained a high concentration of GUVs, sizes ranging from 20 to 70 μm.

Computational analysis of VDAC recognition sequence of HKI— N-terminal sequences in data bases, UniProtKB/Swiss-Prot (release 2013_01 of 09-Jan-13: 538849 entries and UniProtKB/TrEMBL (release 2013_01 of 09-Jan-13: 29266939 entries), were scanned using ScanProsite (31) for similarities against the mitochondrial recognition element of the HKI (residues 1–8).

Confocal microscopy— 2 μL of freshly prepared vesicle solution was applied to the well of a microscope slide, and a cover slide set above the sample. Samples were examined with a Leica SP5 X MP confocal/multiphoton microscope system with an inverted microscope front end equipped with A HCX PL APO CS 63.0*x*1.40 OIL UV objective lens. A drop of microscope immersion oil (n=1.518) was placed between the cover glass and the tip of the microscope objective. The light source was a 250 W halogen lamp, which transmitted incoherent light (400-700 nm) via a fiber optic light guide to the microscope. The optical sections were acquired in 1 micron vertical steps. The images were digitized in a format of 512 x 512 pixels (8 bits) and stored in the TIFF format. The fluorescence emission and excitation were followed each specific fluorophore. Commercial confocal software (Leica) was used for image analysis.

RESULTS

Search for the HKI mitochondrial recognition element in other proteins – HKI and HKII interact with mitochondria through the first (N-terminal) 26 residues (17, 18). Some or all of these residues form a helix, the N-terminus of which could reach Glu73 of VDAC. In models of membrane-associated VDAC, Glu73 is buried halfway in the mitochondrial outer membrane, requiring minimally an α-helix of 8 residues to span the outer leaflet of the mitochondrial outer membrane. ScanProsite was used for scanning proteins against a defined motif. The specific motif used here are the first eight residues of HKI and HKII: M-I-A-[A or S]-[Q or H]-L-L-A. The search revealed HKI and HKII from 32 organisms (Table 1), one predicted membrane protein in from *Pseudomonas stutzeri* (strain A1501), and 43 uncharacterized proteins from different organisms. Of the uncharacterized proteins, most come from higher eukaryotes (mammals, birds and reptiles), and are likely hexokinases, but the remaining are from species of *Pseudomonas* and have probable homology to that of the predicted membrane protein of

Pseudomonas stutzeri (strain A1501). All characterized proteins (all of them HKI or HKII) have peptide sequences that make exact matches to the motif. The motif seems restricted to hexokinases of higher eukaryotes, suggesting a fundamental purpose in the hexokinase-mitochondrion interactions.

TABLE 1. Results from M-I-A-[A or S]-[Q or H]-L-L-A sequence motif search (ScanProsite).

#	Proteins	Organisms	Seq. (1-8)
1	**Hexokinase-1**	**Bovine**	**MIAAQLLA**
2	**Hexokinase-1**	**Human**	**MIAAQLLA**
3	**Hexokinase-1**	**Sumatran Orangutan**	**MIAAQLLA**
4	**Hexokinase-1**	**Rat**	**MIAAQLLA**
5	**Hexokinase-2**	**Grevy's Zebra**	**MIASHLLA**
6	**Hexokinase-2**	**Horse**	**MIASHLLA**
7	**Hexokinase-2**	**Human**	**MIASHLLA**
8	**Hexokinase-2**	**Pig**	**MIASHLLA**
9	**cDNA FLJ75392, highly similar to Homo sapiens hexokinase II (HKII) mRNA**	**Human**	**MIASHLLA**
10	**cDNA FLJ78173, highly similar to Homo sapiens hexokinase 1 (HK1) mRNA**	**Human**	**MIAAQLLA**
11	**cDNA FLJ56506, highly similar to Hexokinase-1 (EC 2.7.1.1)**	**Human**	**MIAAQLLA**
12	**Hexokinase-2**	**Horse**	**MIASHLLA**
13	**Hexokinase-2**	**Horse**	**MIASHLLA**
14	**Hexokinase-1**	**Chinese Hamster**	**MIAAQLLA**
15	**Hexokinase-1**	**Naked Mole Rat**	**MIAAQLLA**
16	**Hexokinase-1**	**Sumatran Orangutan**	**MIAAQLLA**
17	**Hexokinase 2**	**Chimpanzee**	**MIASHLLA**
18	**Hexokinase-1 isoform HKI**	**Rhesus Macaque**	**MIAAQLLA**
19	**Hexokinase-2**	**Rhesus Macaque**	**MIASHLLA**
20	**Hexokinase-1 isoform HKI**	**Rhesus Macaque**	**MIAAQLLA**
21	**Hexokinase 2**	**Chimpanzee**	**MIASHLLA**
22	**Hexokinase 2**	**Chimpanzee**	**MIASHLLA**
23	**Hexokinase 1**	**Chimpanzee**	**MIAAQLLA**
24	**Hexokinase 1**	**Bovine**	**MIAAQLLA**
25	**Hexokinase 1, isoform CRA_d**	**Mouse**	**MIAAQLLA**
26	**Hexokinase2**	**Chicken**	**MIASHLLA**
27	**Hexokinase1**	**Chicken**	**MIAAQLLA**
28	**Hk1 protein**	**Western clawed frog**	**MIAAQLLA**
29	**Hexokinase 1a**	**Atlantic Cod**	**MIAAQLLA**

TABLE 1 Continued

30	**Hk1-A protein**	**African Clawed Frog**	**MIAAQLLA**
31	**Hexokinase 1**	**Zebrafish**	**MIAAQLLA**
32	**Hexokinase 1**	**Zebrafish**	**MIAAQLLA**
33	**Uncharacterized protein**	**Bovine**	**MIAAQLLA**
34	**Uncharacterized protein**	**Chicken**	**MIAAQLLA**
35	**Uncharacterized protein**	**White Tufted ear Marmoset**	**MIAAQLLA**
36	**Uncharacterized protein**	**White Tufted ear Marmoset**	**MIAAQLLA**
37	**Uncharacterized protein**	**Horse**	**MIAAQLLA**
38	**Uncharacterized protein**	**Duckbill Platypus**	**MIAAQLLA**
39	**Uncharacterized protein**	**Rhesus Macaque**	**MIASHLLA**
40	**Uncharacterized protein**	**White Tufted ear Marmoset**	**MIASHLLA**
41	**Uncharacterized protein**	**Giant Panda**	**MIASHLLA**
42	**Uncharacterized protein**	**Northern White-Cheeked Gibbon**	**MIASHLLA**
43	**Uncharacterized protein**	**Rabbit**	**MIASHLLA**
44	**Uncharacterized protein**	**Lowland Gorilla**	**MIASHLLA**
45	**Uncharacterized protein**	**African Elephant**	**MIASHLLA**
46	**Uncharacterized protein**	**Tasmanian Devil**	**MIASHLLA**
47	**Uncharacterized protein**	**Crab-eating Macaque**	**MIASHLLA**
48	**Uncharacterized protein**	**Small-Eared Galago**	**MIAAQLLA**
49	**Uncharacterized protein**	**Zebra Finch**	**MIAAQLLA**
50	**Uncharacterized protein**	**Chicken**	**MIASHLLA**
51	**Uncharacterized protein**	**Chicken**	**MIASHLLA**
52	**Uncharacterized protein**	**Pig**	**MIAAQLLA**
53	**Uncharacterized protein**	**Thirteen-Lined Ground Squirrel**	**MIAAQLLA**
54	**Uncharacterized protein**	**Dog**	**MIAAQLLA**
55	**Uncharacterized protein**	**Chinese Softshell Turtle**	**MIAAQLLA**
56	**Uncharacterized protein**	**Mouse**	**MIAAQLLA**
57	**Uncharacterized protein**	**Mouse**	**MIAAQLLA**
58	**Uncharacterized protein**	**Western clawed frog**	**MIASHLLA**
59	**Uncharacterized protein**	**Three-Spined Stickleback**	**MIAAQLLA**
60	**Uncharacterized protein**	**Three-Spined Stickleback**	**MIAAQLLA**
61	**Uncharacterized protein**	**Medaka Fish**	**MIAAQLLA**
62	**Uncharacterized protein**	**Japanese Pufferfish**	**MIAAQLLA**

TABLE 1Continued

63	**Uncharacterized protein**	**Japanese Pufferfish**	**MIAAQLLA**
64	**Uncharacterized protein**	**Japanese Pufferfish**	**MIAAQLLA**
65	**Uncharacterized protein**	**Japanese Pufferfish**	**MIAAQLLA**
66	**Uncharacterized protein**	**West Indian Ocean Coelacanth**	**MIAAQLLA**
67	**Uncharacterized protein**	**Spotted Green Pufferfish**	**MIAAQLLA**
68	**Uncharacterized protein**	**Spotted Green Pufferfish**	**MIAAQLLA**
69	**Uncharacterized protein**	**Nile Tilapia**	**MIAAQLLA**
70	**Uncharacterized protein**	**Nile Tilapia**	**MIAAQLLA**
71	**Predicted membrane protein. (strain A1501)**	**Pseudomonas**	**MIAAHLLA**
72	**Uncharacterized protein (strain DSM 4166 / CMT.9.A)**	**Pseudomonas**	**MIAAHLLA**
73	**Uncharacterized protein (strain:ATCC17588/DSM5190/CCUG11256/JCM5965/LMG11199/NCIMB11358/Stanier221)**	**Pseudomonas**	**MIAAHLLA**
74	**Uncharacterized protein CCUG 29243**	**Pseudomonas**	**MIAAHLLA**
75	**Uncharacterized protein TS44**	**Pseudomonas**	**MIAAHLLA**
76	**Uncharacterized protein KOS6**	**Pseudomonas**	**MIAAHLLA**

VDAC embedded in gigantic unilamellar vesicles— The dehydration method produced vesicles in the presence and absence of VDAC in reproducible amounts and size. GUVs produced in the absence of VDAC did not localized TNP-ATP in contrast to GUVs produced in the presence of VDAC (Fig. 1). Previous studies show that TNP-ATP binds to VDAC with high affinity (Chapters 2 & 3 of this thesis). The outer ring of fluorescence is consistent with the localization of TNP-ATP in the membrane (only in the presence of VDAC), and is a consequence of curvature of vesicles and a focal plane of thickness smaller than the diameter of the vesicle. This result indicates VDAC has become embedded in the membrane of GUVs so that its TNP-ATP binding site is accessible to solution.

Localization of interactive proteins— The determination of whether HKI can bind to GUVs with and without VDAC involved a set of HKI constructs involving two fluorescence labels. Nonspecific binding of polyhistidyl-tagged HKI to the mitochondrial outer membrane occurs (Chapter 2 of this thesis). In order to limit membrane binding to the N-terminal tail of HKI, the N-terminal half was tagged with the green fluorescent protein (GFP) and alternatively the FlAsH tagged tetracysteine motif (Fig. 2). Although GFP is a commonly employed fluorophore, it might

still bind nonspecifically to the GUV or even VDAC. Hence, in order to confirm binding due exclusively to the N-terminal tail of HKI, a “tail-less” N-terminal HKI tagged with GFP served as a negative control.

The FlAsH tagged tetracysteine motif provided an alternative experimental approach that confirmed the behavior of the GFP-tagged constructs. Nonspecific interactions due to the FlAsH-modified tetracysteine motif were ruled out by the absence of membrane-associated fluorescence in the presence of the “tail-less” N-terminal half HKI with the FlAsH-modified tetracysteine motif. The results (Fig. 2) taken together show that the GUV must have VDAC in order to bind an HKI-construct, and that the HKI construct must have its first 26-residues in order for binding to occur. Moreover, binding to the GUV with VDAC occurs with just the first 26 residues of HKI.

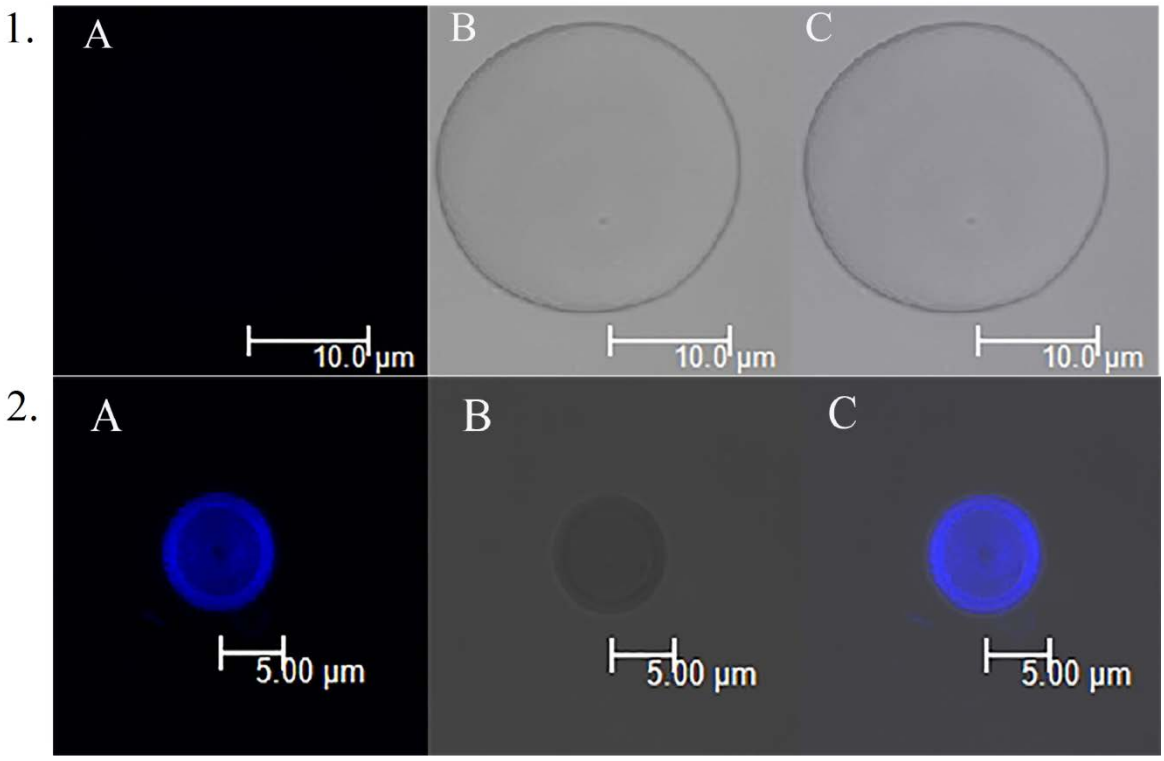

FIGURE 1. GUV captures VDAC. Panels A, B, and C represent illuminating fluorophores, normal light view, and the superposition of images A and B, respectively. The fluorophore is TNP-ATP with at excitation 409 nm and emission at 530 nm.

If images of Fig. 1 & 2 are scanned, and transformed to relative fluorescence intensities (observed intensity relative to background intensity). The distribution of relative fluorescence through a diametric cross-section of the GUV appears as in Fig 3. Two peaks represent each

edge of the GUV, with background fluorescence taken outside the GUV. Comparison of peak fluorescence levels from different samples (Fig. 4) are complicated by three considerations. Firstly, fluorescence intensity is a nonlinear function of fluorophore concentration. Hence, peak intensities at saturation are insensitive to increases in fluorophore concentration. Secondly, fluorescence intensity will vary with vesicle size. Larger vesicles would elevate fluorescence intensity in the peaks due to less membrane curvature and more membrane perpendicular to the pathway of the fluorescence scan. Vesicles used in data collection are approximately of the same size (60±10 microns), so that differences greater 20% should reflect different loads of the protein on the membrane. Thirdly, the amount of protein construct added to each sample is the same, but the molecular weight of each construct differs. Hence, the molar concentration is different. In fact, the molar concentration of N-terminal HKI tagged with GFP is approximately one-half of that of the tail tagged with GFP. The variation in peak fluorescence for the GFP constructs indicates N-terminal HKI tagged with GFP reaches a substantially higher level than the 26-residue tail tagged with GFP.

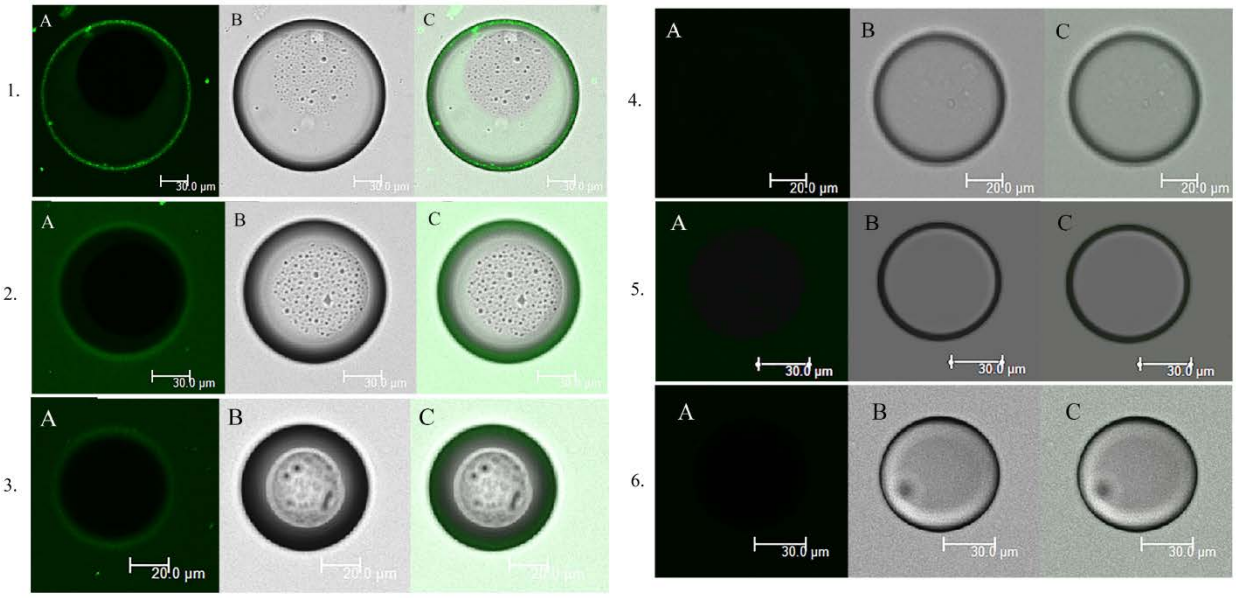

FIGURE 2. Interaction between VDAC-embedded GUVs with N-terminal HKI fluorophores. (Panel 1) N-terminal half HKI tagged with GFP (excitation 488 nm and emission 509 nm). A, B and C represent the illuminating fluorophore view, normal light view, and the superimposition of A and B, respectively. (Panel 2) N-terminal half HKI with the FlAsH-modified tetracysteine motif (excitation 508 nm and emission 528 nm). (Panel 3) N-terminal 26 residues of HKI tagged with GFP. (Panel 4) N-terminal half HKI (without the first 26 residues) tagged with GFP (excitation 488 nm and emission 509 nm). (Panel 5) N-terminal 26 residues of HKI tagged with

FlAsH-modified tetracysteine without VDAC at GUV. (Panel 6) N-terminal half HKI tagged with GFP added to GUV without VDAC. In each instance, 2 μM of HKI construct was added to the well of the microscope slide. VDAC came from the same preparation. GUVs were prepared freshly as described in the Methods Section.

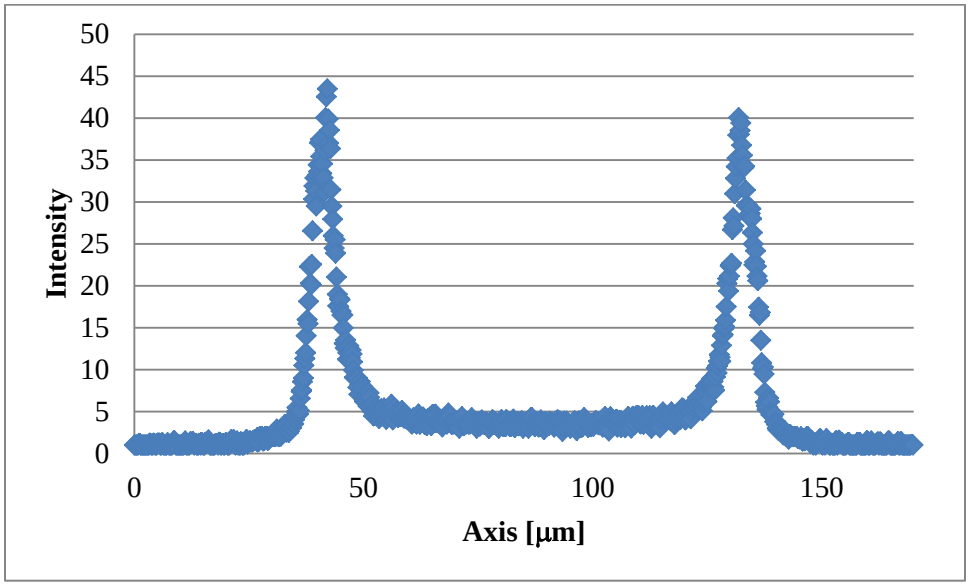

FIGURE 3. Intensity scan along the diameter of a GUV with bound N-terminal HKI tagged with GFP. Fluorescence of GFP-tagged N-terminal-HKI localizes to the membrane giving the observed pattern.

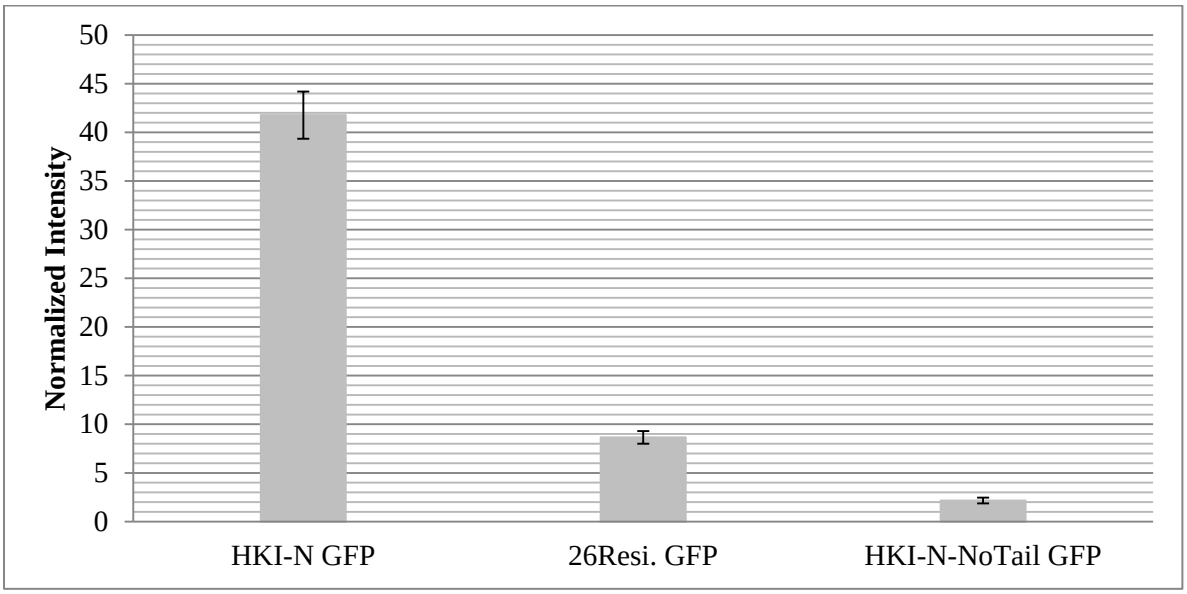

FIGURE 4. Relative peak intensity of bound HKI constructs. Relative peak intensity captured by the analysis presented in Fig. 3.

Release of N-terminal HKI by glucose 6-phosphate and ATP— TNP-nucleotides, nucleotides, and glucose 6-phosphate release HKI from the outer membrane of the mitochondrion (Chapter 2, this thesis). The release phenomenon is pH dependent, with maximum binding of HKI (and release) occurring at pH 7.4. The overlap of the excitation/emission spectra for TNP-nucleotides with that of GFP- or FlAsH-tagged fluorophores preclude the use of TNP nucleotides as release agents; however, other effective release agents (ATP and glucose 6-phosphate) do not interfere. GFP fluorescence decreases in response to additions of glucose 6-phosphate and ATP (Fig. 5). Fluorescence intensities are determined as above (Figs. 3 & 4), and are limited by the nonlinear relationship between fluorescence and fluorophore concentration and variation in vesicle size (Fig. 6); however, GFP fluorescence clearly diminishes in response to releasing ligand.

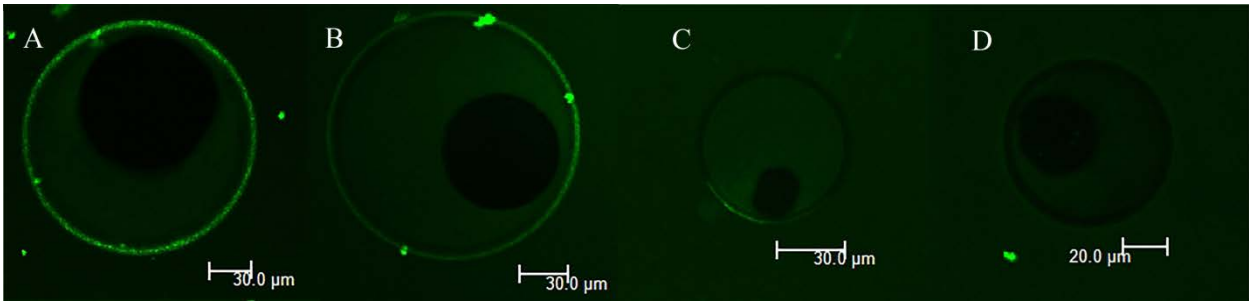

FIGURE 5. Effect of glucose 6-phosphate and ATP on fluorescence intensities from N-terminal HKI tagged with GFP. N-terminal half HKI tagged with GFP (A). N-terminal half HKI tagged with GFP followed by the addition of 10 mM glucose 6-phosphate (B). N-terminal half HKI tagged with GFP followed by the addition of 20 mM glucose 6-phosphate (C). N-terminal half HKI tagged with GFP followed by the addition of 10 mM ATP (D). Excitation 488 nm and emission 509 nm. The pH of each added ligand was adjusted to 7.4 (equal to the pH of the buffer used in making the GUV).

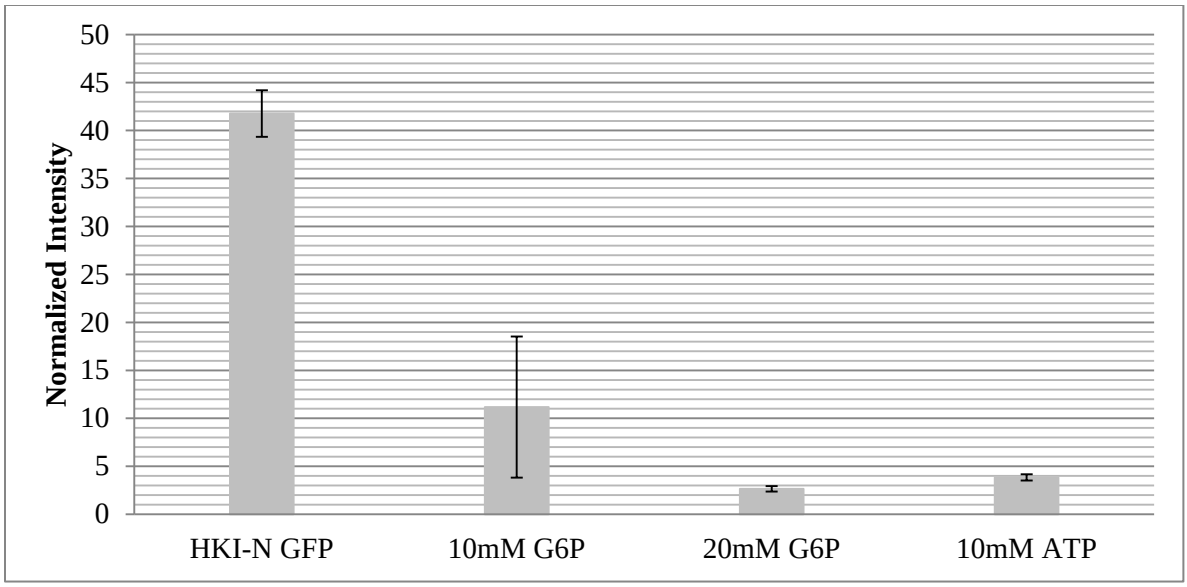

FIGURE 6. Comparison glucose 6-phosphate (G6P) and ATP in releasing HKI constructs. The left-most bar represents the fluorescence due to GUV-bound N-terminal half HKI tagged with GFP, whereas the other represent fluorescence remaining after the addition of the releasing ligand.

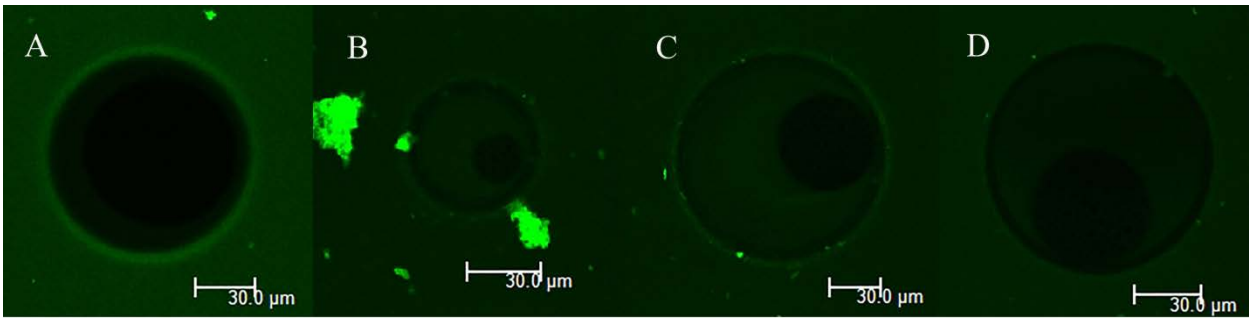

FIGURE 7. Effect of glucose 6-phosphate and ATP on fluorescence intensities from N-terminal HKI tagged with FlAsH-modified tetracysteine. N-terminal half HKI tagged with FlAsH-modified tetracysteine (A). N-terminal half HKI tagged with FlAsH-modified tetracysteine followed by the addition of 10 mM glucose 6-phosphate (B). N-terminal half HKI tagged with FlAsH-modified tetracysteine followed by the addition of 20 mM glucose 6-phosphate (C). N-terminal half HKI tagged with FlAsH-modified tetracysteine followed by the addition of 10 mM ATP (D). Green blotches represent protein aggregates. Excitation 508 nm and emission 528 nm. The pH of each added ligand was adjusted to 7.4 (equal to the pH of the buffer used in making the GUV).

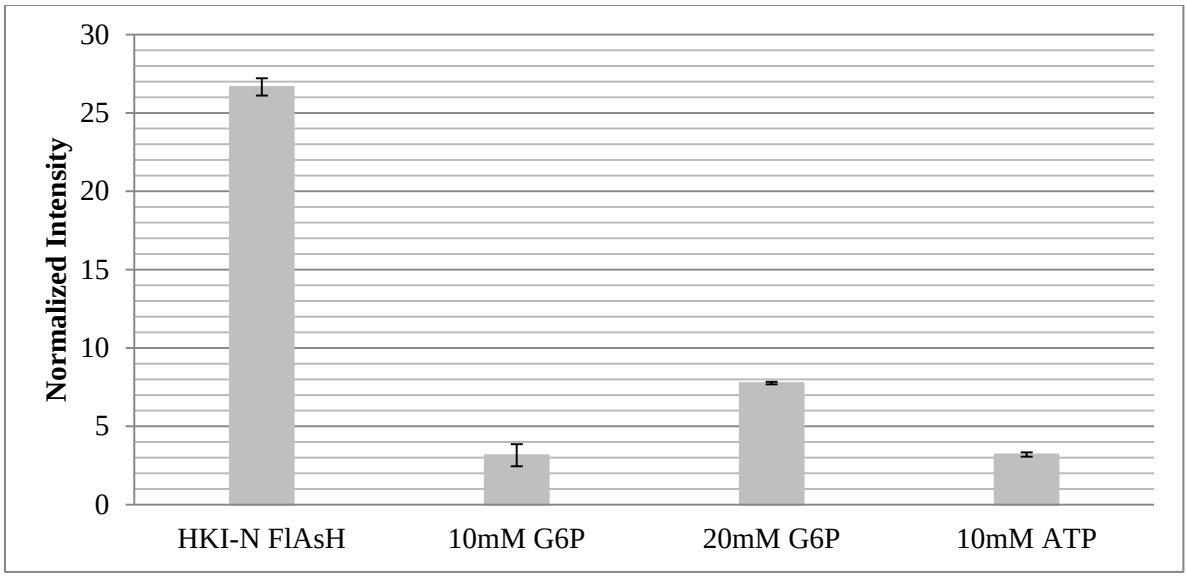

FIGURE 8. Comparison of glucose 6-phosphate (G6P) and ATP in releasing HKI constructs. The left-most bar represents the fluorescence due to GUV-bound N-terminal half HKI tagged with FlAsh, whereas the others represent fluorescence remaining after the addition of the releasing ligand.

The release of N-terminal HKI tagged with FlAsH-modified tetracysteine is comparable to the GFP construct (Figs. 7 & 8). These data indicate more than a 4-fold loss of fluorescence intensity relative to that of N-terminal half HKI tagged with FlAsh modified tetracysteine.

Release of the 26-residue N-terminal tail of HKI— Glucose 6-phosphate and ATP release HKI from the mitochondrion (and also GUVs containing VDAC); however, the mechanism of release from the mitochondrion differs. Glucose 6-phosphate releases HKI from the mitochondrion by binding to the glucose 6-phosphate binding site in the N-terminal half of HKI (32), whereas ATP releases HKI by binding to VDAC (Chapters 2&3, this thesis). The tagged constructs having just the 26-residue N-terminal tail of HKI (and lacking the glucose 6-phosphate binding site) should not be released by glucose 6-phosphate. Indeed, this appears to be the case as the 26-residue N-terminal tail tagged with GFP remains bound in the presence and absence of glucose 6-phosphate (Figs 9 & 10). ATP, however, diminishes bound construct, although the change in fluorescence is small relative to the variation observed over samples having from 0–20 mM glucose 6-phosphate.

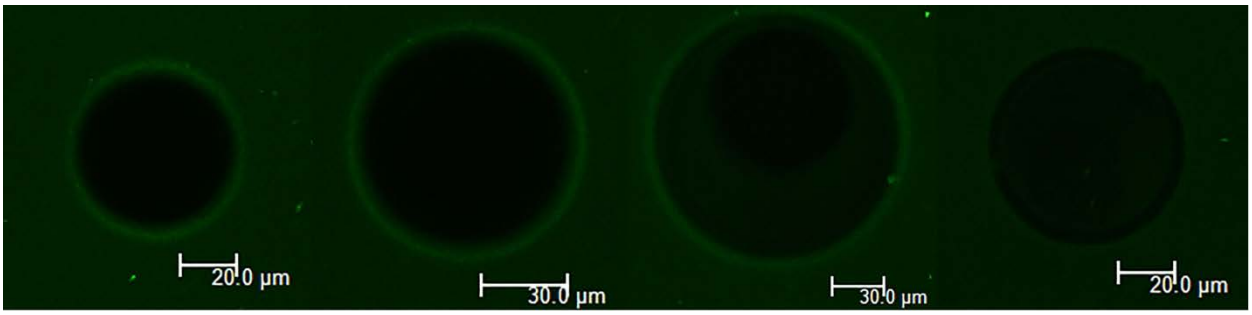

FIGURE 9. Effect of glucose 6-phosphate and ATP on membrane bound constructs incorporating the 26-residue N-terminal tail of HKI. Constructs are tagged with GFP (excitation, 488 nm; emission, 509 nm). From left to right, no glucose 6-phospahte, 10 mM glucose 6-phosphate, 20 mM glucose 6-phosphate and 10 mM ATP. All pictures were taken under the illuminating fluorophores.

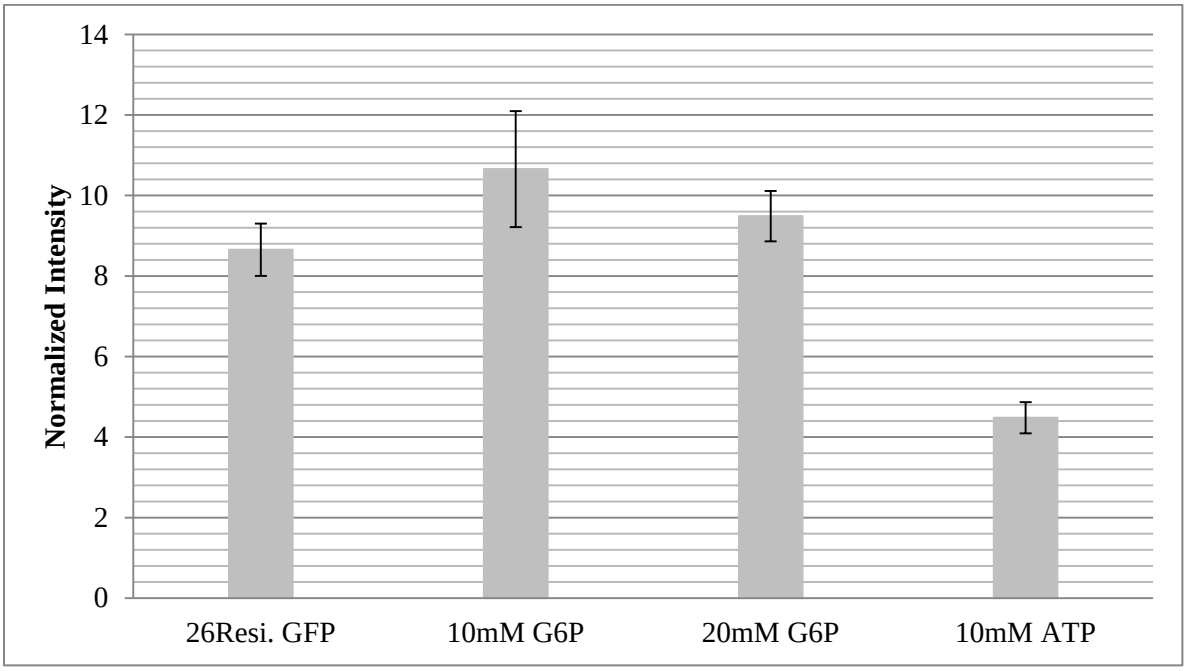

FIGURE 10. Comparison of glucose 6-phosphate (G6P) and ATP in releasing 26-residue N-terminal HKI constructs. The left-most bar represents the fluorescence due to GUV-bound 26-residue N-terminal HKI tagged with GFP, whereas the others represent fluorescence remaining after the addition of the releasing ligand.

DISCUSSION

The results represent the first demonstration that VDAC alone is necessary and sufficient to localize HKI to the membrane. Other factors, such as the involvement of pro-apoptotic proteins, post-translational modification of VDAC, and polarization of the mitochondrial outer membrane, probably modulate HKI binding to the mitochondrion, but the fundamental

characteristics of the VDAC-HKI interaction are determined primarily by elements of VDAC and HKI.

The N-terminal sequence motif of HKI and HKII is limited primarily to proteins of higher eukaryotes (this study). Proteins that have the N-terminal sequence motif have either been characterized biochemically as hexokinases or have high sequence identity to a characterized hexokinase. This observation, combined with a two-component interaction involving HKI and VDAC, suggests a specific binding site on VDAC for the N-terminal tail of HKI (and HKII). Studies of Maskey *et al.* (MS thesis), implicate residue positions 1, 4 and 8 in the interaction between the N-terminal tail of HKI and VDAC. Positions 1, 4 and 8 define a contiguous face of an α-helix that could mate with a complementary surface of VDAC. In fact, the mutation of the N-terminal methionine of HKI (Met1Leu) reduces binding affinity to the mitochondrion by 10-fold. The complementary surface of VDAC that recognizes the N-terminal tail of HKI is unknown; however, Glu73 lies on the outer surface of the VDAC barrel, and would localize approximately midway between the outer and inner leaflets of the membrane bilayer. A three-turn α-helix (approximately 16 Å in length) would extend midway to Glu73. Coarse-grain modeling localizes the 1-4-8 face of the α-helix to the exterior of the VDAC barrel in the vicinity of Glu73 (Maskey, MS thesis).

The GUV system presented here could be a useful tool in the systematic investigation of interactions of HKI (and HKII) with VDAC. The GUV has but one component (VDAC) embedded in its membrane. Hence, any protein that binds to the GUV-VDAC system but not to GUV alone, must bind directly to VDAC or to a membrane structure maintained by VDAC. Hence, the effect of VDAC mutations on the binding of HKI, along with supporting CD spectra to verify the VDAC fold (Chapter 3, this thesis), could map out the binding site on VDAC for HKI. Currently the only approach to the characterization of VDAC mutants is by change in phenotype. The mutation of Glu73 of VDAC to glutamine in yeast results in a cell line that is barely viable, and in fact probably survives only because expression levels of wild-type VDAC (VDAC-1) are not eliminated entirely and other genes of VDAC (VADC-2 and -3) may complement the Glu73Gln mutation.

Pig liver mitochondria comparably bind N-terminal half HKI and wild-type HKI (Chapter 2, this thesis) using an ELISA assay; however, these binding experiments are complicated by variations in mitochondrial preparations and in the stability of HKI constructs.

Specifically, the polyhistidyl-tagged wild-type HKI has a half-life of 48 hours (as measured by specific activity). The instability is due to the polyhistidyl tag attached to the C-terminal half, and results in nonspecific binding (binding that cannot be reversed by glucose 6-phosphate or nucleotides). The constructs used here eliminate the C-terminal half of HKI, eliminating catalytic activity as readout of HKI levels, but providing a means of directly visualizing the binding of HKI to VDAC vesicles.

HK is the “guardian of the mitochondria” (17), controlling the open and closed state of VDAC. Indeed, the addition of HKI terminates ion conductance through VDAC in patch-clamp experiments. The VDAC pore itself, however, can open to a size no larger than the diameter of its barrel (<36 Å) and that size is insufficient to pass cytochrome c. The flow of cytochrome c out of the mitochondrion is the hallmark of the mitochondrial pathway of apoptosis. Presumably, multiple molecules of VDAC cluster into a complex in order to create a sufficiently large pore. Pro-apoptotic proteins presumably stabilize this macro-pore (some have called this the permeability transition pore), whereas the HKI complex of VDAC antagonizes macro-pore formation. The TNP-ATP bound state of VDAC exhibits uniform fluorescence, without punctate patterns indicative of VDAC clusters (Fig. 1). The addition of N-terminal half HKI tagged with GFP makes a punctate pattern indicative of HKI clusters (Fig. 2); however, fluorescence-emission clusters could simply be indicative of nonspecific aggregation. The punctate pattern is not evident in images that expose VDAC-GUVs to N-terminal half HKI tagged with FlAsH-modified tetracysteine. The experiments here do not indicate the formation of VDAC clusters, and in fact, experiments were not designed to produce such clusters.

VDAC cluster formation may also be sensitive to the orientation of membrane-embedded VDAC. Presumably 50% of VDAC molecules spontaneously insert into the membrane of GUVs with their true outer face directed inward (backward insertion). If so, then the mixture of two differently oriented populations of VDAC might interfere with macro-pore formation.

REFFERENCES

1.Wilk, S. (2005) Apoptosis. Sci. STKE. 285, tr16.

2.Czerski, L; Nunex, G. (2004) J. Mol. Cell. Cardiol. 37, 643-52.

3.Lemasters, J J; Holmuhamedov, E. (2006) Biochim. Biophys. Acta. 1762, 181-90.

4.Tsujimoto, Y; Shimizu, S. (2002) Biochemie. 84, 187-93.

5.Vyssokikh, M Y; Brdiczka, D. (2003) Acta. Biochim. Pol. 50, 389-404.

6.Abu-Hamad, S; Arbel, N; Calo, D; Arzoine, L; Israelson, A; Keinan, N; Ben-Romano, R; Friedma, O; Shoshan-Barmatz, V. (2009) J. Cell. Sci. 122, 1906-16.

7.Tajeddine, N; Galluzzi, L; Kepp, O; Hangen, E; Morselli, E; Senovilla, L; Araujo, N; Pinna, G; Larochette, N; Zamzami, N; Modjtahedi, N; Harel-Bellan, A; Kroemer, G. (2008) Oncogene. 27, 4221-31.

8.Yuan, S; Fu, Y; Wang, X; Shi, H; Huang, Y; Song, X; Li, L; Song, N; Luo, Y; (2008) FASEB. J. 22, 2809-20.

9.Madesh, M; Hajnoczky, G. (2001) J. Cell. Biol. 155, 1003-10.

10.Shimizu, S; Matsuoka, Y; Shinohara, Y; Yoneda, Y; Tsujimoto, Y. (2001) J. Cell Biol. 152, 237-50.

11.Zheng, Y; Shi, Y; Tian, C; Jiang, C; Jin, H; Chen, J; Almasan, A; Tang, H; Chen, Q. (2004) Oncogene. 23, 1239-47.

12.Abu-Hamad, S; Zai, H; Israelson, A; Nahon, E; Shoshan-Barmatz, V. (2008) J. Biol. Chem. 283(19), 13482-90.

13.Ghosh, T; Pandey, N; Maitra, A; Brahmachari, S K; Pillai, B. (2007) PLoS. ONE. 2, e1170.

14.Godbole, A; Varghese, J; Sarin, A; Mathew, M K. (2003) Biochim. Biophys. Acta. 1642. 87-96

15.Lu, A J; Dong, C W; Du C S; Zhang, Q Y. (2007) Fish. Shellfish. Immunol. 23, 601-13

16.Zaid, H; Abu-Hamad, S; Israelson, A; Nathan, I; Shoshan-Barmatz, V. (2005) Cell. Death. Differ. 12, 751-60.

17.Robey, R B; Hay, N. (2005) Cell. Cycle. 4, 654-58.

18.Neumann, D; Bückers, J; Kastrup, L; Hell, S W; Jakobs, S. (2010) PMC. Biophys. 3, 1-15.

19.Perevoshchikova, I V; Zorov, S D; Kotova, E A; Zorov, D B; Antonenko, Y N. (2010) FEBS. Lett. 584, 2397-402.

20.Arzoine, L; Zilberberg, N; Ben-Romano, R; Shoshan-Barmatz, V. (2009) J. Biol. Chem. 284, 3946-55.

21.Shoshan-Barmatz, V; Zakar, M; Rosenthal, K; Abu-Hamad, S. (2009) Biochim. Biophys. Acta. 1787, 421-30.

22.Azoulay-Zohar, H; Israelson, A; Abu-Hamad, S; Shoshan-Barmatz, V. (2004) Biochem. J. 377, 347-55.

23.Yehezkel, G; Hadad, N; Zaid, H; Sivan, S; Shoshan-Barmatz, V. (2006) J. Biol. Chem. 281, 5938-46.

24.Yehezkel, G; Abu-Hamad, S; Shoshan-Barmatz, V. (2007) J. Cell. Physiol. 212, 551-61.

25.Rostivtseva, T K; Kazemi, N; Weinrich, M; Bezrukov, S M. (2006) J. Biol. Chem. 281, 37496-506.

26.Skaff, D A; Kim, C S; Tsai, H J; Honzatko, R B; Fromm, H J. (2005) J. Biol. Chem. 280, 38403-9.

27.Bradford, M M. (1976) Anal. Biochem. 72, 248-254.

28.Yehezkel, G; Abu-Hamad, S; Shoshan-Barmatz, V. (2007) J. Cell. Physiol. 212, 551-61.

29.Engelhardt, H; Meins, T; Poynor, M; Adams, V; Nussberger, S; Welte, W; Zeth, K. (2007) J. Membrane Biol. 216, 93-105.

30.Moscho, A; Orwar, O; Chiu, T D; Modi, P B; Zare, N R. (1996) Proc. Natl. Acad. Sci. U.S.A 93, 11443-447.

31.De Castro, E; Sigrist, C J A; Gattiker, A; Bulliard, V; Langendijk-Genevaux P S; Gasteiger, E; Bairoch, A; Hulo, N. (2006) Nucleic Acids Res. 34, W362-5.

32. Skaff, D A; Kim, C S; Tsai, H J; Honzatko, R B; Fromm, H J. (2005) J. Biol.Chem. 280, 38403-9.

CHAPTER 5: COMBINED HALIDE AND ADDUCT STABILIZATION OF β-KETOACYL-(ACYL-CARRIER-PROTEIN) SYNTHASE III

A paper to be submitted to the Journal of Biological Chemistry

Muneaki Watanabe[8], Aaron Marcella, Basil Nikolau, Adam Barb and Richard B. Honzatko[1,9]

From the Roy J. Carver Department of Biochemistry, Biophysics and Molecular Biology

Iowa State University, Ames, IA 50011

Running title: Importance of binding compounds at FabH active site

Keywords: FabH; CPM; Acetyl CoA; Malonyl-CoA; fluorescence

Background: FabH governs the principal priming reaction for fatty-acid biosynthesis in *Escherichia coli*, and efforts to manufacture non-native fatty acids through the introduction of engineered enzymes must take into account enzyme stability *in vivo*.
Results: The Cys112 acetyl-adduct form of FabH in the presence of halide anions optimizes the stability of the enzyme.
Conclusion: FabH *in vivo* is most likely present as the acetyl adduct of Cys112, which is an intermediate state of a reaction cycle.
Significance: Engineering FabH in order to prime fatty-acid biosynthesis with variants of the acetyl group must consider the chemical and conformational stability of the enzyme intermediate.

ABSTRACT

β-Ketoacyl–(acyl-carrier-protein) synthase III (FabH) catalyzes the first condensation reaction of fatty acid biosynthesis. Highly purified FabH from *Escherichia coli* is unstable at elevated concentrations and precipitates irreversibly from solution. Stability problems aside, the enzyme can be crystallized, resulting in atomic-resolution structures. The basis of FabH instability is explored here by experiments in x-ray crystallography and thermal denaturation. Conditions of crystallization enhance the thermal stability of FabH through a nonspecific mechanism; however, the presence of halide ions (chloride and bromide), enhances the thermostability of FabH by specific mechanisms subject to saturation. FabH crystallizes readily when prepared rapidly from an *E. coli* expression system. Such crystals have well-defined electron density for an acetyl adduct, covalently linked to the active-site cysteine (Cys112). The covalent adduct forms a charged complex with a chloride anion that sterically prevents hydrolysis of the acetyl adduct. Co-crystallization of FabH with acetyl-CoA provides a clear and detailed image of a substrate/product complex of FabH to a resolution of 1.4 Å, however, the

active site has a mixture of Cys112 with an acetyl adduct, and Cys112 without adduct but in a disulfide linkage to the thiol group of CoA. Finally, a partially unfolded form of FabH has been trapped in crystals. Evidently, FabH achieves relatively high levels of stability as the acetyl adduct of Cys112, paired with a suitable anion, such as a chloride. The “resting” state of the enzyme *in vivo* may be the intermediate form after the priming reaction and before its reaction with malonyl-acyl carrier protein.

INTRODUCTION

A significant effort in the engineering of enzymes and biosynthetic pathways is necessary in order for bio-renewable chemicals to replace or provide alternatives to petroleum-derived chemicals. The biosynthesis of a diverse set of natural (1, 2) or unnatural (3, 4) compounds is catalyzed by condensing enzymes. Many of these enzymes are part of the Type II fatty acid synthase system, which is the primary pathway for the production of fatty acids in bacteria. In *Escherichia coli* fatty-acid biosynthesis involves enzymes FabB, FabF, and FabH (β-ketoacyl-(acyl-carrier-protein) synthase-I, -II and -III respectively). FabH is distinct from FabB and FabF because it uses acetyl-coenzyme A (acetyl-CoA) over acyl-ACP (acyl carrier protein) in the primary *in vivo* initiation reaction of fatty-acid biosynthesis (5, 6). Acetyl-CoA first transfers its acetyl moiety to the sulfur atom of FabH Cys112, releasing CoA. Malonyl-ACP then binds to FabH and undergoes decarboxylation, generating a resonance-stabilized carbanion that reacts with the acetyl adduct attached to Cys112. The net reaction is the condensation of malonyl-ACP and acetyl-CoA to product acetoacetyl-ACP (9).

FabH is ideally positioned as a regulator of the fatty acid biosynthesis in *Escherichia coli* (7, 8). Fatty acids produced from biosynthetic pathways are used in the production of retail fuels (7); however, procedures to scale-up microbial production using alternative carbon sources requires extensive engineering of metabolic pathways and enzymes (10-15). The development of dynamic sensor-regulator systems for non-natural products derived from fatty acids also presents challenges (16).

Molecular dynamic simulations of FabH, with and without bound ligands, suggest the free enzyme (no bound ligands and no adduct) is the least stable form of FabH (17). Hence, if engineered forms of FabH are to be used in the production of non-natural fatty acids, a strategy to stabilize FabH constructs *in vivo* while permitting catalysis is a necessary attribute. Wild-type

FabH, however, is unstable, and at elevated concentrations precipitates irreversibly from solution. The instability of the wild-type enzyme will likely hinder efforts in protein engineering and the use of FabH in the biosynthesis of novel fatty-acids. In this study, x-ray crystallography, thermal denaturation and enzyme kinetics are used to explore factors critical to the stability of FabH. Rapid isolation of FabH from *E. coli* yields the acetyl adduct of Cys112, observed in crystal structure determinations. The unexpected stability of the acetyl adduct of Cys112 is linked to the presence of a chloride ion, which protects the acetyl adduct from hydrolysis and thereby guards against the inadvertent oxidation of Cys112. Stability of any mutant form of FabH would necessarily include a mechanism to protect its key active site residue.

EXPERIMENTAL PROCEDURES

Materials— Acetyl Coenzyme A (Acetyl-CoA), Malonyl Coenzyme A (Malonyl-CoA), 7-Diethylamino-3-(4'-maleimidylphenyl)-4-methylcoumarin (CPM) and Diethylaminoethyl (DEAE)–sepharose came from Sigma. Kanamycin sulfate was from Invitrogen. Diethylaminoethyl (DEAE) – sepharose, Toyopearl HW-55 was from Tosoh bioscience. Isopropyl-1-thio-β-D-galactopyranoside (IPTG) came from Anatrace. Oligonucleotides were from the Iowa IDT.

Cloning of β-ketoacyl-(acyl carrier protein) synthase III and β-ketoacyl-(acyl carrier protein) synthase III mutants— β-Ketoacyl-(acyl carrier protein) synthase III (FabH) was cloned into a pET-29a vector. FabH mutants were created through PCR modification. A serine residue was introduced at position 112 (C112S mutation of FabH) by using the forward primer, 5’-CATTTGACGTTGCAGCAGCCAGCGCAGGTTTCACCTATGCATT-3’, and its revers complement. The construct was confirmed by DNA sequencing facility at Iowa State University.

Expression and purification of FabH— FabH expression and purification follows protocols in the literature (18) with modifications. *E.coli* strain BL21 (DE3) cells were transformed with FabH plasmids. Transformed cells were grown at 37 °C in a shaking incubator until OD600 reached 0.9 and then induced with 0.5 mM IPTG. At the moment of induction, temperature was reduced to 18 °C. After 16–18 hrs, cells were pelleted and re-suspended in 20 mL lysis buffer (25 mM Tris-HCl, 50 mM NaCl, 5 mM DTT, pH = 7.5). The cell suspension was sonicated three times at 40% of full amplification for 1.5 min. Cell debris were removed from the lysate by centrifugation at 16,000 rpm for 1 hr at 4 °C. The clarified lysate was applied to HPLC

DEAE column and followed by a linear gradient from 50 mM to 1 M NaCl using lysis buffer conditions. Fractions containing FabH as determined by SDS–PAGE were concentrated to 5 mL using a 10 kDa-cutoff ultrafiltration membrane (Millipore) and applied to Toyopearl HW-55F column (Tosoh). The HW-55F column was run at a flow rate of 1 mL/min. Buffer used was 100 mM NaCl, 25 mM Hepes, 5 mM DTT, pH = 7.0. The fractions containing FabH were determined by SDS-PAGE.

Expression and purification of holoACP— Holo-ACP expression and purification also follow protocols with modifications (18). Holo-ACP was expressed in *E. coli* BL21 (DE3) cells harboring a pETDuet™-vector (EMD-Millipore) containing the apo-ACP and holo-ACP synthase genes under control of individual T7 promoters. Apo-ACP was cloned into BamHI and EcoRI of the first multiple cloning site (MCS) while holo-ACP synthase was inserted into the NdeI and XhoI restriction sites in the second MCS of the pETDuet™ vector. The holo-ACP expression cassette includes a His-tag at the N-terminus and the holo-ACP synthase cassette includes no modifications. *E. coli* cells were transformed with the protein expression vector and grown to OD600 = 0.9 at 37 °C in a shaking incubator and then induced with 0.5 mM IPTG. At the moment of induction, the temperature was reduced to 18 °C. After 16 hrs cells were pelleted and re-suspended in 25 mL lysis buffer (20 mM Tris-HCl, 500 mM NaCl, 1 mM β-mercaptoethanol pH = 8.1). The cell suspension was sonicated three times at 40% of maximum amplication for 1.5 min. Cell debris were removed from the lysate by centrifugation at 16,000 rpm for 1 hr at 4 °C. The supernatant was applied to nickel-NTA column (Qiagen) pre-equilibrated with lysis buffer. The column was washed with 25 mL of the base buffer 20 mM Tris, 500 mM sodium chloride, 1 mM β -mercaptoethanol, pH 8.1, then washed again with 25 mL of the base buffer plus 5 mM imidazole, followed by 25 mL of the base buffer plus 25 mM imidazole. Protein was eluted with a buffer consisting of the base buffer plus 150 mM imidazole. Fractions were analyzed by a 15% SDS–PAGE gel. Fractions containing holo-ACP as determined by SDS–PAGE were concentrated to 5 mL using a 3 kDa-cutoff ultrafiltration membrane (Millipore) and applied to Toyopearl HW-55F column (Tosoh). The HW-55F column was run at a flow rate of 1 mL/min. The buffer was 100 mM NaCl, 25 mM Hepes, pH 7.5. The fractions containing holo-ACP were determined by SDS-PAGE.

FabH activity assays— A fluorometric assay was adapted (19) to monitor the appearance of CoA via a reaction of a fluorescent reagent 7-diethylamino-3-(4-maleimidophenyl)-4-

methylcoumarin (CPM) with the newly formed CoA thiol. The FabH assay was conducted with 50 μM malonyl-CoA, 10 μM CPM, and 50 mM Hepes buffer, pH 7.0, at 25 °C in a volume of 1 mL. Acetyl-CoA and FabH concentrations ranged from 20 to 100 μM and 0.5 to 2 μM, respectively. Fluorescence was measured with excitation at 384 nm and emission at 470 nm using a SLM 4800/8000 Spectrophotometer.

FabH ThermoFluor Assays— The quantitative real-time PCR (qPCR) system StepOnePlus was used to run Protein Thermal Shift™ assays to screen for buffer conditions that affect the thermal stability of FabH. FabH (2 μg) in 20 mM Hepes pH 7.0 with 5X Sypro Orange was combined in wells of a 96-well PCR reaction plate with varying salt concentrations (0–1.2 M). Temperature was scanned from 25 to 95 °C at a rate of 1 °C per minute.

FabH crystallizations and data collections— FabH crystals were grown by the hanging-drop vapor diffusion in 96-well sitting-drop plates. FabH (10–20 mg/mL) in 20 mM Hepes pH 7.0, 100 mM NaCl was combined with the well solutions in a 1:1 ratio to give a final droplet size of 3 μl. The ratio of solutions was varied when substrates and/or acyl carrier protein were added, but the drop size did not appear to affect the quality or the size of the crystals. The trays were equilibrated at room temperature. Prior to data collection, crystals were looped and immediately flash-frozen in liquid nitrogen. All diffraction data were collected at 100 K using a MAR300 CCD detector on the Advanced Photon Source beamline 23-ID-B (GM/CA-CAT). At a crystal-to-detector distance of 350 mm, 180 frames were collected using an oscillation range of 1 degree and a 10–20 μm beam size. Data were processed using HKL-3000 (20). Additional analysis, molecular replacement and refinement were performed using PHENIX (21).

RESULTS

Conditions that stabilize FabH— Solution conditions must stabilize a protein in order to facilitate crystal nucleation and growth. Conversely, the successful growth of a protein crystal infers a condition that stabilizes the protein. A screen for successful growth conditions often vary concentrations of polyethylene glycol (PEG), halide salts, ammonium sulfate, and also pH. Given that FabH (and any engineered form of FabH) must be stable under physiological conditions, the pH is fixed at 7.0. The systematic variation in the concentration of PEG was not pursued because at concentration beyond 10% (w/v) PEG, the thermal denaturation assay gave no signal indicative FabH unfolding (data not shown). The variation of halide and ammonium

sulfate concentration, however, did indicate increases in thermal denaturation temperature as salt concentration increased (Fig. 1). The mechanism of stabilization, however, was not the same for each salt. NaBr, for instance, exhibits a curve consistent with a specific binding site for Br^- or Na^+ (K_d = 60±10 mM for wild-type FabH), with little or no nonspecific binding by either Br^- or Na^+ at higher concentrations. The effects of NaCl and ammonium sulfate on the other hand, are consistent with multiple binding sites for the anions (as Na^+ had no effect at high concentrations when introduced as NaBr). In the presence of ammonium sulfate, wild-type FabH and C112S FabH produced isomorphous crystals (same R32 space group and unit cell parameters); however, crystals of C112S FabH diffracted to higher resolution (~2 Å) relative to the wild-type enzyme (~2.8 Å). The difference in the crystal quality correlate well with the difference in thermal stabilities of wild-type and C112S FabH (Fig. 2). The serine mutant has higher stability than wild type FabH regardless of salt concentration, indicating a stabilization effect of approximately 4 °C due to a change in a single atom.

Influence of sodium chloride on FabH activity— FabH activity is assayed by the liberation of CoA from acetyl-CoA. Malonyl-CoA cycles the enzyme back to its free form by its reaction with the enzyme-adduct formed when free enzyme reacts with acetyl-CoA (priming reaction). In initial velocity kinetics, acetyl-CoA concentration varied from 20 to 100 μM, whereas the concentration of malonyl-CoA (second substrate) was fixed at 50 μM. Data and calculated constants are in Fig. 3 and Table 1. Specific activity (4 μmol/min/mg) and K_m (0.04 mM) are close to literature values (5.9 μmol/min/mg and 0.04 mM respectively) (5, 22). FabH activity is modeled by the Ping-Pong mechanism in an approach-to-equilibrium assay to determine NaCl inhibition using DynaFit. FabH with a ping-pong mechanism can exist in two states, E and a chemically modified form of the enzyme E*. The modified enzyme is hereafter called the adduct form of FabH. In such mechanisms, the first substrate, acetyl-CoA, binds, changes the enzyme to E* by transferring the acetyl group to the active site, and is then released as CoA. Only after the first substrate is released can secondary substrate, malonyl-CoA, bind and react with the acetylated enzyme, regenerating the unmodified E form. $E + A \rightarrow EA \rightarrow E^*P \rightarrow E^* \rightarrow E^*B \rightarrow E + Q$, where E is FabH, A and B are acetyl-CoA and malonyl-CoA, respectively, P and Q are products (CoA and acetoactyl-CoA), and E* is the intermediate (acetyl-adduct) state of FabH. NaCl is assumed to inhibit the second reaction governed by FabH.

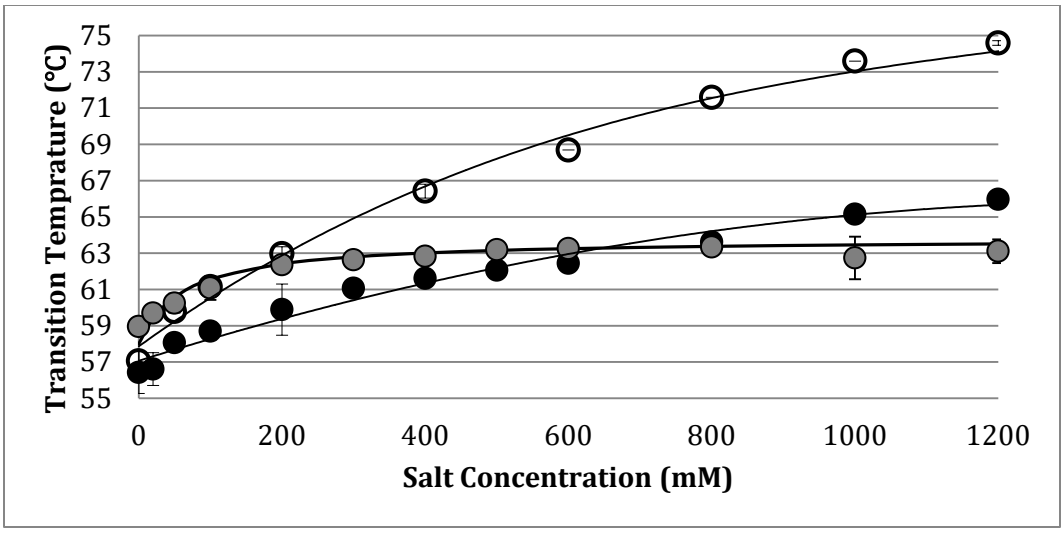

FIGURE 1. Denaturation temperature as a function of salt concentration. The transition temperature rises with increasing concentrations of ammonium sulfate (○), NaCl (●), or NaBr (●). Thermal scans used 1.0 mg/mL wt-FabH, 5x Sypro Orange, and 50 mM Hepes buffer, pH 7.0.

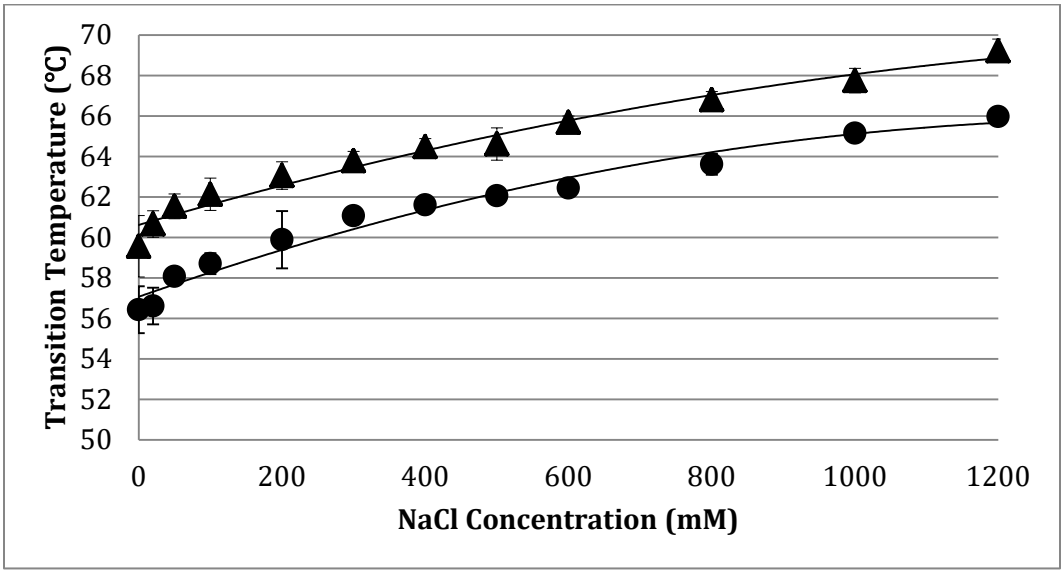

FIGURE 2. Denaturation temperature as a function of NaCl concentration of wild-type and C112S FabH. Thermal scans used 1.0 mg/ml wt-FabH (●), C112S-FabH (▲), 5x Sypro Orange, and 50 mM Hepes buffer, pH 7.0.

The model was modified to add NaCl inhibition, $E^* + I \rightarrow E^*I$ where I is the NaCl as an inhibitor. Enzyme concentration and substrate concentrations were fixed, whereas equilibrium constants were treated as adjustable parameters using DynaFit. Experimental and calculated data

are plotted in Fig. 4. Increasing NaCl concentrations inhibits the production of CoA with a K_i value of 71 mM for wild-type FabH.

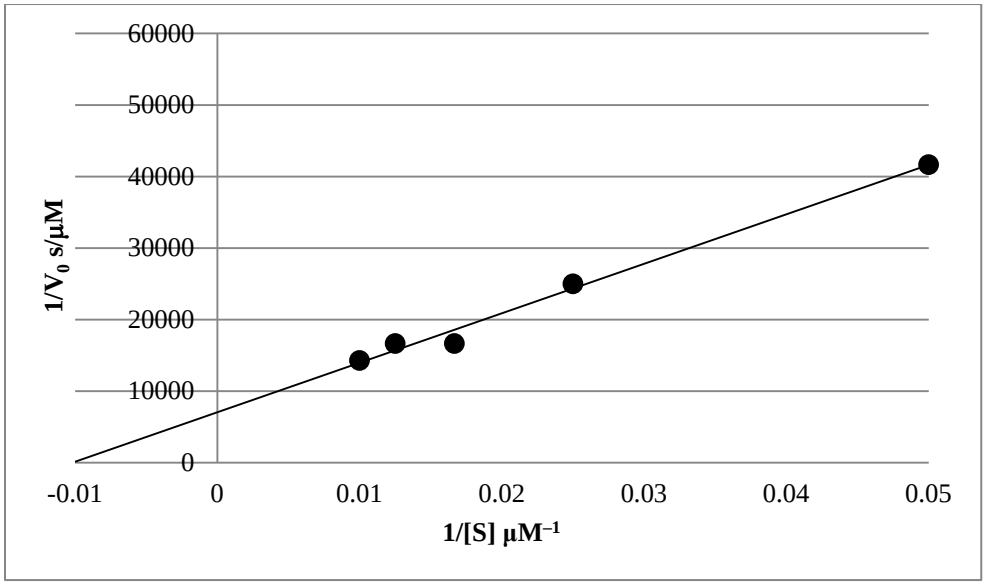

FIGURE 3. Confirming FabH enzyme activity using double-reciprocal plots. Plots represent rate of CoA production at varying total concentration of acetyl-CoA added to 1 µM wild-type FabH, 50 µM malonyl-CoA, 20 µM 7-diethylamino-3-(4'-maleimidylphenyl)-4-methylcoumarin (CPM), and 50 mM Hepes, pH 7.0.

TABLE 1. Values for kinetic parameters for wild-type FabH. K_m , apparent $V_{max,}$ specific activity (SA) and k_{cat} come from initial velocity kinetics, whereas K_i for inhibition due to NaCl comes from approach-to-equilibrium data.

Km (mM)	Apparent Vmax (µM/s)	SA (µmol/min/mg)	kcat (s^{-1})	Ki (mM)
0.04 (3)	0.001 (1)	4 (5)	2 (3)	70 (60)

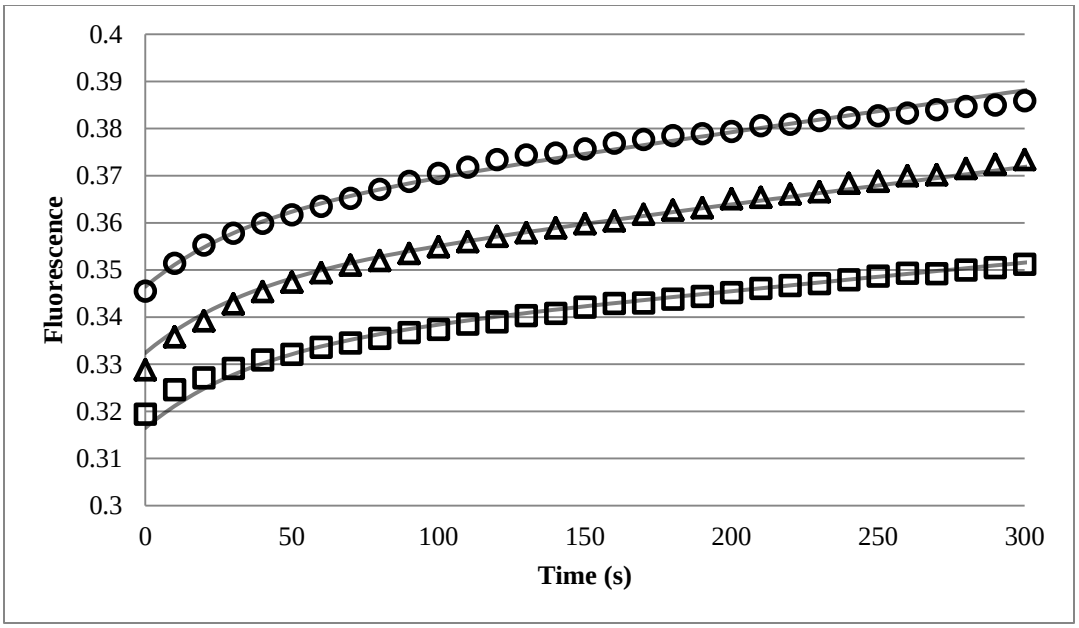

FIGURE 4. Effect of NaCl on enzyme activity. Plots represent production of CoA at varying total concentration of NaCl: 0 (○), 25 (△), and 100 mM (□) added to 2 μM wt-FabH, 50 μM malonyl-CoA, 100 μM Acetyl-CoA, 20 μM 7-diethylamino-3-(4'-maleimidylphenyl)-4-methylcoumarin (CPM), and 50 mM Hepes buffer, pH 7.0. Each solid line was calculated using a theoretical model fitted to data points by DynaFit.

Crystallization and data collection of FabH— Crystals grew within two days from droplets that combined protein, well and ligand solutions in a volume ratio of 1:1:1. Droplets had a volume of 3 μL. Details regarding the FabH constructs and conditions of crystallization appear as footnotes to column headers of Table 2. The key finding was the presence of the acetyl adduct in wild-type FabH and C112S FabH without the addition of acetyl-CoA. n other words, the protein isolated from *E.coli* came with the acetyl adduct in place, and this adduct resisted hydrolysis throughout protein isolation and crystallization.

Analysis of crystal structures— A bromine ion (Fig. 5) appears consistently in crystals which came from crystallization conditions that included NaBr (columns 3—5 of Table 2). This binding site is not located at the FabH active site, but instead close to the dimer interface. The presence of a single, well-defined site for bromide is consistent with thermal denaturation (Fig. 1). Surrounding functional groups from the protein are proton donors in hydrogen bonds with donor-acceptor distances from 3 to 4 Å. The thermal parameter (B) for bromide is 28 $Å^2$ (assuming full occupancy), whereas thermal parameters for atoms of neighboring side chains average to 19 $Å^2$. The refinement of Cl^- at this site (again assuming full occupancy) results in a B-value of 14 $Å^2$.

TABLE 2. Data collection and refinement statistics.

	wt-FabH with adduct and CoA	wt-FabH disordered	SeMet wt-FabH with Adduct	C112SFabH	C112SFabH with adduct
Lattice	Tetragonal	Tetragonal	Orthorhombic	Orthorhombic	Orthorhombic
Resolution range	36 - 1.45	45 - 2.25	35 - 2.02	48 - 2.01	45 - 2.00
Space group	P 41 21 2	P 41 21 2	P 21 21 21	P 21 21 21	P 21 21 21
Unit cell (a/b/c)	a=b=72.54, c=102.07	a=b=72.556, c=98.08	a=64.23,b=67.11, c= 161.14	a=63.63,b=65.40, c=143.97	a=64.12,b=66.87 c=162.02
Total reflections	536,959	176,820	418,690	119,118	257,478
Unique reflections	48,509	13,008	45,456	38,371	47,376
Mosaicity Range	0.32-0.96	0.32-0.92	0.53-1.39	0.24-0.96	0.20-0.98
Completeness (%)	98.8 (96.1)	99.7 (97.7)	97.9 (83.8)	93.6 (66.7)	99.0 (93.4)
Mean I/sigma(I)	18.9 (1.92)	21.2 (2.02)	41.4 (6.85)	9.03 (2.01)	18.5 (4.82)
R-symm	0.08	0.12	0.2	0.085	0.147
R-meas	0.087	0.12	0.206	0.116	0.178
Rpim	0.034	0.077	0.081	0.079	0.099
R-work	0.147 (0.264)	0.210 (0.286)	0.163 (0.216)	0.158 (0.197)	0.169 (0.223)
R-free	0.176 (0.267)	0.244 (0.336)	0.195 (0.245)	0.195 (0.223)	0.215 (0.267)
No. of atoms	2981	2162	5303	5307	5452
Protein	2438	2126	4733	4749	4784
Water	490	34	544	535	631
Ligand	53	2	25	23	37
Protein residues	317	286	634	634	634
RMS(bonds)	0.01	0.004	0.003	0.003	0.004
RMS(angles)	1.62	1	1.02	0.74	1.04
Ramachandran favored (%)	97	95	97	97	97
Average B-factor	19.3	59	34.9	19.9	27.4
Protein	16.7	59.1	34.3	19	26.4
Ligand	23	82.8	41.3	32.3	35.6
Solvent	31.9	53.9	39.7	27.1	34.5

Footnotes to Table 2.

Column 1: Protein solution, 10–20 mg/mL wild-type FabH in 20 mM Hepes pH 7.0 and 100 mM NaCl. Well solution, 50 mM MgCl, 0.1 M Tris Base pH 8.5, and 29% PEG 4000. Ligand solution,10 mM acetyl CoA in 20 mM Hepes pH 7.0.

Column 2: Protein solution, 10 mg/mL wild-type FabH and 20 mg/mL holo-ACP in 20 mM Hepes pH 7.0 and 100 mM NaCl. Well solution, 0.2 M calcium acetate, 0.1 M sodium cacodylate pH 6.5, and 22% PEG 8000. Ligand solution, 10 mM acetyl CoA in 20 mM Hepes pH 7.0.

Column 3: Protein solution, 10–20 mg/mL selenomethionine (SeMet) wild-type FabH in 20 mM Hepes pH 7.0 and 100 mM NaCl. Well solution, 0.3 M NaBr, 0.1 M Hepes pH 7.0, and 25% PEG 8000. Ligand solution, water.

Column 4: Protein solution, 10–20 mg/mL C112S FabH in 20 mM Hepes pH 7.0 and 100 mM NaCl. Well solution, 0.2 M NaBr, 0.1 M Hepes pH 7.0, and 27% PEG 8000. Ligand solution, water. The crystal was removed from its protein droplet and soaked in a droplet of 20 mM Hepes pH 7.0 solution for several hours before flash-freezing.

Column 5: Protein solution, 10–20 mg/mL C112S FabH in 20 mM Hepes pH 7.0 and 100 mM NaCl. Well solution, 0.3 M NaBr, 0.1 M Sodium cacodylate pH 7.0, and 26% PEG 6000. Ligand solution, water.

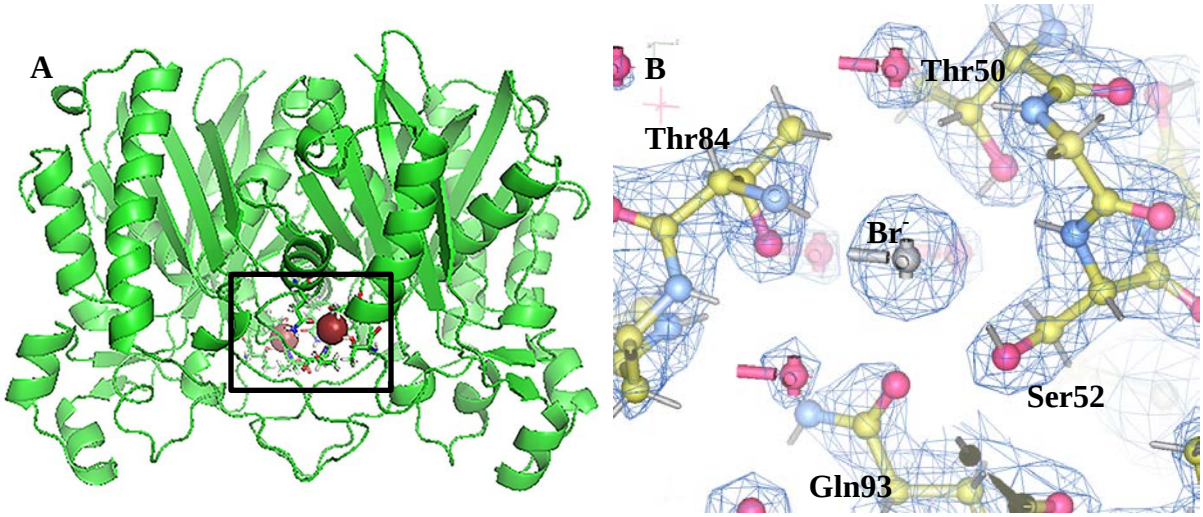

FIGURE 5. The binding of bromide to FabH. (A) Ribbon drawing showing the bromide site relative to the dimer interface. Bromide is indicate by the magenta sphere. (B) Electron density and protein side chains near the bound bromide. The box in Panel A is the region of viewing in Panel B.

Electron density here becomes much weaker in structures that come from crystallization conditions that exclude NaBr, suggesting that the observed density is largely due to bound Br^-.

Electron density for chloride appears juxtaposed to the carbonyl carbon of the acetyl adduct of Cys112 or Ser112 (structures represented by columns 3 and 5 of Fig. 6; Table 2). Cl^- (at full occupancy) refines at these positions with B-values of 14 $Å^2$, which is comparable to B-values of the acetyl adduct. The B-values for water molecules refined in the same density were below 5 $Å^2$. Regardless of the mutation at position 112, the acetyl adduct appears associated with strong electron density, and refines with atomic B-values comparable to those of neighboring residues of the protein. In addition, the carbonyl group of the acetyl adduct hydrogen bonds with backbone amides of Gly306 and Cys112 (or Ser112), presumably localizing negative charge on the oxygen atom, and thereby generating positive charge on the carbon atom of the carbonyl. That positive charge in turn is stabilized by the juxtaposed chloride ion.

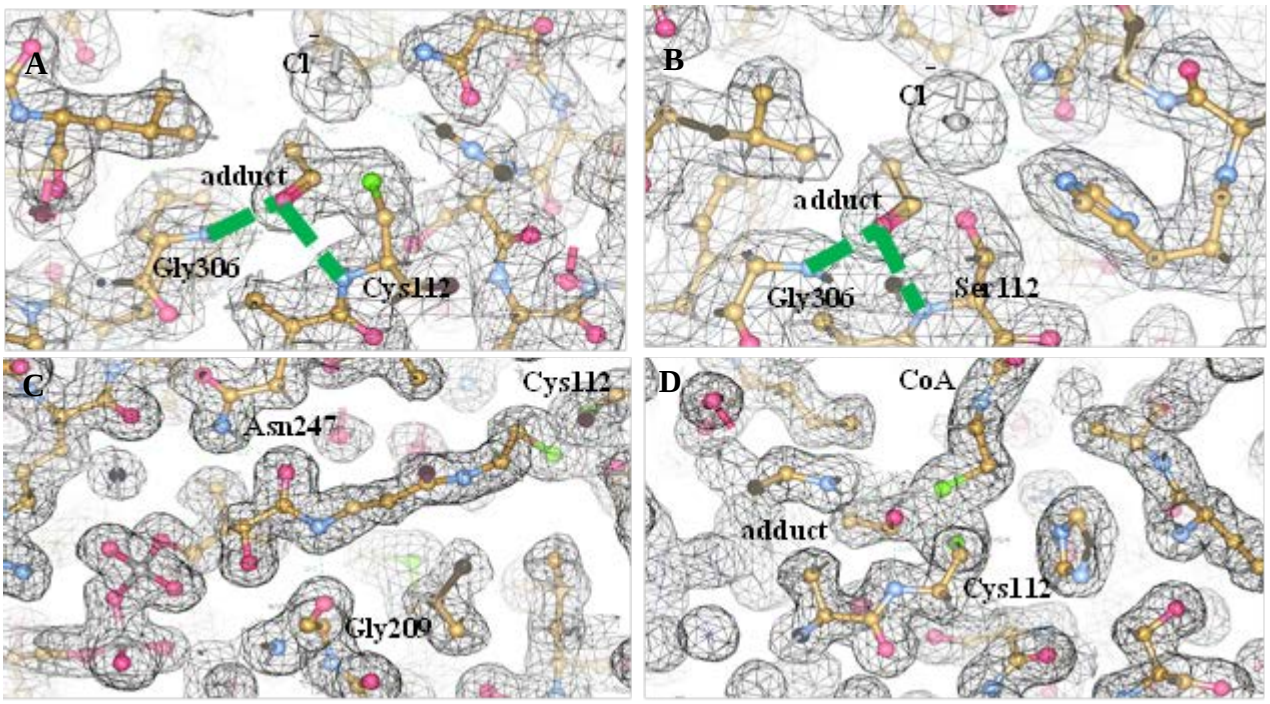

FIGURE 6. Halide, acetyl adduct, and the CoA-bound active site. (A) Wild-type FabH with adduct and Cl^-. (B) C112S-FabH with adduct and Cl^-. (C) Mixed acetyl-CoA/CoA-adduct complex showing the CoA moiety in an extended conformation. (D) Electron density reflecting a mixed state of CoA disulfide-linked to Cys112 and adduct-lined to Cys112.

Exposure of crystals to a solution without NaCl results in the loss of the adduct (structure represented by column 4 of Table 2). Electron density in proximity to the site assigned to Cl^- is diminished and can be explained by a water molecule, the B-values for which match those of the surrounding protein atoms.

CoA appears to form a disulfide link Cys112 (Fig. 6). Electron density in the active site indicates a mixed state, with fractional occupancy by the acetyl adduct and CoA, with CoA dominant. CoA is in strong electron density (Figs. 6C & 6D) and the distal amide group of the pantothenate moiety hydrogen bonds with Asn247 and Gly209. The same residue pair likely recognizes the proximal amide group of the pantothenate moiety of malonyl-ACP (Fig. 7). The adenyl and phosphoryl groups of CoA interact with the active site as observed in a CoA complex in which the disulfide bond is absent (23). The observation of a disulfide-linked CoA at the active site of FabH suggest a purpose in forming the acetyl adduct of Cys112 and stabilizing it through a charge interaction with Cl^- (see Discussion section).

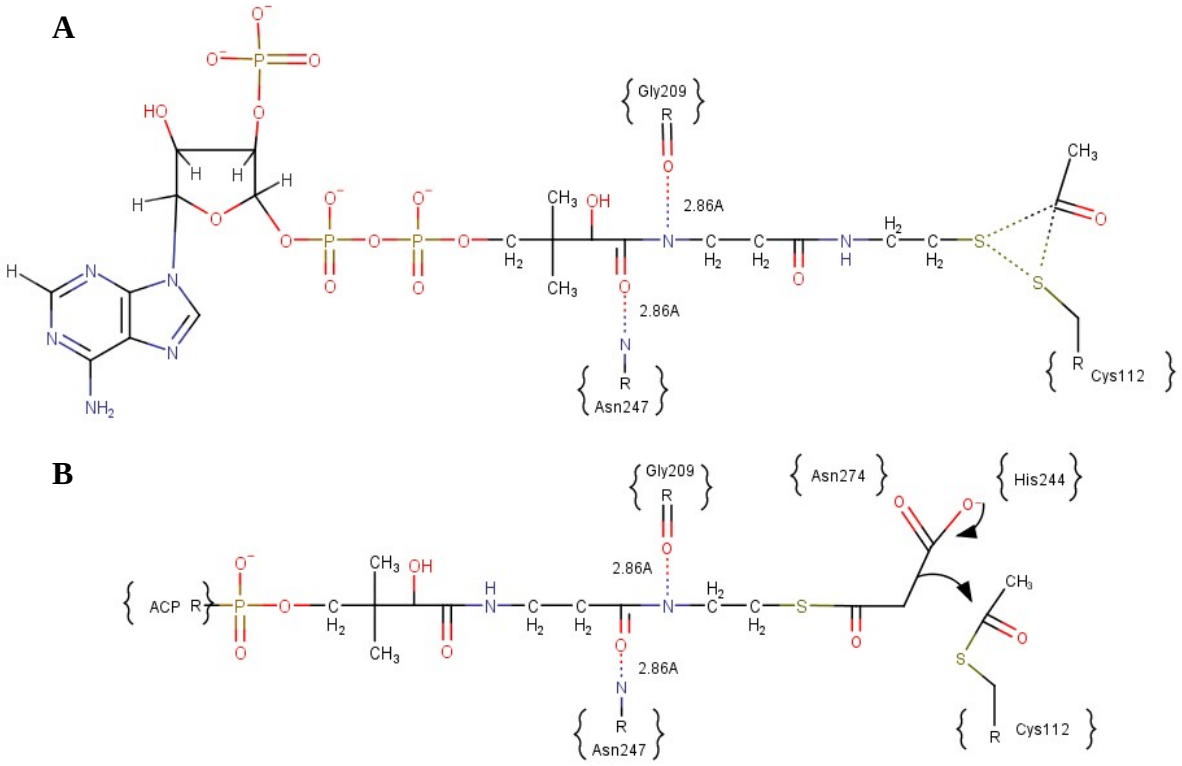

FIGURE 7. Recognition of malonyl-ACP relative to acetyl-CoA. (A) The distal amide linkage of acetyl-CoA is recognized by hydrogen bonds involving Gly209 and Asn247. In order to provide sufficient space for the acetyl adduct and the malonyl moiety of malonyl-ACP, we suggest recognition of the proximal amide linkage of the pantothenate moiety of malonyl-ACP by Gly209 and Asn247 (B).

The disordered structure of FabH, missing 28 residues from a long loop that covers the active site (Fig. 8), has been observed before (23) and is presented here without detailed analysis; however, this opened conformation of FabH has no acetyl adduct at Cys112, and no electron density for Cl^{-}.

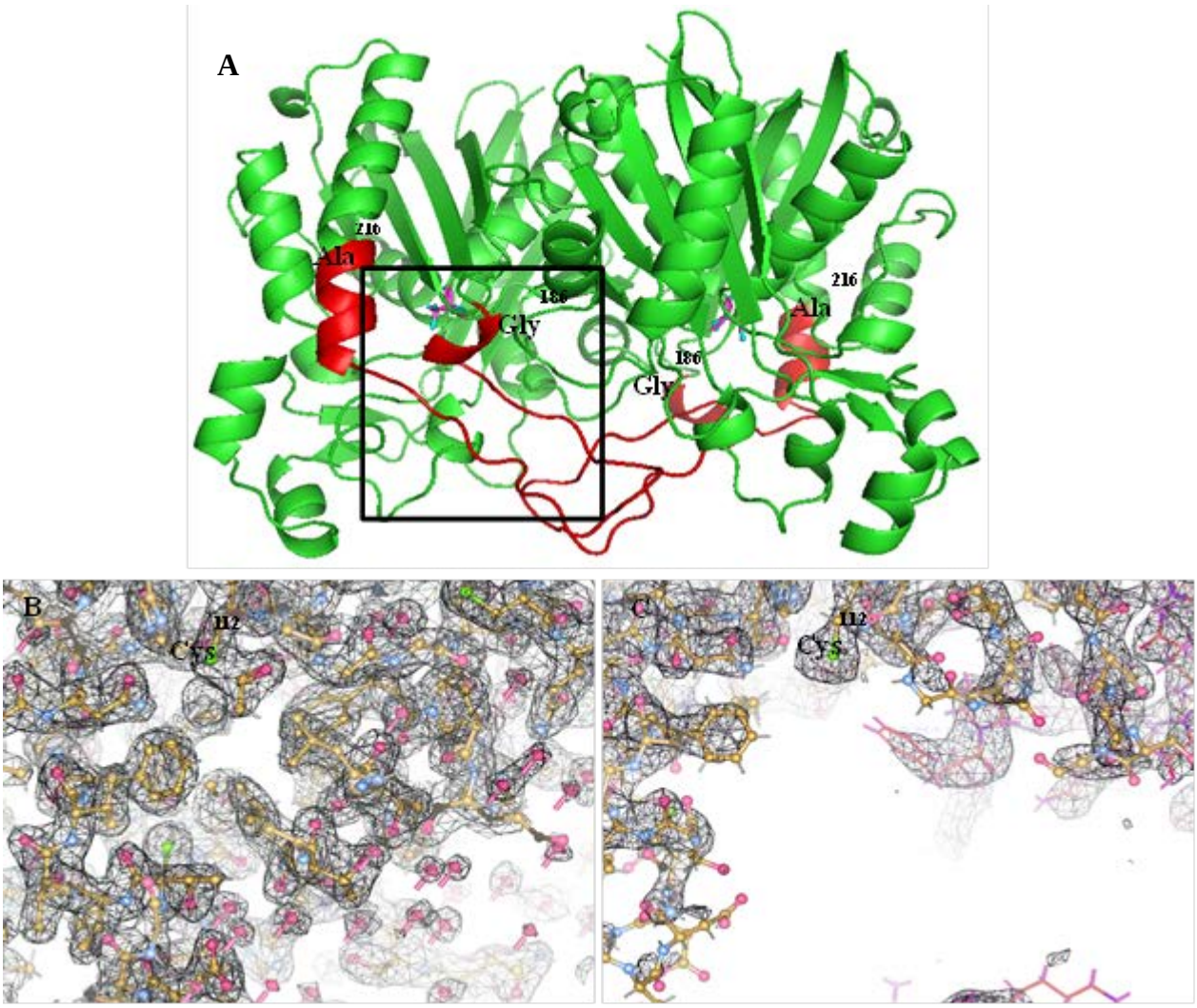

FIGURE 8. Disorder in the wild-type FabH. Dimer of wt-FabH (A) showing region of disorder (red). The side chain of Cys112 marks the active site. Electron density in proximity to Cys112 in the ordered dimer (B) and locally disordered dimer (C). Region of viewing indicated by the box in Panel A.

DISCUSSION

FabH when over-expressed in *E. coli*, comes through rapid preparations with the acetyl adduct in place as revealed by crystal structures. The persistence of this intermediate state (the state that occurs after the priming reaction) is unexpected, and suggests that a stabilization mechanism protects the acetyl adduct of Cys112 from hydrolysis. Moreover, the result indicate sthat the intermediate (acetyl-adduct) state of FabH may be that which dominates *in vivo*.

No law of nature requires that an enzyme prefer its ligand free state. An enzyme goes through a catalytic cycle. The cycle can begin with the primed (acetyl-adduct) state, undergo

reaction with malonyl-ACP, release products, and “finish” with the priming reaction to regenerate the acetyl adduct. The “resting” state of the enzyme, then could be as easily the primed state as the unmodified (free) state. In fact, there may be an advantages in maintaining an acetyl-modified as opposed to an unmodified enzyme in vivo. The thiol group of Cys112 is reactive, and evidently can form other kinds of adducts, the formation of which may not be easy to reverse. The disulfide bond formed between the sulfur atom of Cys112 and the sulfur atom of CoA could be one such adduct. The presence of CoA in the active site designed to fit CoA blocks other metabolites from entering the active site. Once formed then, what chemical process can reduce a disulfide linkage that is blocked and buried in the core of the enzyme, short of unfolding the protein and exposing that link to the solvent? Hence, a mechanism that maintains the acetyl-adduct of Cys112 can protect FabH from inadvertent and damaging chemistry.

Thermal denaturation data here shows that the acetyl adduct of Cys112 is likely to enhance thermal stability of FabH. Crystal structures indicate the presence of Cl^- in what is probably an electrostatic interaction with the partial positive charge of the carbonyl carbon of the acetyl adduct. Cl^- inhibition of FabH with a K_i of ~70 mM (comparable to physiological levels of Cl^-) is consistent with crystallographic data. We suggest then, that acetyl adduct is stabilized by electrostatic pairing with an anion, and that the most likely anion involved in this process is Cl^-. As further evidence, exposure of crystals to a solvent free of NaCl, results in the loss of the acetyl adduct.

With respect to the goal of engineering FabH to accept something other than an acetyl adduct in the priming reaction, an additional consideration of enzyme stability emerges from this study. The goal is to form an adduct complex leaving key active site residues in place and retaining the anion stabilization/protection mechanism. The anion preferably should be Cl^-, as it is plentiful and relatively constant in concentration in vivo. Cl^- does not form strong hydrogen bonds, and hence is easily displaced by malonyl-ACP. The challenge lies in expanding the volume of the active to accommodate an adduct significantly larger than the acetyl group without destabilizing the enzyme in its adduct-free state.

REFFERENCES

1.Cornan, J E; Rock, C O. (1996) ASM Press, 612-638.

2.Magnuson, K; Jackowski, S; Rock, C O; Cornan, J E. (1993) Microbiol. Rev. 57, 522-542

3.Cane, D E; Walsh, C T; Khosla, C. (1998) Science 282, 63-68

4.McDaniel, R; Thamchapipenet, A; Gustafsson, C; Fu, H; Betlach, M; Ashley, G. (1999) Proc. Natl. Acad. Sci. U. S. A. 96, 1846-1851

5.Heath, R J; Rock, C O. (1996) J. Biol. Chem. 271, 10996-11000

6.Tsay, J T; Oh, W; Larson, T J; Jackowski, S; Rock, C O. (1992) J. Biol. Chem. 267, 6807-6814

7.Blatti, J L; Michaud, J; Burkart, M D. (2013) Curr. Opin. Chem. Biol. 17, 496-505.

8.Howard, T P; Middelhaufe, S; Moore, K; Edner, C; Kolak, D M; Taylor, G N; Parker D A; Lee, R; Smirnoff, N; Aves, S J; Love, J. (2013) Proc. Natl. Acad. Sci. U.S.A. 110, 7636-41.

9.Volpe, J J; Vagelos, P R. (1976) Physiol. Rev. 56, 339-417.

10.Youngquist, J T, Lennen, R M; Ranatunga, D R; Bothfeld, W H; Marner, W D 2nd; Pfleger, B F. (2012) Biotechnol. Bioeng. 109(6), 1518-27.

11.Liu, T; Vora, H; Khosla, C. (2010) Metab. Eng. 12(4), 378-86.

12.Steen, E J; Kang, Y; Bokinsky, G; Hu, Z; Schirmer, A; McClure, A; DelCardayre, S B; Keasling, J D. (2010) Nature 463(7280), 559-62.

13.Wargacki, A J; Leonard, E; Win, M N; Regitsky, D D; Santos, C N; Kim, P B; Cooper, S R; Raisner, R M; Herman, A; Sivitz, A B; Lakshmanaswamy, A; Kashiyama, Y; Baker, D; Yoshikuni, Y. (2012) Science 335(6066), 308-13.

14.Handke, P; Lynch, S A; Gill, R T. (2011) Metab. Eng. 13(1), 28-37.

15.Dellomonaco, C; Rivera, C; Campbel, P; Gonzalez, R. (2010) Appl. Environ. Microbiol. 76(15), 5067-78.

16.Zhang, F F; Carothers, J M; Keasling, J D. (2012) Nat. Biotechnol. 30(4), 354-59.

17.Misra, N; Patra, M C; Panda, P K; Sukla, L B; Mishra B K. (2013) J. Biomol. Struct. Dyn. 31(3), 241-57.

18.Marcella, M A; Jing, F; Barb, W A. (2015) Protein Expr. Purif. Yprep 4708.

19.Chung, C C; Ohwaki, K; Schneeweis, J E; Stec, E; Varnerin, J P; Goudreau, P N; Chang, A;Cassaday, J; Yang, L; Yamakawa, T; Kornienko, O; Hodder, P; Inglese, J; Ferrer, M; Strulovici, B; Kusunoki, J; Tota, M R; Takagi, T. (2008) Assay Drug Dev. Technol. 6, 361–74.

20.Minor, W; Cymborowski, M; Otwinowski, Z; Chruszcz, M. (2006) Acta. Cryst. D62, 859-66.

21.Adams, P D; Afonine, P V; Bunkoczi, G; Chen, V B; Davis, I W; Echols, N; Headd, J J; Hung, L W; Kapral, G J; Grosse-Kunstleve, R W; McCoy, A J; Moriarty, N W; Oeffner, R; Read, R J; Richardson, D C; Richardson, J S; Terwilliger, T C; Zwart, P H. (2010) Acta. Cryst. D66, 213-21.

22.Khandekar, S S; Konstantinidis, A K; Silverman C; Janson C A; McNulty D E; Nwagwu S; Van Aller, G S; Doyle M L; Kane, J F; Qiu, X; Lonsdale, J. (2000) Biochem. Biophys. Res. Commun. 270, 100-107.

23.Qiu, X; Jason, C A; Smith, W W; Head, M; Lonsdale, J; Konstantinidis, A K. (2001) J. Mol. Biol. 307, 341-56.

CHAPTER 6: GENERAL CONCLUSIONS

TNP-nucleotides and ATP release HKI from the mitochondrion; however, results of Chapter 2 eliminate nucleotide binding to HKI as the basis for release. The findings of Chapter 2 are negative, determining mechanisms that are not responsible for ATP-release of HKI, and attributing the phenomenon to ATP binding to VDAC.

Suspecting a role for VDAC is easy; proving that ATP binds to hVDAC-1 and releases HKI is difficult. In fact, the evidence for a high-affinity binding site on VDAC for ATP is weak. Analogs of ATP may bind tightly, but no specific residue of VDAC is linked unequivocally to an ATP binding site. Work of Chapter 3 identifies Lys256 as a major determinant in ATP and TNP-AMP binding to VDAC. Moreover, the incorporation of tryptophan at two positions 7 and 18 of the N-terminal helix of VDAC indicates tighter association of that helix with the core of VDAC in the presence of TNP-ATP, than in its absence. These observations suggest a stable complex of ATP and TNP-nucleotides with VDAC.

How then does VDAC pass ATP from the intermembrane space of the mitochondrion to the cytosol if it forms a complex of high stability with ATP? Some have suggested VDAC localizes to tight junctions between outer and inner membranes of the mitochondrion. Components of tight junctions include the adenylate translocator of the inner membrane, VDAC of the outer membrane and a HKI at the outer membrane surface. These proteins co-purify from detergent-solubilized mitochondria, but whether the 500 kDa complex is relevant to the organization of proteins at the tight junction is unknown. Nonetheless, VDAC alone may be an incomplete system, and that interactions with the adenylate translocator and/or HKI may regulate/facilitate the function of VDAC. On the other hand, VDAC could function independently of other proteins, and as suggested in Chapter 3, could have two binding sites for ATP. The site of high-affinity could bind and stabilize a closed pore. As ATP concentrations build in the intermembrane space of the mitochondrion, a second molecule of ATP binds to VDAC at the low affinity site. The pore opens in response to the second binding event, and in so doing destabilizes the tight binding site for ATP, allowing the nucleotide to pass on to the cytosol. Hence, ATP plugs the pore of VDAC, waiting for the mitochondrion to generate an ATP gradient that thermodynamically pushes ATP into the cytosol.

Evidence of ATP binding to VDAC leading to the release of HKI comes in Chapter 4. Here a vesicle system of embedded VDAC and surface-bound N-terminal half HKI qualitatively

reproduces the interaction of HKI with the outer membrane of the mitochondrion. The N-terminal half of HKI releases from VDAC-embedded vesicles in response to glucose 6-phosphate and ATP as does HKI from the mitochondrion. The N-terminal "tail" of HKI also binds to VDAC-embedded vesicles (but not to vesicles without VDAC). The N-terminal tail does not release in response to glucose 6-phosphate, which is an expected outcome as the glucose 6-phosphate binding site is not included in the tail construct. Release of the tail by ATP, however, is less effective than for the N-terminal half, suggesting structural elements of the N-terminal half besides the tail are involved in the recognition of VDAC.

It is not unreasonable to suggest the next experiment to be done in the investigation of interactions between VDAC and HKI. Clearly, the incorporation of any of the VDAC mutant proteins into vesicles is feasible. The 15 lysine mutants of VDAC exhibit wild-type CD spectra, indicating wild-type protein folds. Incorporation of K256M VDAC would test whether the high-affinity binding site for ATP is responsible for the release of the N-terminal half of HKI. Moreover, using the model for the complex of VDAC and N-terminal half HKI (Maskey, MS thesis) specific mutations of N-terminal half HKI can identify other structural determinates of HKI involved in VDAC recognition.

The second part of the thesis focuses on factors that stabilize FabH. Not surprisingly, additives frequently used in the crystallization of proteins enhanced the stability of FabH; however, the mechanism of stabilization varied. Br^- binds to a single site, readily observed in crystal structures of FabH. The protective effects of Br^- seem limited to a single site as the temperature of thermal denaturation plateaus at concentrations of Br^- above 150 mM. Bromide stabilization of FabH is fortuitous, and likely not physiologically significant.

The mechanism of chloride stabilization seems more complex, involving multiple binding sites. At concentrations of approximately 100 mM Cl^-, however, a single chloride anion appears juxtaposed to the acetyl adduct of Cys112, suggesting an electrostatic charge interaction between the anion and partial positive charge of the carbonyl carbon of the acetyl adduct. The presence of chloride here may account for the isolation of the Cys112-adduct form of FabH from *E. coli*, and suggests the predominant state of the enzyme *in vivo* as the adduct intermediate. The presence of chloride protects the acetyl adduct of Cys112 from hydrolysis, and the adduct form of the enzyme protects the thiol of Cys112 from oxidation. The occurrence of a disulfide linked molecule of CoA to the sulfur atom of Cys112 is an example of a dead-end reaction that could

happen *in vivo*. Hence, we hypothesize that the role of chloride in conjunction with the acetyl adduct is physiological, protecting FabH from rogue chemical reactions involving Cys112. We suggest then, that in engineering FabH to accept different substrates in the priming reaction, that the protective mechanism of chloride be retained.

ACKNOWLEDGMENTS

I would like to thank Dr. Richard Honzatko, my major professor, for his guidance through my graduate career. I would like to thank him for his encouragement and support as a teacher and a mentor, and above all. My appreciation extends to my colleagues: Dr. Lu Shen, Dr. Yang Gao, Dr. Nimer Mehyar, Nidhi Shah, Manjit Maskey, and Dr. Nathanial Ginder for their help and support. In addition, I would like to express my gratitude to Dr. Morgan Milton and Dr. Jun-Yang Choe for their help and useful advice. Thanks extend to Dr. Alan Robertson and Dr. Richard Martin for their help using their laboratory. Special thanks for my committee member for their encouragement and help through the years of my research.

Finally I thank my parents and friends for their understanding and support.